



Feasibility of Scaled NASA Dragonfly Capsule for Through-Model Radiation Measurements in X2 Expansion Tube.

Robert Hawken

School of Science, Technology & Engineering
University of the Sunshine Coast

Supervisor: Dr. T. Tian (UniSC)

Industry Advisors:

Dr. C. James (UQ)
Dr. A. Brandis (NASA)
Professor R. Morgan (UQ)

ENG 402 Engineering Thesis

Undergraduate thesis as part of the Bachelor of Mechanical Engineering (Honours)

October 2024

Abstract

In 2028, NASA is launching a drone mission to explore the atmosphere and surface of Saturn's largest moon Titan, called Dragonfly. The aim of this thesis is to; perform an engineering feasibility study for a scaled Dragonfly planetary entry capsule model, suitable for through-model radiation experiments at the University of Queensland. The research involved a literature review on previous Titan entry, current Dragonfly entry models and standard capsule scale model designs. A replication of the Genesis sample return capsule was first created, then scaled up to the 4.5 m Dragonfly diameter. A 90 mm model was chosen to investigate the optic fibre through-model placements to the stagnation point, forebody shoulder and an aftbody shoulder location from the same sting, to replicate the sensor locations of the DrEAM instrumentation suite. Three initial sting designs were created to limit the near wake flow interactions towards the top of the models, by placing the stings towards the bottom shadow regions. A bottom aft-shoulder mounted sting was deemed as the most appropriate, which involved modifications to the shadow region capsule geometry. To improve the understanding of the Titan environment for forthcoming simulations, a comparison was made using NASA's CEA program between the post-shock CN mole fractions at 0.98 N₂, 0.15 CH₄ & 0.05 Argon or 0.98 N₂ & 0.02 CH₄. The last mixture showed a 35% increase in immediate post-shock CN mole fractions, which was the Titan atmosphere composition referred to throughout this thesis to further understand CN interactions at scale. The optimised scale model design was experienced to hypersonic Ansys simulation, which aided in validating that this new design would not impede optic fibre measurements taken towards the instrumentation region. The optimised sting design had an optic fibre bend radius of between 61 mm & 84 mm, within the operating specifications of the manufacturer. A brief binary scaling investigation illustrated the complexity of creating the required immediate post-shock CN concentration at the scale required for X2. Finally, a number of recommendations were listed to improve the understanding of the Titan post shock environment at scale. However, this scale model and sting arrangement is suitable for through-model assessments of Dragonfly radiative heating for the X2 expansion tube at UQ.

Certificate of Authorship

This is to certify that the thesis titled "Feasibility of Scaled NASA Dragonfly Capsule for Through-Model Radiation Measurements in X2 Expansion Tube" submitted by Robert Hawken to the University of the Sunshine Coast in partial fulfilment of the requirements for the degree, Bachelor of Engineering (Mechanical) (Honours) is my own work.

I, Robert Hawken, declare that the thesis is my original work, except where explicitly acknowledged. All sources consulted or referred to in this thesis have been duly cited and acknowledged and the content of this thesis has not been submitted, in part or in whole, for any other degree or qualification at any other academic institution.

I hereby declare that except where specific reference is made to the work of others, the contents of this dissertation are original and have not been submitted in whole or in part for consideration for any other degree or qualification in this, or any other university. This dissertation is my own work and contains nothing which is the outcome of work done in collaboration with others, except as specified in the text and Acknowledgements.

November 2024



Signature

Wednesday 13th November, 2024

Acknowledgements

I would like to acknowledge my supervisors, Dr Tongfei Tian, Professor Richard Morgan, Dr. Aaron Brandis and especially Dr. Chris James.

These people have shaped my personal and professional life throughout my second undergraduate degree. Not only through high standards, wisdom and guidance, they are the first people to maintain a nurturing environment my un-extinguishable curiosity.

Thank you for giving me every opportunity, whilst sharing your knowledge and wisdom, as I transform from student to colleague.

Thank you for constantly going above and beyond for your students.

As we are *your* students.

As long as the candle burns, there is time to make repairs.

- Rabbi Salanter, 19th-century Rabbi

Dedication

I would like to dedicate this thesis to my loving parents, siblings, friends and academic staff who have forged an environment for me to become the person, I ought to become.

"We choose to go to the Moon in this decade and do the other things, not because they are easy, but because they are hard; because that challenge is one that we are willing to accept, one we are unwilling to postpone".

- President John F. Kennedy, Sept. 12, 1962, Rice University, Houston

Table of Contents

Abstract	ii
Certificate of Authorship	iii
Acknowledgements	iv
Dedication	v
List of Figures	xii
List of Tables	xv
Nomenclature	xvii
1 Introduction	1
1.1 Motivation	1
1.2 Stakeholder & Industry Advisor Consultation	3
1.3 Aim	3
1.4 Planetary Entry Background	3
1.4.1 Entry Capsules	3
1.4.2 Hypersonic Wind Tunnels at UQ	4
1.4.3 Hypersonic Chemistry & Entry Radiation	6

1.5	Project Need and Outcomes	6
1.6	Project Scope	7
1.7	Methodology	8
1.8	Thesis Outline	8
2	Literature Review	10
2.1	Chapter Introduction	10
2.2	The NASA Dragonfly Mission	11
2.3	Understanding Hypersonic Temperatures	14
2.4	Atmospheric Entry Heating Thermodynamics	16
2.5	Previous Titan Entry Radiative Inconsistencies	19
2.5.1	Hypersonic Radiation Simulation Codes	20
2.6	Current Dragonfly Mission Radiative Inconsistencies	22
2.7	Instrumentation of NASA Dragonfly Entry Capsule	24
2.8	Capsule Scaling Methods for Experimental Testing	25
2.9	Optic Fibre Through-Model Radiation Testing	27
2.10	Chapter Summary	28
3	Design Methodology	29
3.1	Chapter Introduction	29
3.2	Capsule Replication	30
3.2.1	Genesis Capsule Replication	30
3.2.2	Dragonfly Capsule Geometry	32
3.3	Initial Model Capsule Scaling for X2	33
3.4	Current Through-model Experimentation at UQ	34
3.4.1	Optic Fibre Bend Radius Limitations	36
3.5	Sting Design Methodology	37

3.5.1	Critical Criteria for Sting Design Variations	38
3.6	Proposed Sting Interface Angles	39
3.6.1	Design 1 - Axial Sting Placement	40
3.6.2	Design 2 - Mid-Shoulder Placement	41
3.6.3	Design 3 - Backshell Sting Placement	42
3.6.4	Design 4 - Aft-Shoulder Sting Placement	43
3.7	Decision Matrix of Preferred Sting Design	44
3.8	Chapter Summary	45
4	Analytical and Simulation Results	46
4.1	Chapter Introduction	46
4.2	Determining Boundary Conditions for Simulations	46
4.2.1	Justification of Boundary Conditions	49
4.3	Analytical Calculations for Dragonfly Entry	49
4.3.1	Analytical Approximation of Initial Atmosphere Conditions	50
4.4	NASA's Chemical Equilibrium for Applications Code	52
4.4.1	Additional Initial Conditions for CEA Calculations	53
4.4.2	Inclusion of Argon in CEA Gas Model	53
4.5	CEA Post-shock Equilibrium Conditions N ₂ & CH ₄	54
4.5.1	CEA Post-shock Species N ₂ & CH ₄	54
4.5.2	Errors with Analytical Post-shock Equations	55
4.6	CEA Post-shock Equilibrium Results N ₂ , CH ₄ & Ar	56
4.6.1	CEA Post-shock species N ₂ , CH ₄ & Ar	57
4.7	Comparison of Post-shock Conditions with Gas Models	57
4.7.1	Comparison of Post-shock Species with Gas Models	58
4.8	Summary of Initial Conditions and CEA results	59

4.9	Computational Fluid Dynamic Assessment of Designs	60
4.9.1	Dragonfly Full Scale Simulations	60
4.10	Ansys Fluent Analysis of Control	61
4.11	Ansys Fluent 90 mm Aft-shoulder Model	62
4.12	Ansys Static Structural Assessment of 90 mm Model	65
4.13	Chapter Summary	66
5	Optimised Design & Experimental Scaling	67
5.1	Chapter Introduction	67
5.2	Optimised Design	68
5.3	Ansys Fluent Methodology of Optimised Design	69
5.4	Results from Optimised Design Analysis	70
5.5	Comparison of Results with Literature	70
5.5.1	Design Feedback from Industry Advisors	73
5.6	Scaling for Hypersonic Wind Tunnel Testing	74
5.6.1	Analytical Binary Scaling Approximations	75
5.6.2	CEA CN Results from Density Scaling	76
5.7	Chapter Summary	78
6	Conclusion	79
6.1	Chapter Introduction	79
6.1.1	Literature	79
6.1.2	Methodology & Initial Analysis	80
6.1.3	Optimisation & Experimental Design	80
6.2	Implications to the Scientific Community	80
6.3	Future Experimental Recommendations	81
6.4	Chapter Conclusion	81

References	82
-------------------	-----------

Appendix	86
-----------------	-----------

List of Figures

1.1	Location of Titan (yellow) within Saturn's sphere of influence [2].	1
1.2	The Entry Descent and Landing phases of the proposed Dragonfly mission [2].	2
1.3	Photographs of Titan from Hyugens Probe [3].	2
1.4	Schematic diagram of Genesis capsule similar to Dragonfly Capsule [4]. . .	4
1.5	X2 Expansion tube facility at UQ.	5
2.1	Artist impression of Dragonfly Quad copter on surface of Titan	11
2.2	Proposed Orbital Mechanics trajectory for Dragonfly [10].	13
2.3	Four atomic temperature modes depicted from lowest to highest energy levels [13]	14
2.4	Two atom molecule, translational and rotational energy movements [13] . .	15
2.5	Triatomic molecule H ₂ O with vibrational and electronic energy movement. [13]	15
2.6	Atmospheric thermochemical interactions at vehicle surface [15].	16
2.7	Ballistic entry orientation for Dragonfly Mission [18].	17
2.8	Comparison of Radiation from CN in simulations & experiments [24]. . . .	20
2.9	Comparison of new 2024 Oxford CN results between facilities [26].	21
2.10	Cyanogen radical CFD Results from Johnson, West & Brandis simulations [7].	22
2.11	Convective & Radiative heat flux from Johnson, West& Brandis [7].	23
2.12	DrEAM sensor locations on the Forebody and Backshell of Dragonfly [23].	24

2.13 Manufactured Apollo 11 test model mounted in X3 Test section in Brisbane by Industry Advisors [5].	26
2.14 Stagnation point through-model CAD of Stardust capsule in X2 [35].	27
2.15 Forebody inside the test section area of X2 Tunnel at UQ [35].	28
3.1 Schematic diagram of Genesis capsule [4].	30
3.2 Schematic diagram recreation of Genesis capsule [4].	31
3.3 Render of Genesis capsule with naming conventions replicated from [4]. . .	31
3.4 Schematic diagram of scaled up Dragonfly capsule at 4.5 m.	32
3.5 1:50 scaled down version of the Dragonfly capsule to 90 mm.	34
3.6 Isometric view of current X2 stagnation point through-model assessment [29].	35
3.7 Close up photograph of stagnation point with 90 mm through-model optic fibre in place with adjacent mounting [29].	35
3.8 Raw optic fibre before forebody of capsule is secured [29].	36
3.9 Mach number of near wake flow field to remain free of sting [7].	37
3.10 90 mm diameter models with 600 μm optic fibre.	38
3.11 Axial Sting.	39
3.12 30° Backshell Sting.	39
3.13 83° Mid-shoulder Sting.	39
3.14 45° Aft-shoulder Sting.	39
3.15 Optic fibre bend radius measurements of Axial Sting.	40
3.16 Optic fibre bend radius measurements of Mid-shoulder Sting.	41
3.17 Backshell sting interface with two styles of optic fibre wiring.	42
3.18 Aft-shoulder sting interface with two optic fibre wiring orientations.	43
4.1 Proposed Dragonfly entry milestones in 2023 by NASA Langley [8].	47
4.2 Second entry trajectory presentation in 2022 [20].	47
4.3 CN production with time and distance from shock wave [7].	58

4.4	NASA Simulations of CN mole fraction and Temperature [20].	60
4.5	90 mm capsule normal wake streamlines at 5.77 km/s.	61
4.6	90 mm capsule transient velocity at 5.77 km/s.	61
4.7	Fluid enclosure and volumetric meshing of aft-shoulder simulation.	62
4.8	Streamline effect from before and after 5.77 km/s impulse with aft-shoulder sting.	63
4.9	Transient analysis of Aft-shoulder sting at 5.77 km/s.	64
4.10	Forebody Meshing at 90 mm diamter with 5 mm shell model.	65
4.11	Forebody Deformation at 90 mm diameter with 5 mm shell model.	66
5.1	Comparison of initial aft-shoulder design and optimised design.	68
5.2	Variation of model geometry to house sting.	69
5.3	Ansys Fluent CFD Results for Optimised Design.	70
5.4	CFD Results from Dragonfly Stability Presentation [36].	71
5.5	Radiative & Convective Heat flux for 3.75 m diameter Dragonfly [36]. . . .	72
5.6	Variation of model geometry to house sting.	73
5.7	Variation of model geometry to house sting.	74

List of Tables

1.1	Scope of the Project.	7
2.1	Comparison of original low energy and proposed new high energy trajectory [10].	12
2.2	Titan and Earth properties [22].	19
2.3	Titan Entry Velocity, Density, and Temperature over Time [7].	25
3.1	Comparison of Capsules with Scaling Factor.	32
3.2	Comparison of Parameters with Scale Models Based on Genesis.	33
3.3	600 μm Optical Fibre Characteristics.	36
3.4	Summation of Scores across Sting Designs.	44
3.5	200 μm Optical Fibre Characteristics.	45
4.1	Dragonfly Entry and Descent Flight Parameters.	48
4.2	Titan Entry Velocity, Density, and Temperature over Time [7].	48
4.3	Gas Properties for N ₂ -CH ₄ Mixture.	50
4.4	Analytical Titan Conditions at 5.77 km/s.	52
4.5	Input reactants and output products available from NASA's CEA code. . . .	53
4.6	Reactant Mole Fractions and Products Including Argon.	53
4.7	Post-shock results from N ₂ & CH ₄ by mole fraction.	54
4.8	Most notable post-shock species 0.98 N ₂ & 0.02 CH ₄	55

4.9	Factor increase based on analytical and CEA post-shock values.	55
4.10	Post-shock results from N ₂ , 1.5 % CH ₄ & 0.5% Ar by mole fraction.	56
4.11	Most abundant Post-shock species including Argon.	57
4.12	Factor increase and percentage difference between initial and post-shock conditions.	57
4.13	Relative mole fraction differences between CH ₄ & N ₂ and Argon Species. .	58
4.14	Summary of Initial and Post-shock conditions of Titan at Maximum heating.	59
5.1	Initial Conditions for Optimised Design Simulations in Ansys Fluent. . . .	69
5.2	X2 Freestream Conditions at 5770 m/s (Max heating).	75
5.3	CEA Results from 1:50 density scaling at 5770 m/s (Max heating).	76
5.4	Most notable post-shock species at 1:50 scaled density.	77

Nomenclature

Roman Symbols

1	Initial condition subscript
2	Post-shock subscript
ϵ	Emissivity of the vehicle's surface or atmospheric gases, dimensionless
γ	Ratio of specific heats, dimensionless
∞	Freestream subscript
ρ	Density of the gas, kg/m^3
σ	Stefan-Boltzmann constant, $5.67 \times 10^{-8} W/m^2 \cdot K^4$
a	Speed of sound, m/s
C_3	Characteristic Energy, km^2/s^2
C_p	Specific heat at constant pressure, $J/kg \cdot K$
h	Enthalpy, $MJ/kg - K$
M	Mach number, dimensionless
P	Pressure, Pa
q_c	Convective heat flux, W/cm^2
q_r	Radiative heat flux, W/cm^2

q_{total} Total heat flux, W/cm^2

R_n Nose radius of the vehicle, m/s

T Temperature, K

U Freestream velocity, m/s

V Velocity, m/s

Ar Argon

Ar^+ Ionized argon

C Atomic carbon

C^+ Ionized carbon

C_2 Diatomic carbon

C_2H Ethyne radical

C_2H_2 Acetylene

C_2N_2 Dicyanoacetylene

C_3 Triatomic carbon

C_4 Tetratomic carbon

C_4N_2 Tetracyanoethylene

C_5 Pentatomic carbon

CCN Cyanomethyl radical

CH Methylidyne radical

CH_2 Methylene radical

CH_3 Methyl radical

CH_4 Methane

CN Cyanogen radical

CN⁺ Ionized cyanogen

CNC Cyanocarbene

e⁻ Electron

H Atomic hydrogen

H⁺ Ionized hydrogen

*H*₂ Dihydrogen

HCN Hydrogen cyanide

HNC Hydrogen isocyanide

N Atomic nitrogen

N⁺ Ionized nitrogen

N⁻ Anionic nitrogen

*N*₂ Nitrogen gas

NCN Dicyano radical

NH Imidogen radical

NH⁺ Ionized imidogen

Acronyms / Abbreviations

CAD Computer-Aided Design

CDR Critical Design Review

CEA Chemical Equilibrium for Applications

CFD Computational Fluid Dynamics

DAVINCI Deep Atmosphere Venus Investigation of Noble gases, Chemistry, and Imaging

DLR Deutsches Zentrum für Luft-und Raumfahrt

DPLR Data Parallel Line Relaxation

DSM Deep Space Maneuver

EAST Electric Arc Shock Tube

EDL Entry, Descent, and Landing

EGA Earth Gravity Assist

HTGD High Temperature Gas Dynamics

NASA National Aeronautics and Space Administration

NEQAIR Non Equilibrium Air Radiation

PDR Preliminary Design Review

S.R.C Sample Return Capsule

TOF Time of Flight

UQ University of Queensland

X2 Hypersonic Expansion Tube at UQ

X3 Hypersonic Expansion Tube at Defence

X3R Hypersonic Reflected Shock Tube at Defence

Chapter 1

Introduction

"Success is walking from failure to failure, with no loss of enthusiasm."

1.1 Motivation

— Winston Churchill

In our solar system, the only moon with a substantial atmosphere is Saturn's moon, Titan (Figure 1.1 in yellow). Titan has a thick 1270 km high atmosphere consisting of 98% Nitrogen (N_2), 2% Methane (CH_4) and surface lakes of liquid methane. It is estimated that Titan's inner surface has four layers of alternating water/ice, which makes Titan a very attractive destination to explore for the possibility of organic life [1].

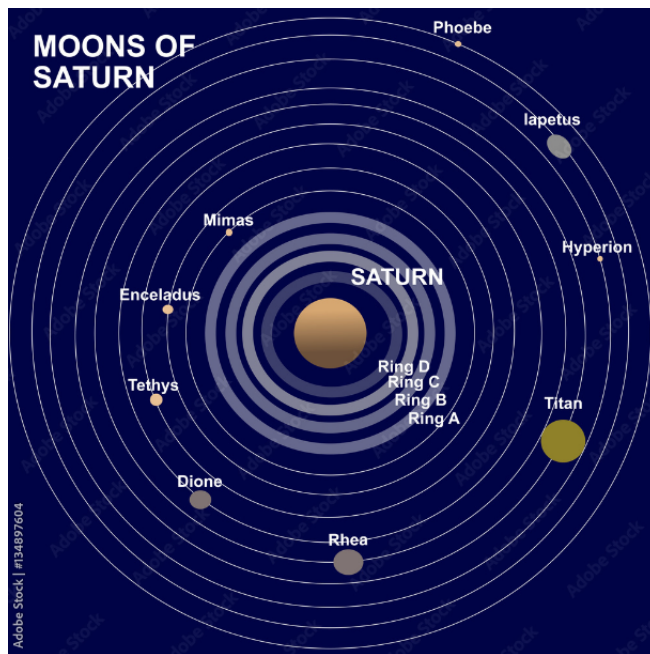


Figure 1.1: Location of Titan (yellow) within Saturn's sphere of influence [2].

The National Aeronautics and Space Administration (NASA) is currently designing a drone to fly around and explore the surface of Titan. The "Dragonfly" mission is apart of NASA's '*New Frontiers*' program, scheduled for a 2028 departure and to arrive on Titan seven years later in 2035 (Figure 1.2). This project will use a 60° sphere cone, 4.5 m diameter capsule to deliver a 450 kg, eight blade quadcopter drone with scientific instrumentation, with the capability of multiple powered flights up to 4 km altitude [3].



Figure 1.2: The Entry Descent and Landing phases of the proposed Dragonfly mission [2].

This is one of the most ambitious un-crewed missions to date, therefore numerous engineering considerations are required to land and operate such a unique payload. In the case of Titan, only the Huygens Probe has entered and landed in 2005 (Figure 1.3). This first probe operated for 90 minutes on the Titan surface transmitting photographs and atmospheric data [3].

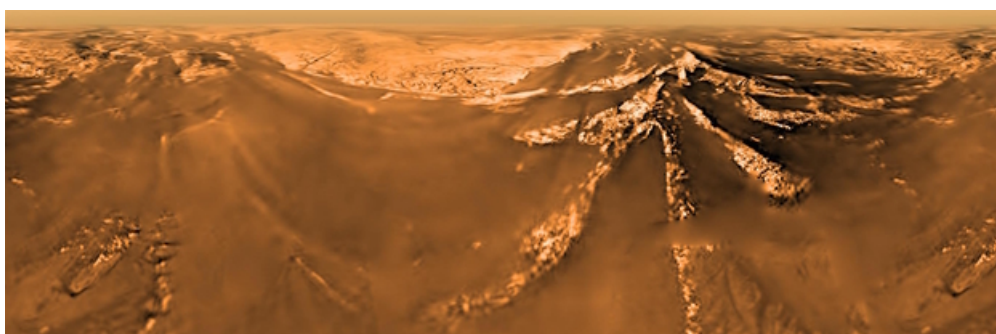


Figure 1.3: Photographs of Titan from Hyugens Probe [3].

1.2 Stakeholder & Industry Advisor Consultation

The investigation of this project has been directly requested by NASA's Lead Aero-thermal engineer for the Dragonfly mission (Industry Advisor, Dr. Aaron Brandis) by video conference. This scoping meeting was organised by the remaining Industry Advisors, Dr. Chris James and Professor Richard Morgan, (April 2024).

Dr. Brandis completed his research on experimental Titan entry at The University of Queensland (UQ) in 2009 and is now leading the aerothermal division for Dragonfly, and has requested a targeted study towards the radiative heating on the Dragonfly entry capsule. The overall concept was to develop a suitable scale model of the Dragonfly entry capsule, in order to experimentally test the radiative heating upon entry, with varying velocities & Nitrogen and Methane concentrations. This project scope is far greater than required for an Undergraduate thesis. Therefore, the experimental feasibility for scaled model ground testing at UQ will be investigated in this document, with the author to act on any recommendations if selected for a Doctor of Philosophy commencing in 2025.

1.3 Aim

The aim of this thesis is to; perform an engineering feasibility study for a scale model of the Dragonfly entry capsule, suitable for through-model radiation experiments in the X2 hypersonic impulse facility at UQ, without adversely interfering with the experimental test flow to the shoulder and backshell. After verifying that a suitable geometry profile can be replicated in X2, the experimental conditions will be determined.

1.4 Planetary Entry Background

To improve understanding of this thesis, background knowledge on interplanetary capsule entry will be briefly presented. The background knowledge is provided here for engineers who are not versed in the planetary entry environment, so the literature review can be targeted towards the specific investigation for this project.

1.4.1 Entry Capsules

Entry capsules are 'blunt' bodies, with a large curved nose covered in a thermally protective external layer (heatshield). Figure 1.4, displays the Genesis Sample Return Capsule (Genesis S.R.C), which is a similar aeroshell design of the Dragonfly entry vehicle.

The primary location required for testing is labelled as the forebody shoulder and aft shoulder (Figure 1.4).

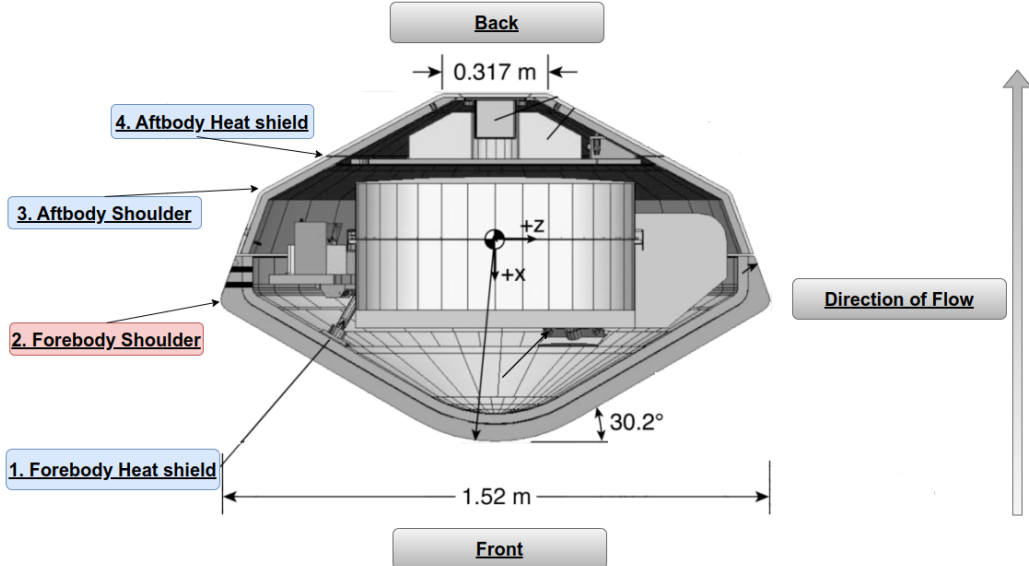


Figure 1.4: Schematic diagram of Genesis capsule similar to Dragonfly Capsule [4].

To experimentally test the chemical changes that occur upon atmospheric entry, scale models of the vehicles are required. However, scaling down a model involves more than just reducing its size; the thermal and chemical changes associated with flight are the properties that need to be accurately recreated. These properties are the driving forces behind the final dimensions of the scale test model [5].

Although numerous papers have investigated radiative Titan entry heating, a vast majority of these studies predate the design specifications of the Dragonfly geometry and trajectory. The studies need to be tailored towards the engineering challenges of this particular mission profile. Based on the results from NASA's Preliminary Design Review (P.D.R) of Dragonfly, a specific scale test model will be designed for hypersonic through-model radiation experiments. For the purpose of this thesis, thermal radiation, radiative heating, and radiative heat transfer will be referred to as radiation.

1.4.2 Hypersonic Wind Tunnels at UQ

Hypersonic wind tunnels are used to recreate similar atmospheric conditions and phenomena found throughout planetary entry. The University of Queensland has developed a number of hypersonic test facilities. Notably the X2 Expansion tube for superorbital ground testing, the T4 reflected shock tunnel for scramjet testing (supersonic combustion), X3/X3R which

is now at the Defence Science Technology Group in Brisbane. These facilities have been designed, maintained and operated by numerous staff, in particular the three Industry Advisors discussed in Section 1.2. Both Dr. Chris James and NASA advisor Dr. Aaron Brandis have completed their experimental planetary entry PhD's under the direct supervision of Prof. Richard Morgan. The close connection to world leading hypersonic researchers, provides a solid teaching and support framework for this thesis.

The impulse facility which will be considered for this analysis is the 25 m, X2 Expansion Tube located at UQ in the Hawken Engineering Building, St. Lucia Campus, QLD, AUS (Figure 1.5). The X2 facility at UQ is one of the worlds fastest free-piston expansion tube (up to 70,000 km/hr). Since, there are only a few of these facilities around the world, NASA, Oxford, and etc, this project is very valuable for experimental research.

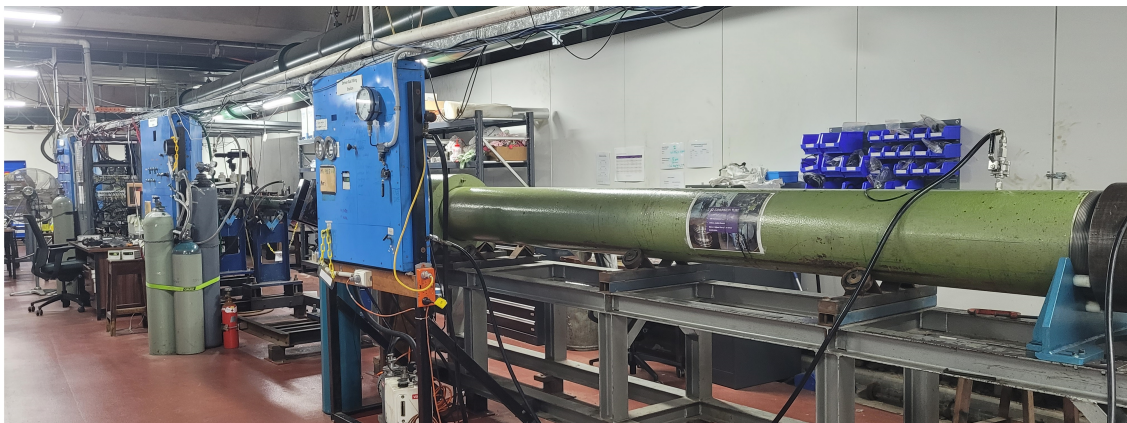


Figure 1.5: X2 Expansion tube facility at UQ.

The X2 Expansion tube includes the reservoir, 10.5 kg piston, compression tube, shock tube, acceleration tube, nozzle and test section. The sections are separated by 1-2 mm steel circular diaphragms, while the diaphragm separating the shock and acceleration tube has a thin Mylar diaphragm. The tunnel sections are normally at atmospheric pressure when not in use. Since the sections will have different gases in testing, they are all initially pumped down to a vacuum.

In order of procedure, the Helium 'driver' gas is filled into the compression tube, then the reservoir is filled to a very high pressure (up to 7 MPa). If the piston is accidentally fired, the diver gas would compress and slow down the piston. The shock tube is filled next with the specific low-pressure atmospheric gas composition for wind tunnel testing, in this case 98% Nitrogen and 2% Methane by volume. The acceleration tube is filled with a very low pressure air, the expansion waves between high pressure and low pressure gas, cause rapid acceleration of the test flow, through the Mylar diaphragm and into the acceleration tube [6].

1.4.3 Hypersonic Chemistry & Entry Radiation

Further knowledge of molecular interactions is required to understand, model and predict how hypersonic flows will interact over an entry vehicle. The first parameter to investigate are the very high temperatures that occur behind the shock wave, and the associated effects on atmospheric chemistry and the vehicle itself.

Although the majority of heating is from convection, thermal radiation measurement techniques onto the capsule are the subject of this thesis. The radiation from the atmosphere will change dramatically throughout the capsule's entry phase, especially when molecules split into atoms, known as dissociation.

Post-shock wave temperatures are able to reach well over 5,000 K upon entry, which changes the composition of the atmosphere locally around the vehicle. In the case of Titan there are numerous collisions which occur, although only a particular interaction will be discussed. The Nitrogen N_2 separates into $N + N$ and Methane CH_4 into various species for example; $CH_2 + 2H$. As the atoms pass over the vehicle, they collide and form a very highly thermally radiative Cyanogen radical CN.

This project is directed towards creating the experimental model of Dragonfly to use new techniques for the UQ Centre for Hypersonics on how the formation and radiation emission of CN radicals will affect the spacecraft radiative heating on this Titan mission.

1.5 Project Need and Outcomes

As the concept and background information have been provided, the need and benefits of the project can be more easily understood. In most planetary entries convective heat flux is dominant at the forebody stagnation point, but minimal along the afterbody of the capsule, hence the afterbody is usually less thermally protected to reduce overall weight.

However, if radiative heat flux is large on the shoulders & afterbody, the lack of thermal protection could lead to material failure in this region and potentially loss of vehicle upon entry. For Dragonfly, one of the primary unknowns is the CN radiative heating of the aft shoulder and backshell due to the changes in atmospheric interactions. Johnston and Brandis indicate that the uncertainties in afterbody radiative heating between 40% and 60% for conditions near peak heating, and radiative heating in the shoulder can be up to 25% higher than the standard stagnation point for the forebody [7].

The need for this investigation is quite evident, as the entry to Titan is nearly two hours long, including parachute phases, from an atmosphere entry interface of 1270 km [8].

For comparison the entry, decent and landing (EDL) for Mars is roughly two - seven minutes [9], which already has the lowest survival rate of entering spacecraft (40%). Most Mars missions are surface landers or rovers, Dragonfly will be landing itself from powered quadcopter flight at the last stage (Figure 1.2). This makes the Titan EDL the longest for any surface-bound vehicle and the Dragonfly payload the most difficult to land.

Therefore, each component of the full mission will need to be *over-engineered* in order to guarantee operational success on Titan. If the experimental techniques outlined in this thesis provide accurate results for Dragonfly, then the Australian researchers operating X2 can be confidently contribute to future NASA missions. Dr. Brandis has also expressed interest in working with UQ towards developing Venus entry assessments for project DAVINCI, launching mid 2030's.

1.6 Project Scope

As this is a very complex project, it is imperative to outline the boundaries of what the scope will actually entail. Table 1.1 details what sections are in scope and what aspects are out of scope for this project.

Table 1.1: Scope of the Project.

Category	In Scope	Out of Scope
Design	3D modelling of the Dragonfly capsule.	Experimentally testing the final product.
Framework	Supporting framework of the model in flow will be developed.	Developing the hypersonic experimental conditions.
Finite Element Analysis	FEA to determine the expected deformation.	Minimal consideration into the testing needs for other projects.
Computational Fluid Dynamics	CFD for streamline analysis of aeroshell to replicate flight.	In-depth analysis of CFD results of radiation heat transfer.
Manufacture	3D printing test models for Optic Fibre installation.	Manufacturing of final model from stainless steel.
Sensors	Basic assessment of optic fibres housed inside the model.	Integration of optic fibres and spectroscopy analysis of results.

This project will focus on the scaled model design and housing suitable for through-model radiation testing. There will be high performance computer simulations required and hypersonic theory which will need to be applied after this thesis is presented, in order to understand the flight and X2 testing environment.

1.7 Methodology

In order to accomplish these numerous sub items, a sequence of development has been produced.

- Investigate the current literature in entry capsule scale model design.
- Gather information on the testing requirements and interface of sensors.
- Design a scale model of the Dragonfly entry capsule.
- Design the supporting mounts for use inside a hypersonic impulse tunnel.
- Prepare finite and fluid analysis required on chosen design.
- Provide alterations and updated iterations to the model and surrounding housing.
- Provide a summary on the experimental testing considerations based on the mission.

1.8 Thesis Outline

Each chapter of this thesis will cover a summary of the previous work and following a conclusion of the discussed information of that chapter.

Chapter 2 will be divided into numerous subsections to aid completion of the primary objective. Initially the literature review will investigate the numerous design considerations involved with scaling of interplanetary entry aeroshells. Once the aeroshell design fundamentals are understood, the research will focus on the additional requirements of the model for radiation testing. Numerous instrumentation factors will be considered and consultation with Industry Advisors towards the accessibility of sensor locations and a modular design.

Furthermore, most entry radiation testing has been conducted on a wide range of geometries, angle of attack, chemical compositions and sensor locations. Therefore, the primary considerations for this current NASA mission will be examined towards replicating a scale model used for the Dragonfly mission from all the obtained information and data.

Chapter 3 will investigate accurate scaling of the Dragonfly entry capsule. Once a suitable model has been drafted, the next aspect is to design a suitable support to house and suspend the model for impulse testing. The proposed range of Titan test gas velocities is between 4000 and 7000 m/s to simulate radiative heating along the entry corridor at these speeds. It is important to consider the boundary layer effects and oblique shock interactions; if any supports were to interfere with experimental and computational testing.

The analytical and numerical boundary conditions will be investigated to improve the quality of the simulations. The numerical modelling, computational fluid dynamics (CFD) and results from finite element analysis will be included in Chapter 4, where the required changes to the desired model will be discovered.

Chapter 5 will pertain the improvements to capsule design on the results from initial streamline testing. Once the profile of a suitable geometry has been established, the hypersonic testing requirements can be determined.

Chapter 6 will provide concluding remarks and the final findings of this investigation with recommendations of Titan entry testing. The aim and goals will be compared to the final product in order to justify that a successful design campaign was reached, which satisfies the future testing requirements of a NASA Dragonfly scale model in X2.

Chapter 2

Literature Review

"Research is what I'm doing, when I don't know what I'm doing."

— Wernher von Braun

2.1 Chapter Introduction

The literature review begins with extra details on the NASA Dragonfly mission and the important parameters to consider investigation. The review will introduce general atmospheric entry considerations involving convective and radiative heating, while highlighting the difficulty of Titan entry. After the Titan entry environment is described, the hypersonic chemistry phenomenon will be reviewed to understand why further experimental Titan entry testing is required for mission success.

Next, the design considerations associated with scaling interplanetary aeroshells needed to replicate the flight environment of Titan. After establishing the fundamentals of scaled aeroshell design, the focus will shift to the specific requirements of the model for through-model radiation testing.

This will involve examining numerous factors related to instrumentation and further consultation with key stakeholders to ensure the accessibility of sensor locations and the feasibility of the design.

Additionally, since most Titan entry testing has been conducted across a broad spectrum of geometries, velocities and sensor locations, this research will specifically address the primary considerations for the current Dragonfly mission. The goal is to replicate a scale model suitable for through-model analysis for the Dragonfly mission using the gathered information.

2.2 The NASA Dragonfly Mission

The Dragonfly mission is aimed to deliver the first ever multi rotor vehicle to another world (Figure 2.1). This project was selected in 2019 as the primary candidate for the next phase of the "New Frontiers" mission schedule by NASA. The previous delivered missions in this schedule include the 2006 'New Horizons' mission to Pluto, 2011 'Juno' mission to Jupiter and the 2023 'Osiris Rex' asteroid sample return.

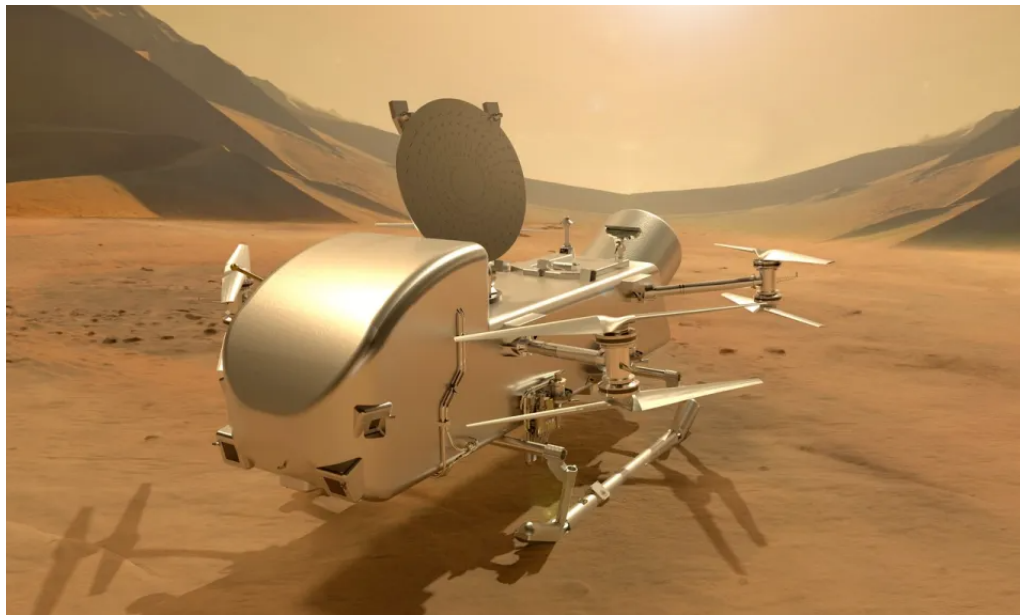


Figure 2.1: Artist impression of Dragonfly Quad copter on surface of Titan

As this thesis aims to improve the knowledge pool for a current project, it is important to understand NASA's project timeline, to underline the importance of this thesis. The mission was originally scheduled for a 2026 departure, but after numerous delays from COVID-19 and budget constraints from International conflicts, departure has now slipped to a 2028. However, this change in timeline allows for the results of this thesis to aid in project research.

The systems engineering program that NASA invented for its missions is now implemented worldwide. The System Requirements Review (SRR) was the first major mission review which occurred in August 2020, to ensure that the project scope and subsystem objectives are understood and feasible. The next phase which Dragonfly passed in February 2023 is the Preliminary Design Review (P.D.R). However, due to the multiple delays in mission deployment between these reviews, the scope and system requirements are still being updated, hindering targeted research for this mission.

Thirdly, is the Critical Design Review (C.D.R) which is scheduled for December 2024, is a notable timeline since this thesis will be completed before then. Therefore, the findings of this research can be used shared with the primary stakeholders during the product design [10]. This is the last engineering design review and therefore, no major design changes should occur after C.D.R (unless mission critical) [11]. It is imperative that the necessary research is conducted and implemented *before* this phase, again highlighting the suitable timing of this thesis.

The delayed timeline will also alter the previously calculated launch, orbital mechanics and thermal entry parameters into Titan. However, NASA engineers have remained positive that only minor design changes are needed between launch options, although minor alterations are ongoing, with an appropriate factor of safety included [10].

Table 2.1 displays key orbital parameters for the original and new proposed launch trajectories. The most notable changes are the increase in Characteristic Energy (C_3), reduction in Time of Flight (T.O.F) by 3.5 years and reduction in both Venus and Mars gravity assists. This reduction in time from an increase in orbital energy will also increase the available power at arrival.

Table 2.1: Comparison of original low energy and proposed new high energy trajectory [10].

Orbital Parameter	Previous Original	New Proposed
Required C_3	$20 \text{ km}^2/\text{s}^2$	$55 \text{ km}^2/\text{s}^2 (2.75x)$
Required launch vehicle (LV)	Medium class (Atlas V-5xx)	Heavy class (Falcon Heavy)
TOF	9.9 years	6.4 years
Venus gravity assists	1	None
Earth gravity assists	3	1
MMRTG power at arrival	82W	91W (+17%)

It is important to note, that the 2.75 times increase in C_3 (hyperbolic excess velocity squared) will increase Dragonfly's entry energy. Therefore, further highlighting the requirement for extended radiation experimentation across a wide variety of entry conditions, regardless of the missions design parameters. It would be a major program failure if the drone was fully built, with a capsule that can only survive a small thermal window. Hence, the requirement to measure and apply a factor of safety on a number of possible entry scenarios.

A visual representation of the most recent launch trajectory is displayed in Figure 2.2. With the change of launch profile that doesn't rely on the position of Earth and Venus for multiple flybys for gravity assists, the mission can now be performed directly with minimal aeroshell thermal design changes.

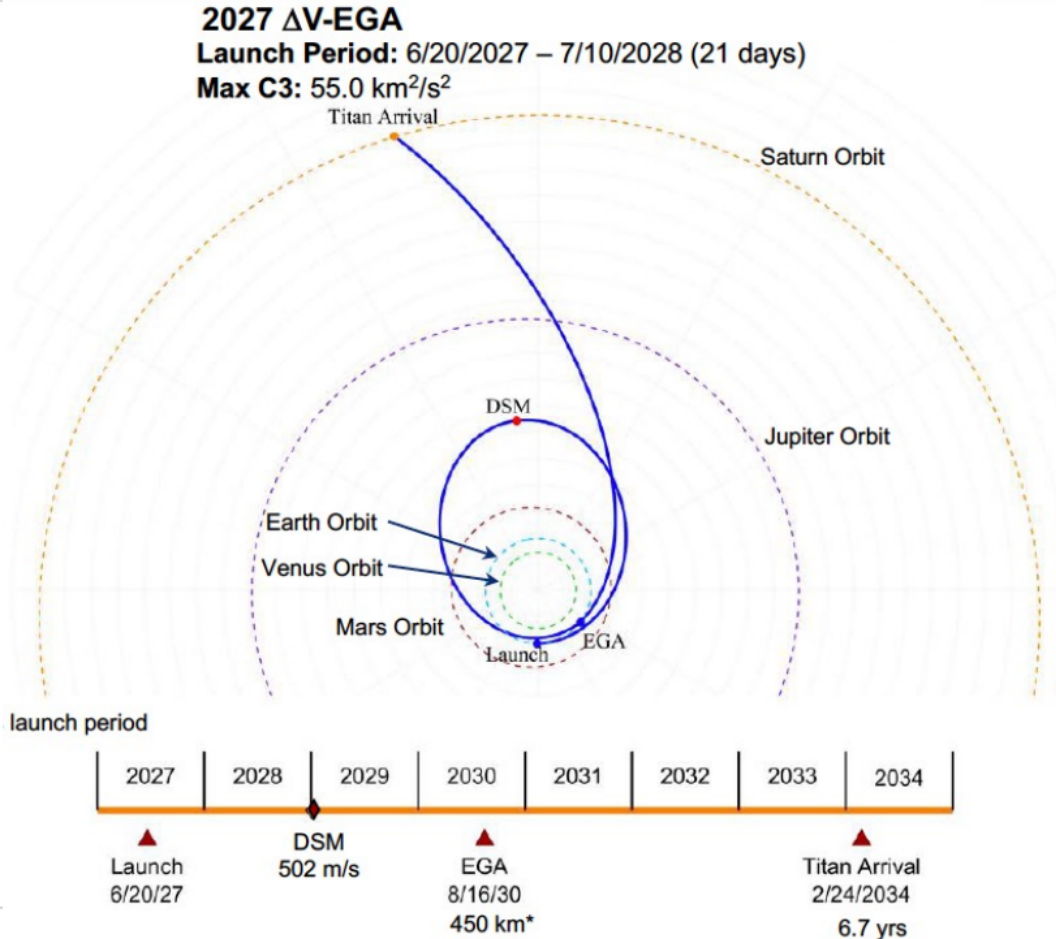


Figure 2.2: Proposed Orbital Mechanics trajectory for Dragonfly [10].

*DSM: Deep Space Maneuver (Use of rocket engines to change course towards Earth flyby).
 *EGA: Earth Gravity Assist (Passing behind Earth at a low altitude will slingshot spacecraft).

Figure 2.2 still labels a 2027 launch, however, as mentioned in the Phase B Mission Design, the same trajectory will be attempted one year later in 2028, adjusting for Titan's new position [12]. The next updated orbital trajectory information is due to be released in the December C.D.R. However, the space vehicle's Entry, Descent and Landing (E.D.L) has aimed to be consistent across these new time frames, as they will all have a high energy entry.

It has been established that; the results of this feasibility study will directly influence the course of Dragonfly testing at UQ and can be used to aid informed decision making by the stakeholders before Dragonfly entry.

The relevant planetary entry principles will be reviewed to aid understanding of how, atmospheric chemical changes dictate the thermal management environment.

2.3 Understanding Hypersonic Temperatures

This section is dedicated to background information towards the concepts of temperature at an atomic and quantum level. This brief review will be focused on the concepts of; how different modes of atomic temperature interact as a gas at hypersonic speeds, which is vital for this project's engineering decision making.

Temperature by itself does not exist, it is the average energy of an atom or molecule [13]. The energy associated with gases that are splitting apart (dissociation) and recombining into other molecules, occurs via probability at the statistical thermodynamic level.

Figure 2.3 depicts the four quantum energy modes in increasing order; translation, rotation, vibration and electronic. Each state also has smaller sub-levels before energy is stored in a different mode.

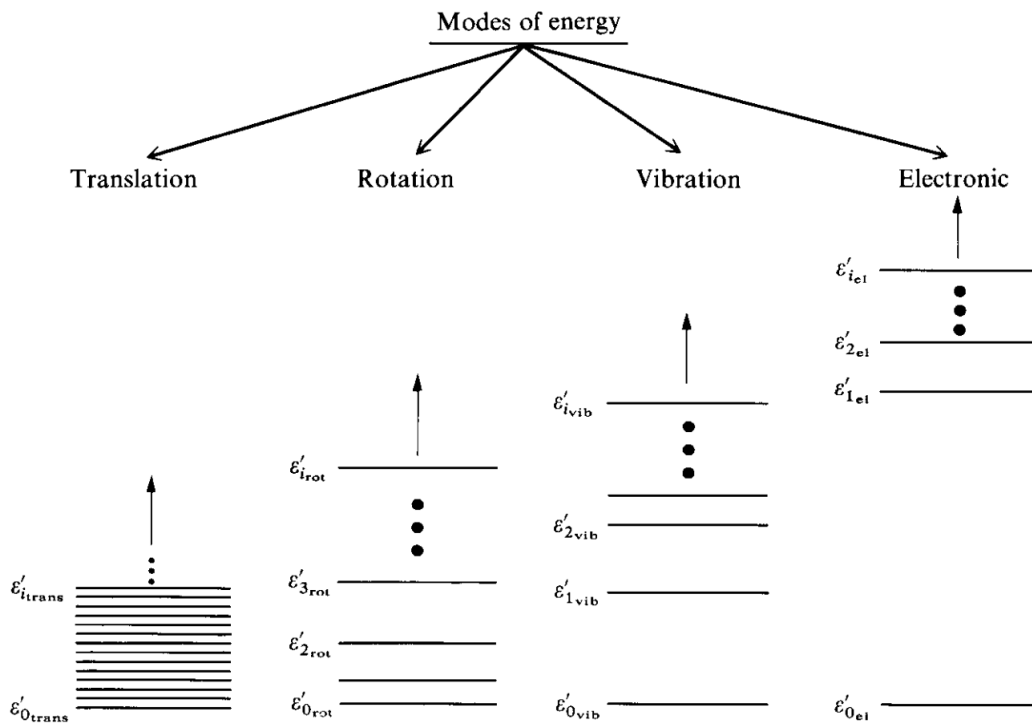


Figure 2.3: Four atomic temperature modes depicted from lowest to highest energy levels [13]

Note that all atoms above absolute zero only have translational and electronic energy, whereas, every molecule can have all four energy modes. This is due to the nature of a single atom for example Nitrogen (N), which can not have a rotational or vibrational energy, as they can only occur in molecules (more than one atom eg. N₂).

Therefore, it is crucial to incorporate how these energy states change as gases change from atomic to molecular forms and vice-versa in an ever changing post-shock environment [13].

For a diatomic molecule like N₂, H₂, CO, CN - Figure 2.4a shows the ‘dumbbell’ model of molecular arrangement. An illustration of translational and rotational energy can be seen for the diatomic molecule about the axis of movement and rotation in subfigures b & c. This also aids the understanding that a single atom doesn’t have a rotational axis to have a rotational energy [13].

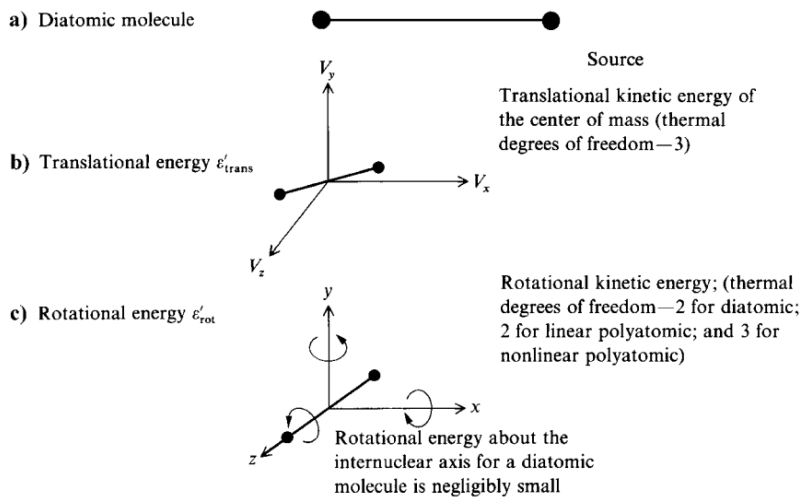


Figure 2.4: Two atom molecule, translational and rotational energy movements [13]

The depiction of a triatomic molecule of H₂O is seen in Figure 2.5, which is similar to the structure of CO₂. Therefore the vibrational and electronic energy trend emerges for Methane (CH₄) and every other molecule with more degrees of freedom to move.

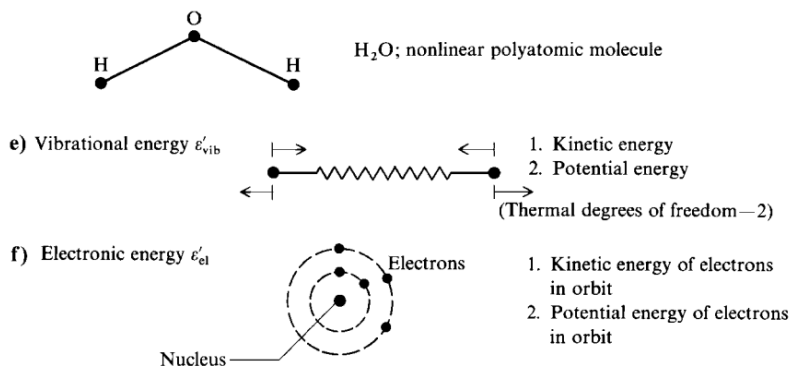


Figure 2.5: Triatomic molecule H₂O with vibrational and electronic energy movement. [13]

2.4 Atmospheric Entry Heating Thermodynamics

Atmospheric entry is a critical phase for any spacecraft, presenting numerous engineering challenges due to the extreme thermal and aerodynamic conditions encountered. This process involves a spacecraft entering a planet's atmosphere from space at over 30,000 kilometres per hour, which leads to intense heating and aerodynamic stresses. The design and analysis of entry vehicles requires a deep understanding of the physical phenomena involved, including the interactions between the vehicle's surface and the atmospheric gases, the generation of shock waves, and the heat transfer mechanisms [14].

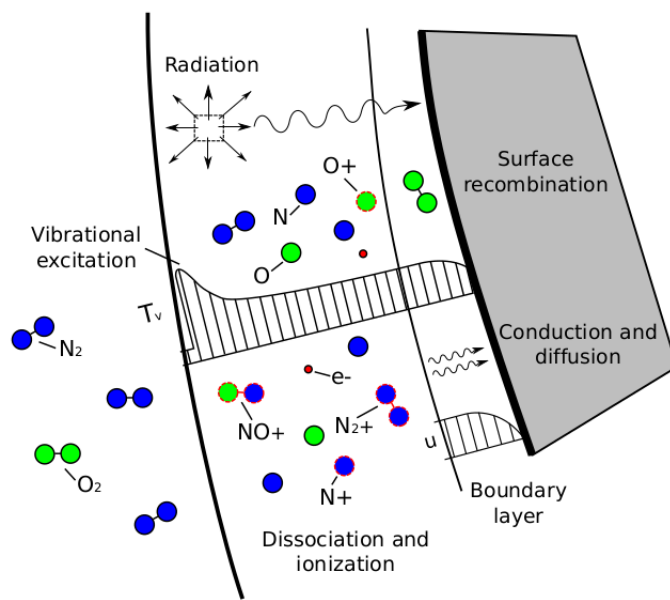


Figure 2.6: Atmospheric thermochemical interactions at vehicle surface [15].

The introduction to atmospheric entry effects will firstly begin with Earth, considering the similarity with our atmosphere having 78% Nitrogen, compared to Titan's 98%. During low Earth orbit entry, spacecraft can be exposed to temperatures exceeding 2,500°C for over 10 minutes [16]. These high temperatures are primarily due to convective heating on the heat shield side of the vehicle, however, radiative heating can occur at faster speeds from the Moon and Mars (Equations 2.1 & 2.2) [16]. The entry trajectory and velocity play significant roles in determining the peak heating rates, but the chemical composition and density of the atmosphere are also crucial factors [14].

Some important parameters to obtain for entry analysis are the type of vehicle trajectory, the altitudes of peak heating, peak deceleration, entry interface and the expected effects of High Temperature Gas Dynamics (HTGD). The vehicle effects from Earth entry are the most

understood to date, so our background of atmospheric interactions will start here. There are three main trajectories that are employed by an entering vehicle; ballistic, skip or equilibrium glide [17]. The first of which, the ballistic entry, is the entry method of the Dragonfly mission [1]. A ballistic entry profile is defined as, the aerodynamic forces provide only a drag force parallel to the direction of descent with no lift force generated (Figure 2.7).

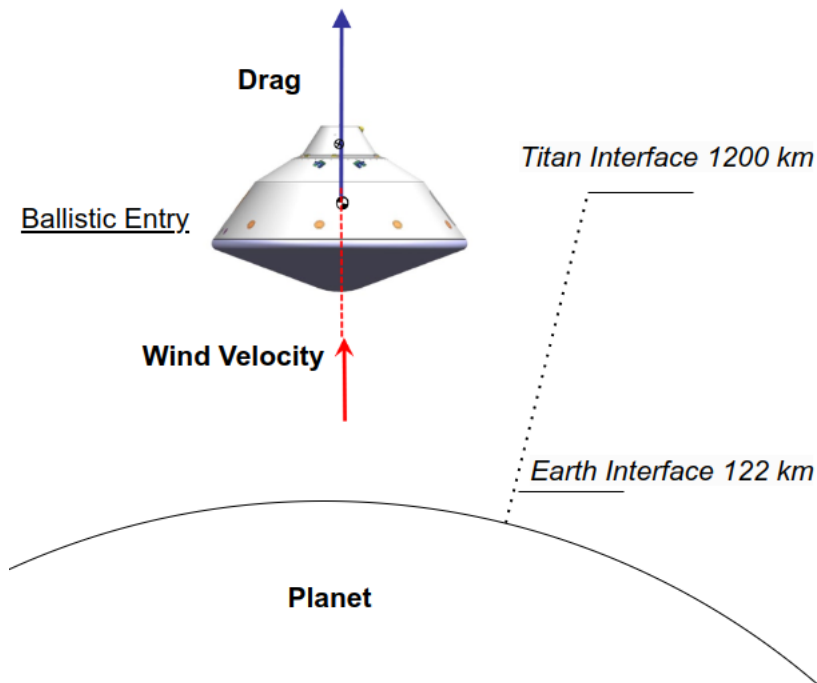


Figure 2.7: Ballistic entry orientation for Dragonfly Mission [18].

Figure 2.7 also depicts the atmospheric interface altitude of Earth and Titan. This is noted as the altitude at which the atmospheric density is substantial enough to have an effect on drag and heating on the vehicle [18]. The entry interface for Earth is 122 km, whereas Titan is nearly ten times higher at over 1200 km [17]. This ten fold difference in atmospheric height is the primary reason as to the vast uncertainty in radiative entry heating upon the two hour EDL phase [8].

Now is an opportunity to further introduce some of the heat flux correlations for Earth entry that was published by the NASA Advisor, Dr. Aaron Brandis for vehicles up to 10 m nose radius [19]. Notice in the following equations that, the radiative heat flux correlation for Earth below 9.5 km/s is regarded as insignificant [19].

With respect to Equation 2.1 and 2.2, \dot{q}_c is convective heat flux, ρ_∞ is freestream density, R_n is nose radius of the capsule, U_∞ is freestream velocity, \dot{q}_{rad} is radiative heat flux, C, a, b and $f(U_\infty)$ represent a complex formula which can be obtained from the original paper [19].

Earth - Convective Heat flux, from $3 \text{ km/s} \leq U_\infty \leq 9.5 \text{ km/s}$

$$\dot{q}_c = 7.455 \times 10^{-9} \rho_\infty^{0.4705} R_n^{-0.52} U_\infty^{3.089} \quad (2.1)$$

Earth - Radiative heat flux ($\geq 9.5 \text{ km/s}$ and altitudes $\geq 38.5 \text{ km}$ Alt $\leq 83.5 \text{ km}$)

$$\dot{q}_{rad} = C R_n^a \rho_\infty^b f(U_\infty) \quad (2.2)$$

While noting these correlations are functions of density, vehicle nose radius and velocity. Although useful for understanding the coupling and impact of convection and radiation, these functions are only useful for air on Earth, therefore new correlations need to be designed for Titan. This is why lengthy and computationally expensive simulations are required for Titan entry heating, as no accurate correlations exist yet. Titan EDL phase has been estimated at over two hours [12] compared to an Earth re-entry between 5-20 minutes and Mars' 7 minutes [17].

Since Titan has over 1270 km of atmosphere to negotiate, as well as Methane concentrations of 0.5 % - 5.5 % throughout the EDL phase, correlations of convective and radiative heating may never occur, hence the need for an in-depth analysis of entry conditions in Chapter 4.

The notion of disregarding radiative heat flux for thin atmospheres & low velocities is a common practice, however, this has proven to be reckless after processing thermal data from real missions [16]. Hence why most missions are now trying to understand both impacts of convective and radiative heating loads across the front and back of the vehicle [19, 20].

Mars entry presents its own set of challenges due to its different atmosphere. The Martian atmosphere is 100 times thinner than Earth's, leading to different aerothermal environments. Due to the 96% Carbon Dioxide composition, peak heating during Mars entry may last only about two minutes, but the vehicles must still be designed to withstand the intense heat fluxes over this period of time [16].

2.5 Previous Titan Entry Radiative Inconsistencies

The entry conditions of Titan are even more unique for two main reasons. It is not only the only moon with a substantial atmosphere, it is also has the highest concentrations of atmospheric and surface liquid methane [20].

Titan's atmosphere is similar to Earth's in terms of nitrogen content but differs significantly in its methane concentration. Near the surface, methane concentrations are approximately 5.5%, decreasing to around 1.5% in the stratosphere [21]. The atmosphere also features a temperature inversion layer and a dense haze layer, impacting visibility and thermal properties during entry. These properties make the atmosphere denser and more complex compared to other planetary atmospheres, influencing the heating experienced during entry.

The Huygens probe, which landed on Titan in 2005, is the only spacecraft to have successfully entered and landed [3]. The probe's entry and descent provided valuable data, but further experimental testing is required to understand the chemical changes that occur upon entry, especially regarding the dissociation and recombination of nitrogen and methane.

Table 2.2: Titan and Earth properties [22].

Parameter	Titan	Earth
Mass	1.345×10^{23} kg	2.2% of Earth's
Diameter	5150 km	12742 km
Scale height	40 km	8.4 km
Entry Interface	1270 km	122 km
Distance from Saturn	1 221 870 km	-
Distance from Sun	1 427 000 000 km	148 670 00 km
Surface temperature	94 K	288 K
Atmosphere Density	5.4 kg/m ³	1.2 kg/m ³
Atmospheric pressure at surface	150 kPa	101.35 kPa
Atmospheric composition	98% N ₂ , 2% CH ₄	79% N ₂ , 21% O ₂
Orbital period	15.95 days	1 day

Radiative heating on Titan is predominantly due to ultraviolet emissions from nitrogen and methane species, especially from the Cyanogen radical (CN) formed during the dissociation of methane and nitrogen molecules [22]. Non-Boltzmann radiation effects, particularly from CN Violet and Red bands, contribute significantly to the radiative heat flux. CN violet appears to produce most of the heating on the forebody and CN red on the backshell [23].

2.5.1 Hypersonic Radiation Simulation Codes

Accurate prediction of heating rates requires sophisticated computational models that account for thermochemical non-equilibrium states and non-Boltzmann radiation effects. NASA uses two computer codes in this instance, DPLR (Data Parallel Line Relaxation) which solves the reacting Navier-Stokes equations for fluids in thermochemical non-equilibrium using finite-volume discretization [24].

NEQAIR (Non Equilibrium Air Radiation) program computes the radiation processes like emission and absorption along a line of sight due to transitions in energy states. Both are key tools for predicting fluid and radiative behaviour during atmospheric reentry [24, 25]. Experimental comparison with computer models, such as shock tube experiments, is essential to ensure their predictive accuracy for informed engineering design.

In 2017 Dr. Brandis performed computational and experimental tests at NASA's Electric Arc Shock Tube (EAST) facility to compare his previous CN Titan results obtained in 2010 at UQ X2 [25]. Very interesting discrepancies were found when comparing the two facilities. Figure 2.8 illustrates the NASA computer code expectations and EAST Test 61 circled in red. However, the UQ results are circled in blue with minimal radiation detected at the 360 - 440 nm bandwidth.

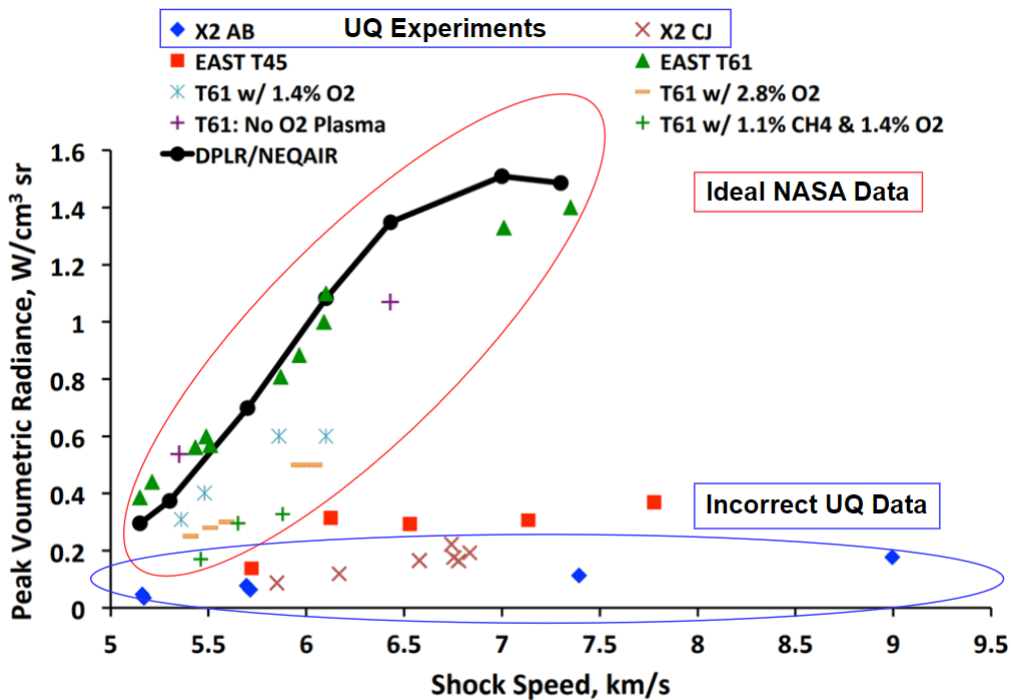


Figure 2.8: Comparison of Radiation from CN in simulations & experiments [24].

This was deemed to occur from accidental atmospheric Oxygen contamination into X2, causing C atoms to bind with O₂ instead of N, which reduced the CN molecule concentration, that DPLR, NEQAIR and EAST T61 expected [24 ,35]

These initial studies performed by Dr. Brandis and other UQ staff paved the way for feasibility for the Dragonfly mission to Titan. These findings necessitated a re-evaluation of the existing data and models [24].

To further display the need to revisit the previous UQ X2 Titan entry experimentation arises from a recent 2024 study from Oxford University [26]. The T6 hypersonic tunnel was used to validate if the NASA models or UQ models were more accurately predict Dragonfly radiative heating (Figure 2.9).

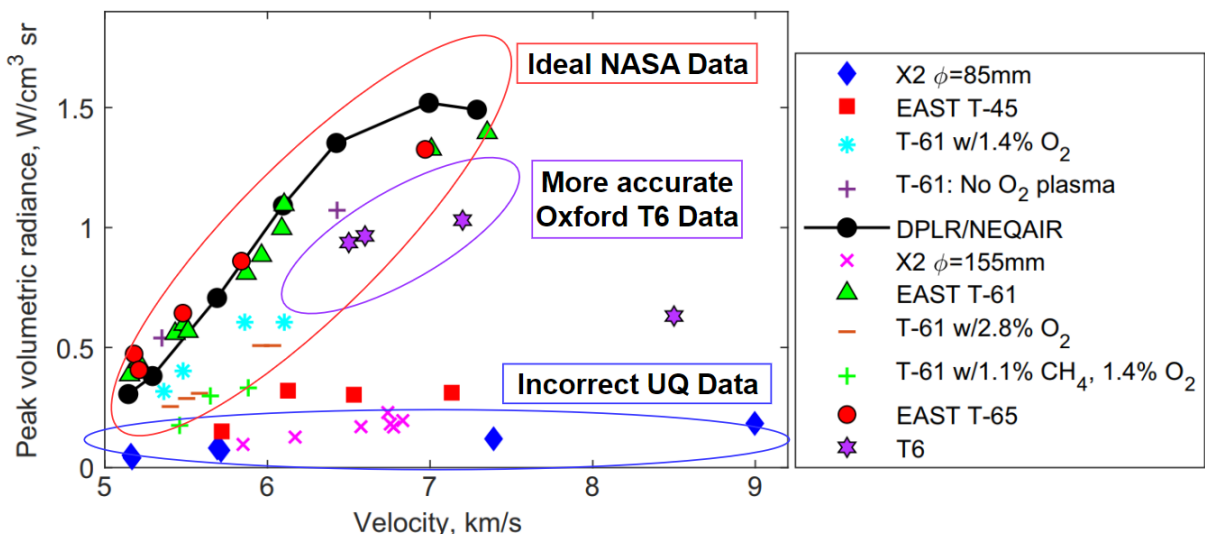


Figure 2.9: Comparison of new 2024 Oxford CN results between facilities [26].

These recent Oxford findings concluded that the results match the NASA code and NASA experiments more closely than the UQ experiments, hence reiterating the need to improve the UQ X2 Titan entry experimental results. Therefore, with the Dragonfly mission in production, this is the perfect time to invest in UQ X2 Titan experimentation to ensure that each simulation and experiment are closely aligned.

The lessons learnt from these validation experiments suggest that the NASA DPLR and NEQAIR codes can accurately predict radiative heating for Titan entry and should be used when developing experimental models. Although due to the restrictions imposed on accessing NASA codes, UQ has developed their own simulation codes which will be improved on in the future works of this thesis. Further display of NASA computer simulations in this thesis will use these programs to reduce errors in replicating their gold standard data.

2.6 Current Dragonfly Mission Radiative Inconsistencies

Titan's atmosphere, composed primarily of nitrogen (98%) and methane (2%), affecting both convective and radiative heating during entry [27]. Studies have also been attempted with up to 5% methane as there is a higher concentration under 160 km due to the methane weather cycle on Titan. However, the highest heat flux occurs around 250 km in altitude, due to the high speeds (5.7 km/s). Trace Argon and Hydrogen is present, they are removed and included a higher methane percentage for simplicity and CN production [7].

Convective heating, was found to produce a peak heat flux at the forebody stagnation point of around 145 W/cm^2 [22]. However, with the addition of radiative heat flux, this number is closer to 291 W/cm^2 (Figure 4.1).

Radiative heating, particularly from CN Violet and CN Red bands, was identified as a significant contributor to the thermal loads on the entry vehicle's afterbody. Experimental measurements from the EAST facility showed variations in shock-layer radiation from CN Violet & CN Red, with discrepancies between predicted and measured values ranging from -50% to +200% depending on velocity and fill pressure [27]. A simulation from NASA of CN Red of Dragonfly aft shoulder is depicted in Figure 2.10, noting the high concentration of CN red across the shoulders [7].

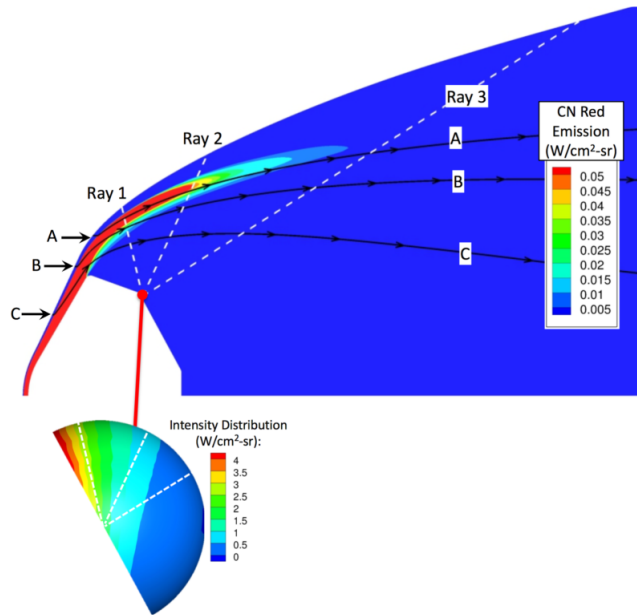


Figure 2.10: Cyanogen radical CFD Results from Johnson, West & Brandis simulations [7].

The Cyanogen species reaches far further around the near and aft shoulders, as most entry cases are only focusing on forebody stagnation results. However, significant thermal protection is required on the shoulders and backshell of Titan entry, than Mars entry [22].

The changes in chemistry reaction schemes have impacted the radiative heating predictions by up to 20% near peak heating and up to 50% later in the trajectory [7]. Further analysis of the radiative and convective heat flux on the shoulders in Figure 2.11 showed that over 90% of the radiative flux reaching the shoulder surface originates from the near-shock flow, which remains in non-equilibrium beyond the initial shock region [7].

Figure 2.11 displays the radiative heating trends on the shoulders of the Dragonfly vehicle upon the simulated entry, with the timescale in Table 2.3, as the vehicle slows from 7.3 km/s (160 s) on entry to approximately 5 km/s (241 s) depicting maximum radiative heating.

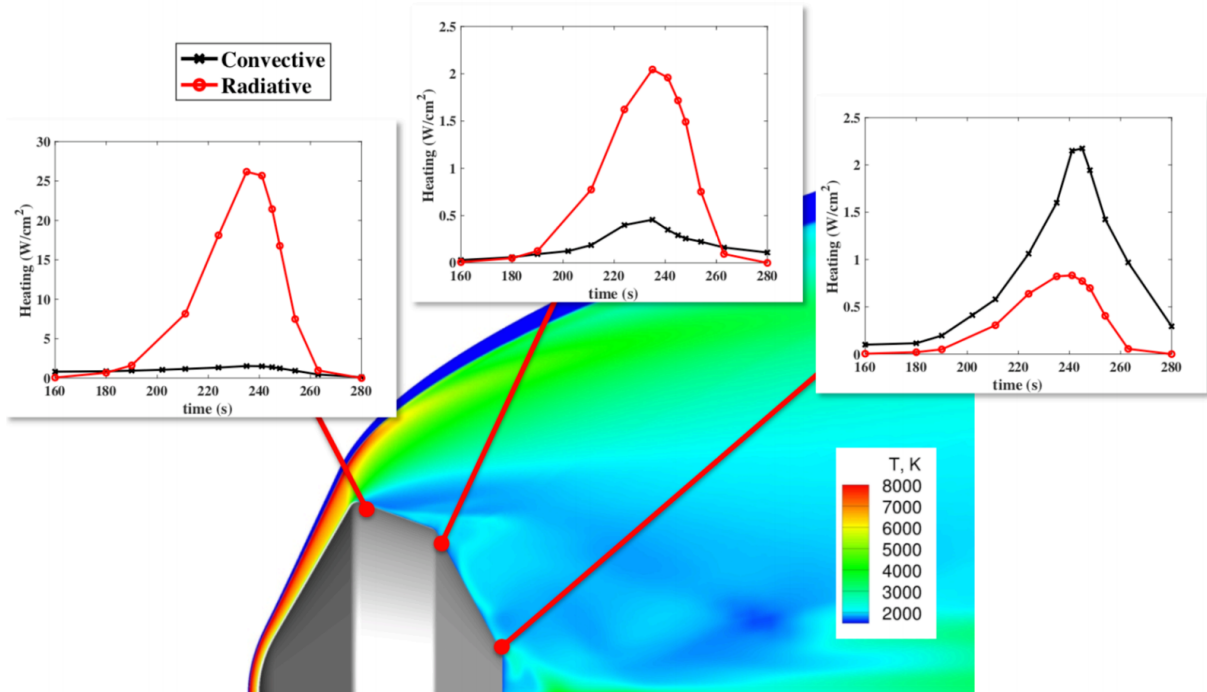


Figure 2.11: Convective & Radiative heat flux from Johnson, West& Brandis [7].

This is extremely important to mention, since with Dr. Brandis' Earth radiation correlation (Equation 2.2), radiative heating was neglected below 9.5 km/s. These two simulations from Johnson, West & Brandis indicate the importance for experimental testing and the development of surface radiation measurements from through-model spectroscopy. It can be seen the nature of how forebody shoulder radiation effects the dissociation reactions on Titan entry. The literature review will now shift towards how to accurately create a scale model in the X2 facility to replicate the chemical changes discussed in the literature review.

2.7 Instrumentation of NASA Dragonfly Entry Capsule

The NASA Dragonfly entry capsule will be instrumented with a wide array of sensors and equipment to gather data upon entry. This experimental suite is termed as Dragonfly Entry Aerosciences Measurements (DrEAM). DrEAM is made up of four main instrument systems, which record a variety of atmospheric entry data [23]. This thesis will focus on the location and role of the COmbined Sensor System for Titan Atmosphere (COSSTA). COSSTA is made up of backshell sensors for radiative & total heat flux and pressure. The main focus is to understand radiative heating from CN and vehicle dynamics upon entry into Titan.

Figure 2.12 depicts the locations of the COSSTA sensors. Sensors labelled C1, C2 and C3 are the heat flux and pressure sensors, whereas the radiometer is coloured blue. It can be noted that the sensors are located on the junction of the aft-shoulder and near backshell of the entry capsule [23]. These sensor locations are in line with the proposed measurement locations being investigated.

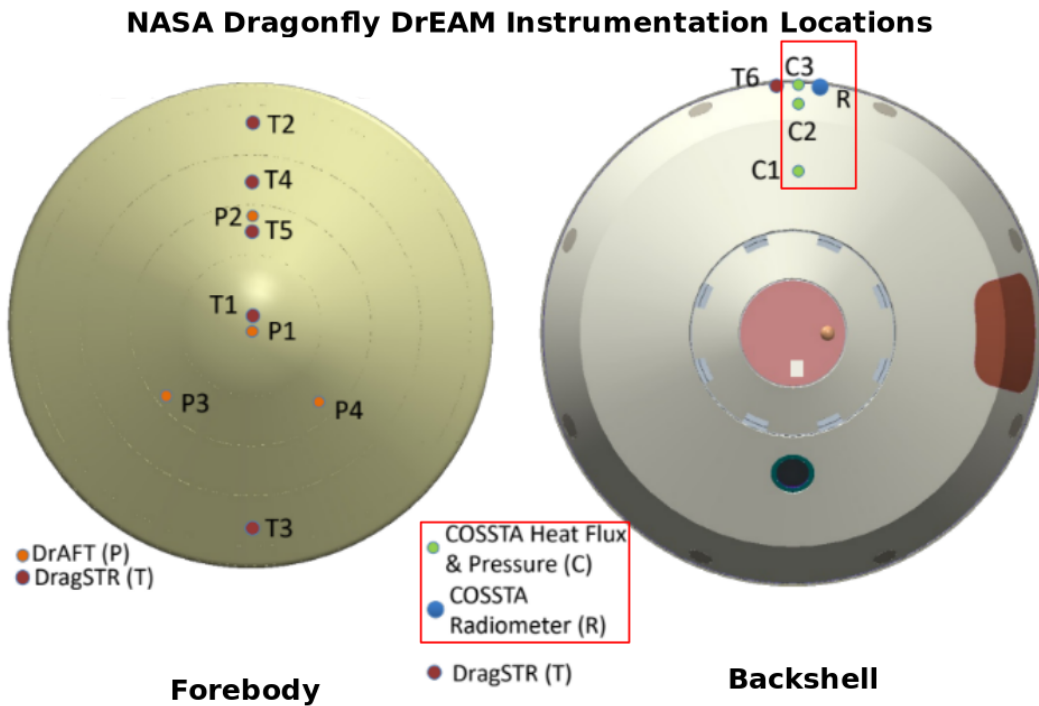


Figure 2.12: DrEAM sensor locations on the Forebody and Backshell of Dragonfly [23].

Deutsches zentrum für Luft und Raumfahrt (DLR) is the German Aerospace Centre in charge of developing the DrEAM sensors. Although the University of Queensland will not be using the same level of sensors, alternative sensors can be supplied which will fit the specific wavelength for CN radicals for this thesis.

2.8 Capsule Scaling Methods for Experimental Testing

The development of scale models for experimental testing is crucial for understanding the thermal and chemical phenomena during planetary entry. However, accurately scaling down a model involves more than just reducing its size; the thermal and chemical properties must also be accurately replicated [13]. This is particularly important for studying the radiative heat flux, which can be a significant component of the total heat load on the vehicle.

The design of entry vehicles has evolved over time, with each mission providing new insights and challenges. From the blunt-body design of the Apollo capsules to the more recent aerodynamic shapes of Mars rovers' aeroshells, engineers have continuously adapted their designs to meet the specific requirements of each mission [5]. The ongoing research and development in this field aim to enhance our understanding of atmospheric entry phenomena and improve the safety and efficiency of future missions.

For scaling, it is important to match the enthalpy (flow energy) of the flight environment, in order to reliably reproduce the matching conditions within the hypersonic wind tunnel.

The proposed entry trajectory throughout the Titan atmosphere for the Dragonfly landing sequence is detailed Table 2.3

Table 2.3: Titan Entry Velocity, Density, and Temperature over Time [7].

Time (s)	Velocity (m/s)	Density (kg/m ³)	Temperature (K)
160	7330	4.40E-06	162
180	7290	1.94E-05	162
190	7240	3.89E-05	162
202	7100	8.74E-05	162
211	6890	1.58E-04	162
224	6350	3.56E-04	162
235	5590	6.64E-04	162
241	5070	9.02E-04	162
245	4700	1.09E-03	162
248	4420	1.24E-03	162
254	3850	1.57E-03	162
263	3080	2.12E-03	160
280	1940	3.26E-03	158

Dr. C James has already successfully created numerous scaled capsule designs. An Apollo forebody section was created and tested in the same impulse facility this project intends to design for (Figure 2.13) [5].

This model was a 40:1 scale and machined from mild steel, however, Figure 2.1 depicts a fixed 28° Angle of Attack (AoA), whereby Dragonfly is 0° due to the ballistic entry style [1].

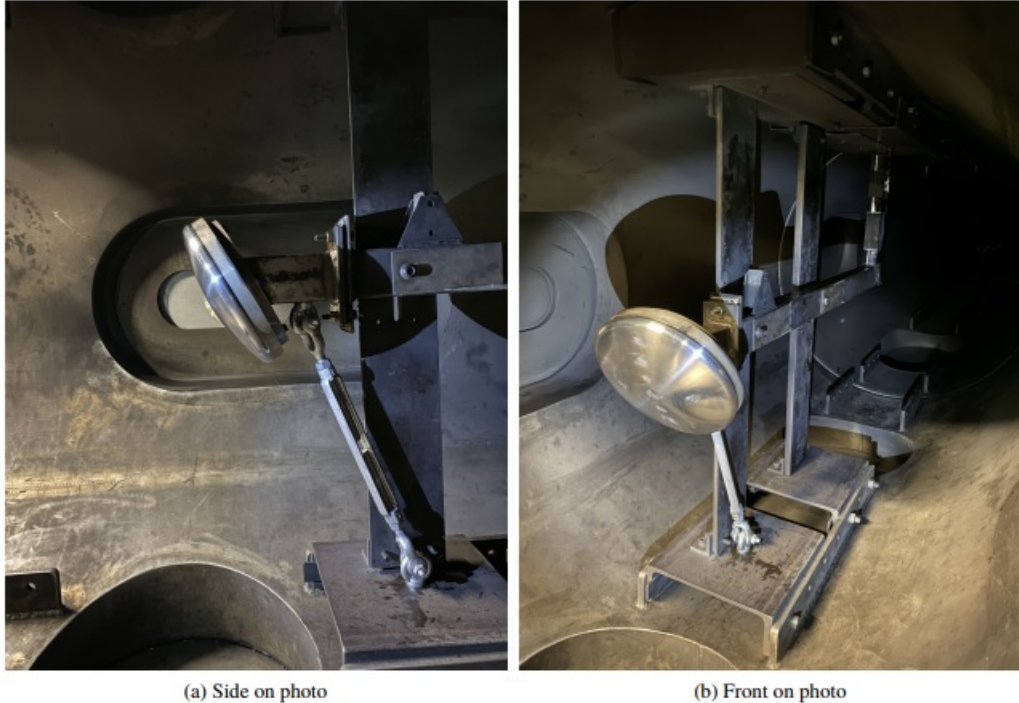


Figure 2.13: Manufactured Apollo 11 test model mounted in X3 Test section in Brisbane by Industry Advisors [5].

The aim of this study was to replicate findings of other institutions such as the NASA Ames Research Centre. Since the X3 impulse tunnel can be used in either expansion or reflected shock mode (X3R), this paper is suitable for investigation due to the close proximity of this thesis.

2.9 Optic Fibre Through-Model Radiation Testing

Conventional radiation measurements in hypersonic wind tunnel testing are taken external the vehicle (radiometers), or using external spectroscopy to record the wavelengths of radiation along the electromagnetic spectrum.

Recent experimental investigations at the X2 expansion tube, are focusing on implementing optical fibres ‘through’ the supporting sting, into the model and mounted flush with the forebody surface. Figure 2.14 depicts the experimental set up of a Stardust capsule (previous NASA mission) in X2.

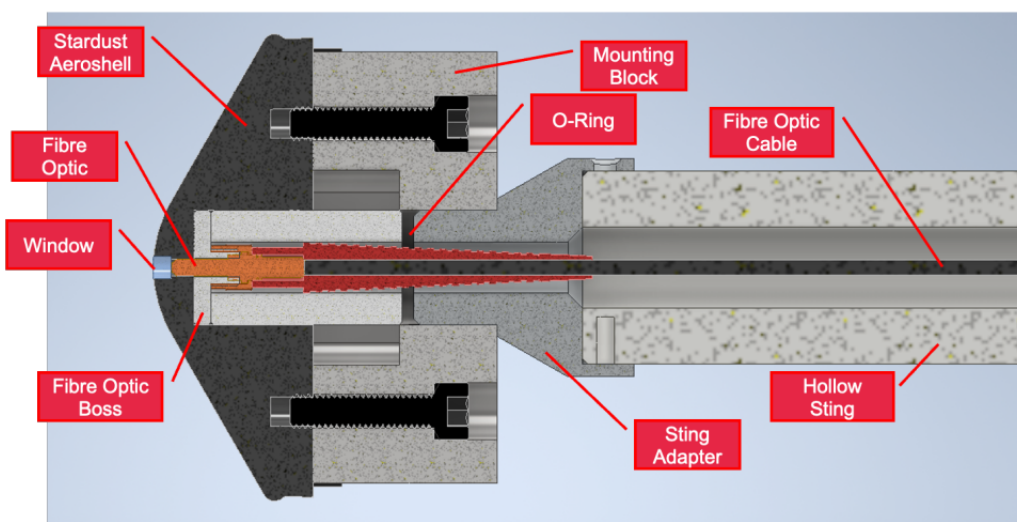


Figure 2.14: Stagnation point through-model CAD of Stardust capsule in X2 [35].

Most notably is the axial mounted sting with the optic fibre remaining ‘unbent’ and passing straight through the model, terminating at the stagnation point of the capsule. The optic fibre is also protected at the surface of the model with a sapphire window. This small (0.25 mm) window is required to ensure that no obstruction to the electromagnetic spectrum through testing, while protecting the fibre itself.

Further testing of through-model spectroscopy UQ involve the Japanese Hayabusa capsule, also involving a straight optic fibre on the forebody stagnation region. This information was presented by Dr. Chris James (Industry Advisor) in September 2024 at the "Radiation of High Temperature Gas" presentation at Oxford University, managed by the European Space Agency [29] . This research by H Subra, R Hawken, C James, M Uren, Y Liu, R Allison, S Lock, awaiting publication, successfully performed optic fibre through-model radiation measurement with a 45 degree sphere cone forebody.

These preliminary results at 18 km/s validate the through-model apparatus. The radiation measurement performed as expected from Alpha-Hydrogen, which peaked at the 656 nm wavelength. The CN radiation is at the 380 nm wavelength which also fits between the sensitivity range of the optic fibres used in this validation test of 250 nm - 1200 nm [29]. As the model and sting designs need to be suitable to fit inside the coreflow of the X2 test section (Figure 2.15).



Figure 2.15: Forebody inside the test section area of X2 Tunnel at UQ [35].

Based from previous and current X2 experiments, it was deemed suitable and the requirement for the model to be completely covered by the hypersonic flow, that a 80 mm - 100 mm scale model should be suitable for CN investigation.

2.10 Chapter Summary

This chapter provided background information for planetary entry with an overview of the Dragonfly mission. A deep insight into the need and importance of the research proposal with various references to previous NASA studies and discrepancies with previous UQ Titan testing. The measurement suite proposed by NASA Ames was introduced followed by the validation of UQ experimentation which can be directly modified to investigate the gaps in the knowledge on radiative Titan entry. A screening of suitable scale model designs and sting frameworks will be created and tested in the following chapters.

Chapter 3

Design Methodology

"Life is pretty simple: You do some stuff. Most fails. Some works. Do more of what works."

— Earl Nightingale

3.1 Chapter Introduction

To investigate the radiative heating on the Dragonfly capsule, a suitable scale model and supporting framework needs to be designed for future experimental testing in X2. Since the current Dragonfly capsule geometry is confidential, the NASA supervisor Dr. Brandis, and supporting literature advised to replicate the geometry of the 60° sphere cone; Genesis S.R.C, which returned to Earth in 2004.

Firstly, the Genesis S.R.C with it's 1.52 m diameter which was depicted in Figure 1.4, will be recreated initially.

Next, an axisymmetric scaled up version of the Genesis S.R.C to the proposed 4.5 m diameter of the Dragonfly capsule. This scaled up iteration will be compared to the publicly available Dragonfly capsule, any design differences will be identified. The design focus will then shift towards the supporting framework required for a scaled down capsule, which will be the most effective inside the X2 Expansion tube.

This chapter will investigate a variety of "stings" which will support the model in the hypersonic wind tunnel test section. Each sting design needs to physically fit inside the test section of X2, to accommodate for the optic fibres which will capture radiation bandwidth data, and to replicate the hypersonic entry effects of Titan's atmosphere.

Chapter three will then conclude with four proposed sting designs, which will be computationally modelled in Chapter four to find an optimal sting design.

3.2 Capsule Replication

As the Dragonfly capsule is still under construction and the exact capsule dimensions are classified information between NASA and Lockheed Martin, it was advised to scale another specific capsule with more publicly available information.

3.2.1 Genesis Capsule Replication

Firstly, the Genesis S.R.C needs to be replicated to a 1:1 scale of the 1.52 m diameter in order to progress towards the Dragonfly model. Figure 3.1 displays the known Genesis dimensions depicted by Desai et al. 2008, in a study post Genesis return, therefore the details of the geometry can be publicly released [4].

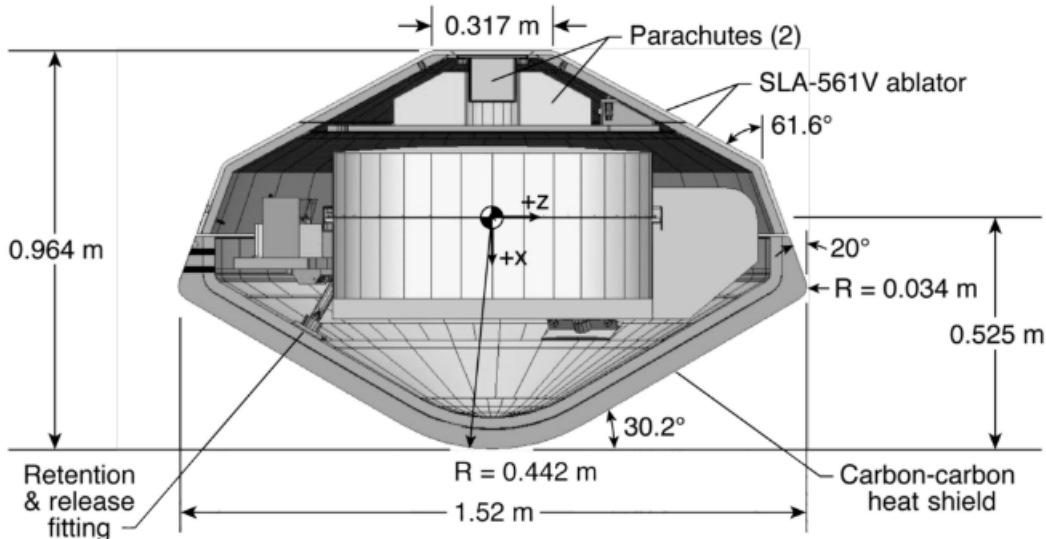


Figure 3.1: Schematic diagram of Genesis capsule [4].

The primary features of this image to note are the, 1.52 m diameter, 60° sphere cone angle ($90^\circ - 30^\circ = 60^\circ$) and nose radius of 0.442 m (Figure 3.1); these traits are the driving dimensions to replicate Genesis as a 3D model.

Since Dragonfly has changed diameters throughout the build phase, most of the research in the literature review was conducted on 2.9x scaled up Genesis capsules [7]. Therefore, it is vital to the future of the project to make an accurate replica of Genesis and infer the geometry to Dragonfly. It was established in the literature review that the initial size of Dragonfly was 3.75 m, although the final confirmed diameter is 4.5 m [20].

An accurate replication of Figure 3.1 was created using OnShape Computer Aided Design (CAD) with the identical dimensions and displayed in Figure 3.2.

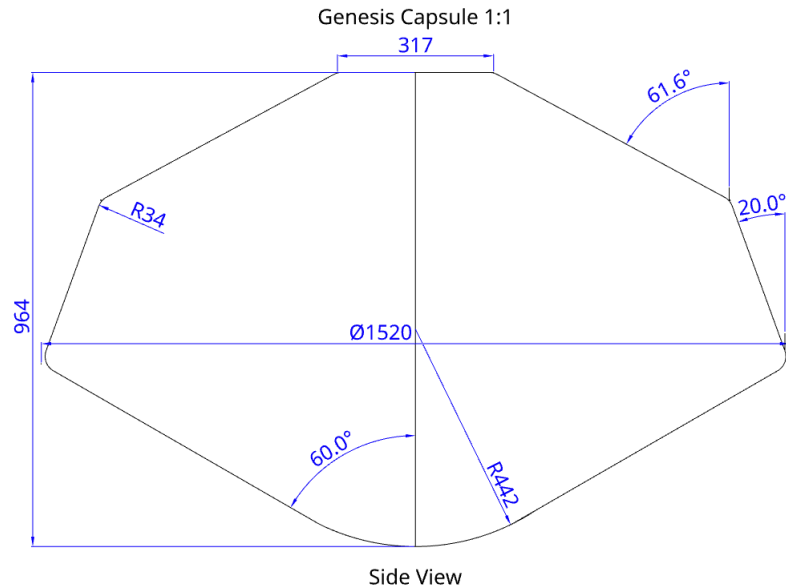


Figure 3.2: Schematic diagram recreation of Genesis capsule [4].

The replication process maintained the same external profile presented in the original work [4]. This is the most important step of this project, since in-depth dimensions of the Dragonfly capsule are not published, accurate replication of the Genesis model is paramount.

A 3D render of the Genesis geometry derived from the same dimensions is displayed in Figure 3.3 to exhibit the capsule's external profile.

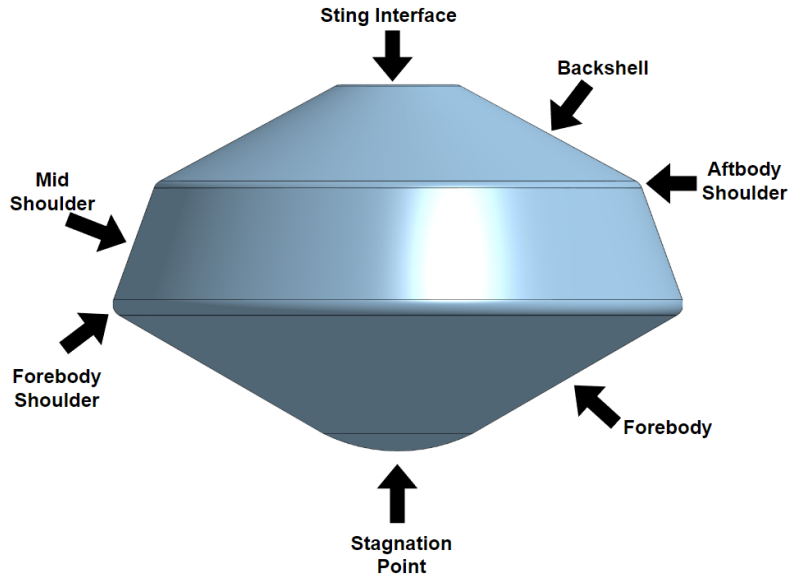


Figure 3.3: Render of Genesis capsule with naming conventions replicated from [4].

3.2.2 Dragonfly Capsule Geometry

The main driving conditions of the capsule include, a 60° sphere cone, now with a 4.5 m diameter and requires an approx $\approx 2.9x$ scaling factor, based on the recommendations from the NASA industry advisor and recent research in the literature review.

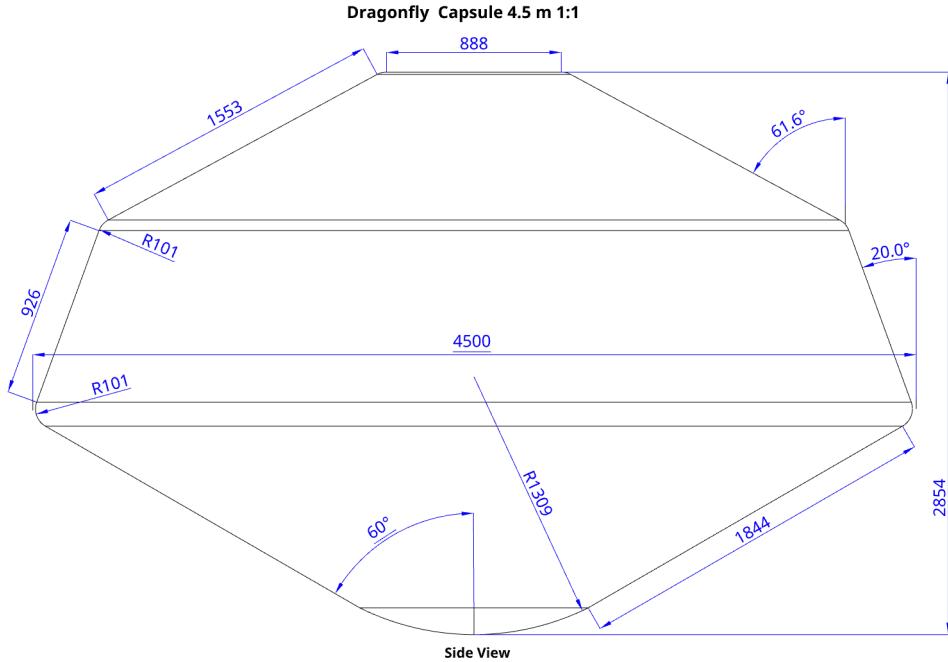


Figure 3.4: Schematic diagram of scaled up Dragonfly capsule at 4.5 m.

A summary of dimensions between Genesis at 1.52 m and the 4.5 m Dragonfly can be seen in Table 3.1. It was noted that uniform scaling occurred for most sections. After verifying scaling to the full size, the scaling down process for the X2 wind tunnel at UQ can begin.

Table 3.1: Comparison of Capsules with Scaling Factor.

Parameter	Genesis 1.52 m	Dragonfly 4.5 m	Scaling Factor
Diameter (mm)	1520	4500	2.96
Sphere Cone θ	60	60	-
Nose Radius (mm)	442	1309	2.96
Height (mm)	964	2854	2.96
Front Panel (mm)	623	1844	2.96
Shoulder Panel (mm)	313	926	2.96
Rear Panel (mm)	525	1553	2.96
Top Panel (mm)	317	888	2.80
Shoulder Radius (mm)	34	101	2.97

3.3 Initial Model Capsule Scaling for X2

After the Dragonfly 4.5 m dimensions were verified, the next phase in the design process is to estimate a scaled down capsule size which will fit into the X2 test section area coreflow, but still suitable to house the optic fibres for radiation measurement. Since the major design process is aimed towards the supporting framework of the test model, this is a necessary requirement.

It was initially estimated as a 80 mm - 100 mm diameter model will suffice to fit inside the testing area of the tunnel and physically house the optical fibres. The final model geometry will be re-examined in Chapter 4 & 5 after the sting design is finalised.

The diameter from 4.5 m to 100 mm, is a 45x reduction in size; and at 80 mm is 56x scaling size. The scaling of interplanetary entry to hypersonic wind tunnels is very complex to recreate the many physical and chemical effects. Therefore, the replication and experimental process is normally at PhD and company level. The methodology of "order of magnitude" accurate scaling will be investigated within the scope of this project.

Table 3.2: Comparison of Parameters with Scale Models Based on Genesis.

Parameter	Scale 80 mm	Scale 100 mm
Sphere Cone Angle	60°	60°
Nose Radius (mm)	23.26	29.07
Height (mm)	50.74	63.42
Front Panel (mm)	32.80	40.97
Shoulder Panel (mm)	16.48	20.59
Rear Panel (mm)	27.63	34.54
Top Panel (mm)	16.68	20.87
Shoulder Radius (mm)	1.79	2.24

Creating upper and lower boundary conditions for the final scaled model for experimental testing inside X2 is a crucial step. The optic fibres that will be inserted inside the model have a maximum bend radius, which must be adhered to. This will ensure adequate signal transmission into the spectroscopy unit for future projects.

The model and sting designs need to be suitable to fit inside the coreflow of the X2 test section (Figure 2.15).

A 90 mm model was designed in between the upper and lower boundary conditions which is a 1:50 scale for testing (Figure 3.5).

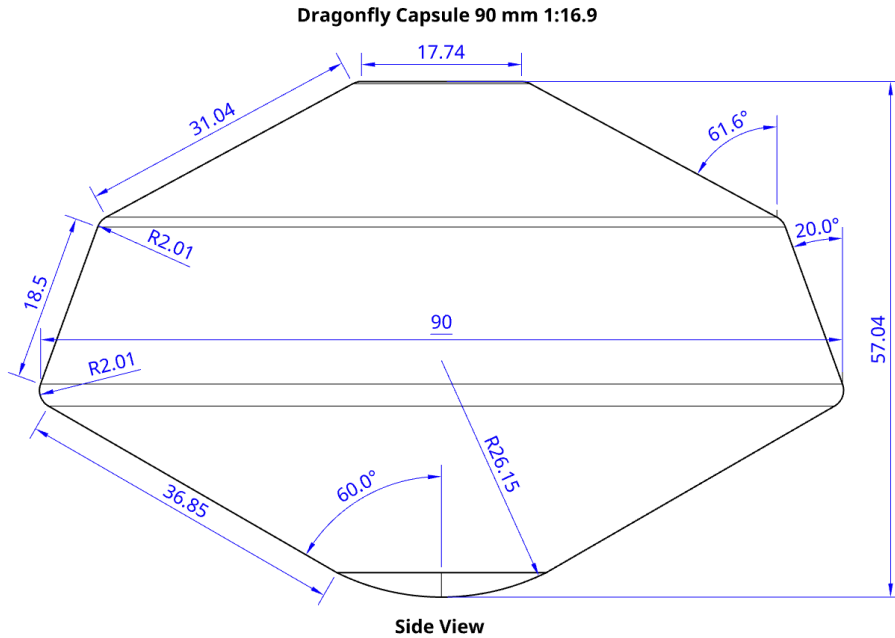


Figure 3.5: 1:50 scaled down version of the Dragonfly capsule to 90 mm.

It was noted that for accuracy a 1:16.9 scale of the original 1.5 m Genesis model (Figure 3.5) was used, rather than a 1:50 scale of 4.5 m Dragonfly. This was completed to reduce potential errors with scaling up and down using CAD software. This process marks another major milestone, as the initial size of the X2 geometry has been decided, and therefore the supporting sting framework can be investigated.

3.4 Current Through-model Experimentation at UQ

The University of Queensland has procured the appropriate optic fibre sensors in order to detect CN in Titan's atmosphere. The optic fibres are currently being tested on another project involving Earth re-entry from a Hayabusa 2 scale model which landed in 2020, however, will be available for this project in parallel [29].

The current stagnation model set up for through-model experimentation which was discussed in Section 2.9 of the literature review is displayed in Figure 3.6 & Figure 3.7.

Moreover, the most important value to determine the most appropriate capsule and sting design is the optic fibre bend radius. Table 3.3 displays the optic fibre parameters with a maximum long term bend radius of 106 mm, this determines that at any point within the sting and model, the fibre should aim to be bent no more than this value. This fibre was used at the single stagnation point in figure Figure 3.7 & Figure 3.8.

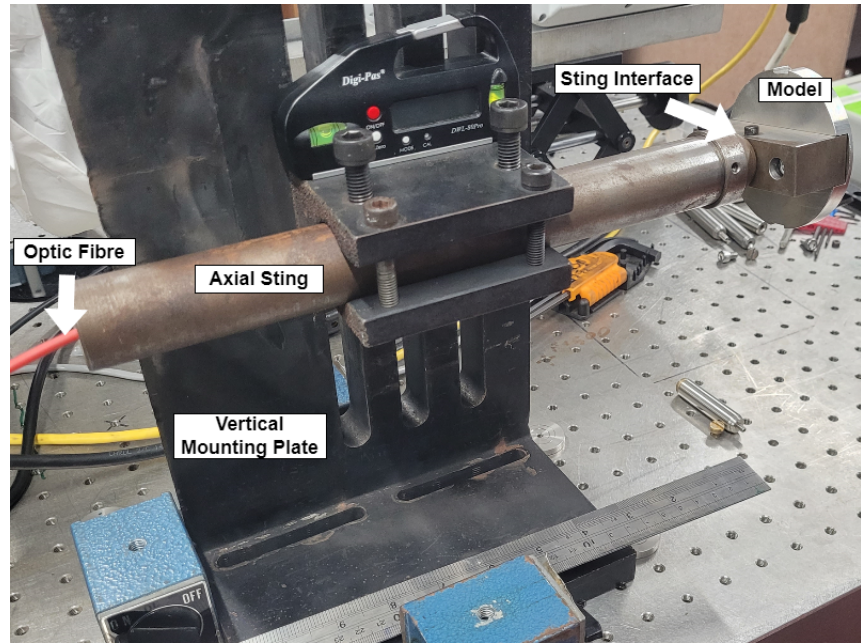


Figure 3.6: Isometric view of current X2 stagnation point through-model assessment [29].

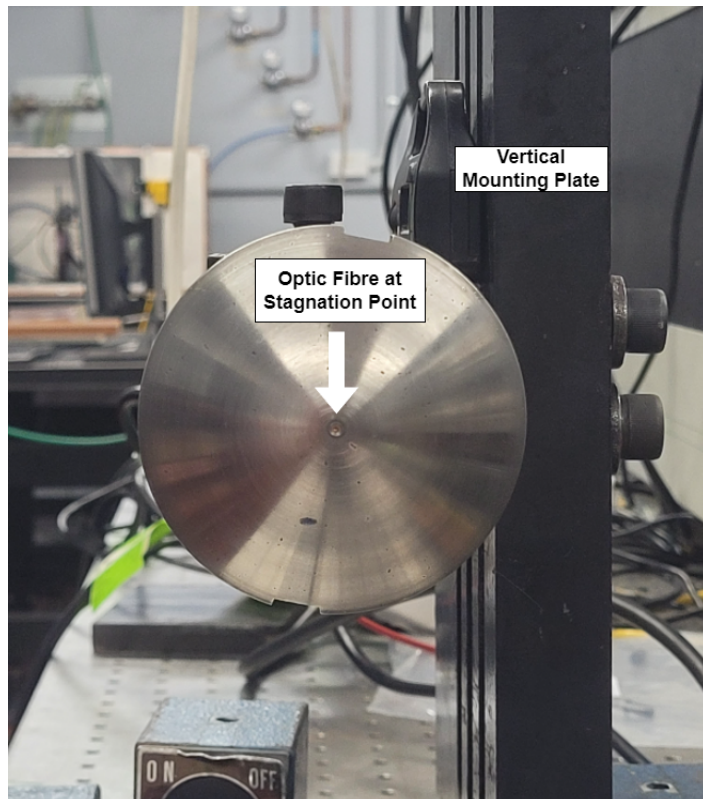


Figure 3.7: Close up photograph of stagnation point with 90 mm through-model optic fibre in place with adjacent mounting [29].

3.4.1 Optic Fibre Bend Radius Limitations

Table 3.3 displays the product information of the current optic fibres from ThorLabs [19]. As mentioned in the literature review, the most important bandwidth ranges of CN radiation are between 360 nm - 440 nm.

Table 3.3: 600 μm Optical Fibre Characteristics.

Parameter	Minimum	Maximum
Wavelength Range (nm)	250	1200
Core Diameter (μm)	660	750
Maximum Attenuation (dB/km)	10	8
Numerical Aperture	0.22	0.24
Bend Radius	Short Term	Long Term
Maximum Bend Radius (mm)	53	106

The current optic fibres used at UQ for the first through-model validation experiment are 600 micrometer (0.6 mm) diameter, which have a recommended bend radius of 106 mm. Following this, the external fibre diameters of up to 0.75 mm, will be used to justify the CAD models (Table 3.3).

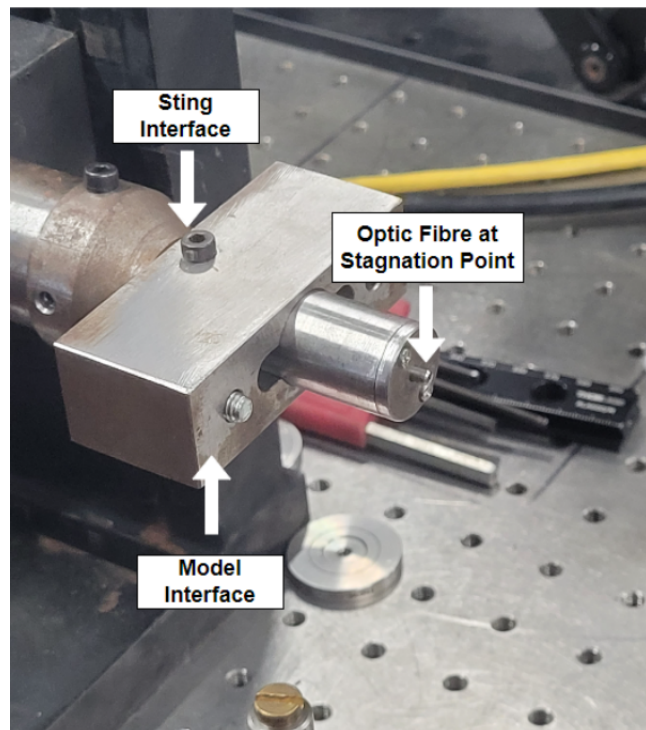


Figure 3.8: Raw optic fibre before forebody of capsule is secured [29].

3.5 Sting Design Methodology

The background optic fibre apparatus at UQ has now been presented, the following sections of this chapter will display a variety of proposed sting mounting locations for scaled experimentation of Dragonfly entry. Figure 3.9 was included in personal communication with Dr. Brandis of the near wake recirculation zone.

The most appropriate sting will *not interfere with this backshell recirculation zone* and will be able to *satisfy the optic fibre requirements* for successful experimental testing.

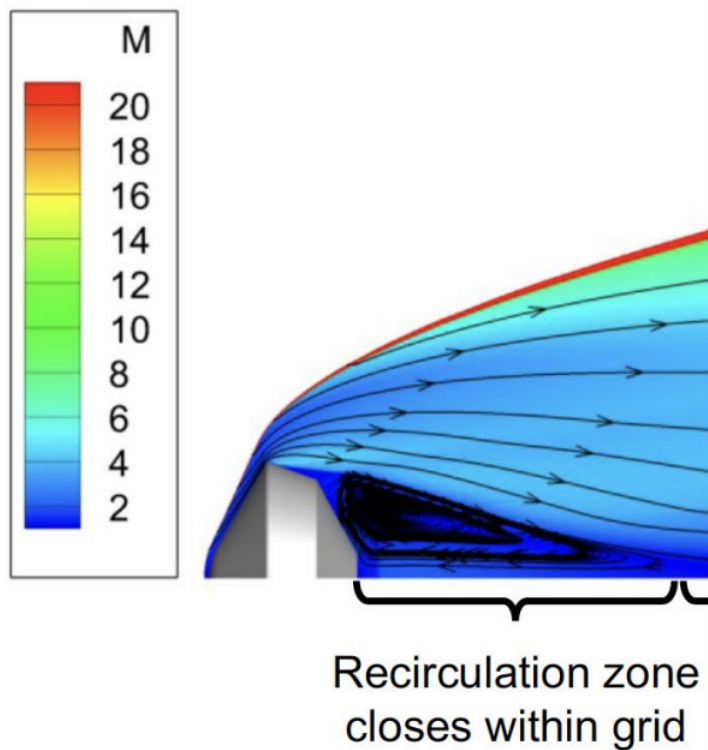


Figure 3.9: Mach number of near wake flow field to remain free of sting [7].

The proposed methods of sting design, will focus on an offset sting attachment which limits interactions with the post-shock CN flow. In the current orientation as Figure 3.9, if the sting interface occurred further towards the "bottom shoulder", the shock wave and hypersonic flow could occur and be measured towards the "top" of the model. Since the model is axis-symmetric, if the optic fibres measured radiation at the "top" shoulder, then the sting can be offset towards the "bottom" shoulder, and reduce the post-shock interactions.

3.5.1 Critical Criteria for Sting Design Variations

There are numerous considerations to account for with the interaction of the capsule model to the sting, which will support the assembly in the test section of X2. These components will be exposed to the 4 km/s - 7 km/s hypersonic flow during the test time. The first consideration is the bend radius of the optic fibres which will transmit the information to the spectrometer.

- Physically fit inside the X2 test section
- The model must fit inside the coreflow of the hypersonic flow
- The three optic fibre locations must be accessible from the one sting
- The bend radius restrictions of the optic fibre cables must be adhered to
- Reduced near wake flow interaction of the top (superior) shoulders

Throughout the literature review, it was evident that the stagnation point, forebody shoulder and aft-shoulder needs to be instrumented to measure CN composition, however, the optic fibres which are primarily glass tubes, have a maximum bending radius of 53 mm - 106 mm.

A 3D printed 90 mm model was constructed in order to physically verify with the optic fibres could indeed be used for this experimental design (Figure 3.10).

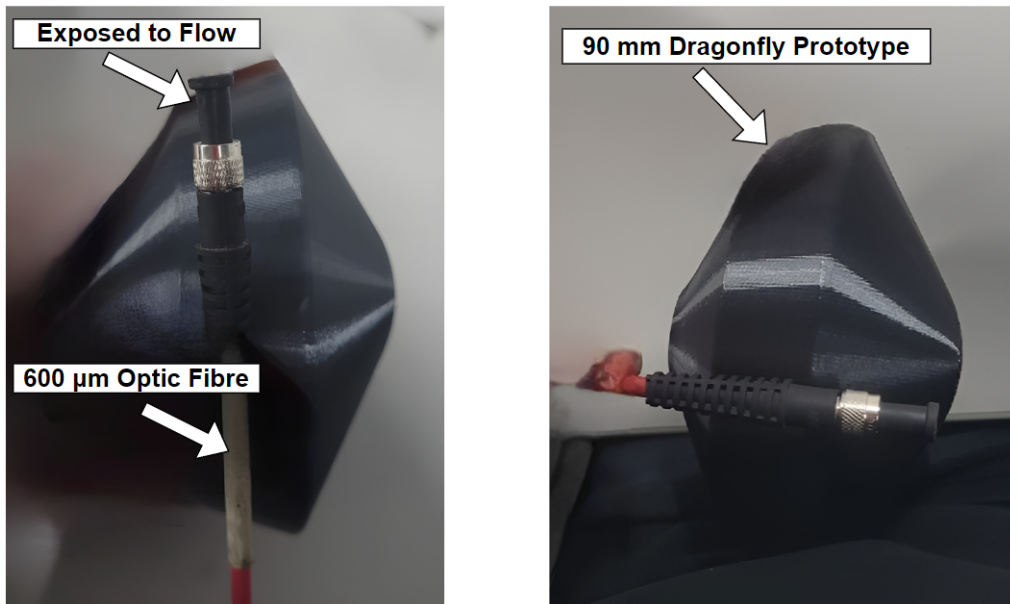


Figure 3.10: 90 mm diameter models with 600 μm optic fibre.

It is clearly evident that the black housing from the optic fibre would need to be removed if appropriate, in order for all three fibres to be installed.

3.6 Proposed Sting Interface Angles

The four proposed sting interface angles are displayed in Figure 3.11 - Figure 3.14. The Axial sting in Figure 3.11 is included as it's the current and long standing method. The backshell sting in Figure 3.12 is installed at a 30° below. The mid-shoulder sting in Figure 3.13 is installed on the 18.5 mm between the foreshoulder and aft-shoulder at a 83° angle. Finally, Figure 3.14 depicts an alternative to the former, installing at a 45° angle on the aft-shoulder. This design would also necessitate a change in geometry for proper sting mounting, however, it will be considered in the initial screening of suitable designs.

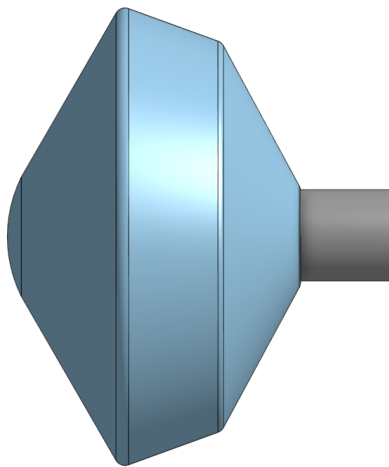


Figure 3.11: Axial Sting.

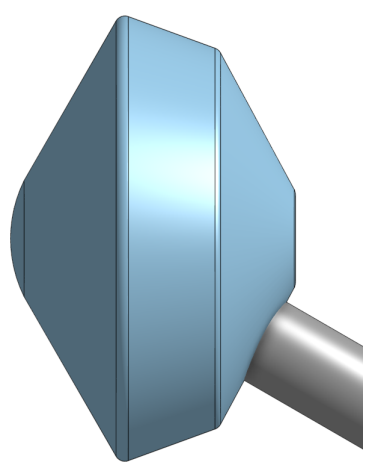


Figure 3.12: 30° Backshell Sting.

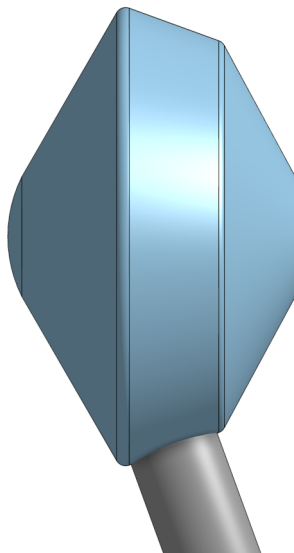


Figure 3.13: 83° Mid-shoulder Sting.

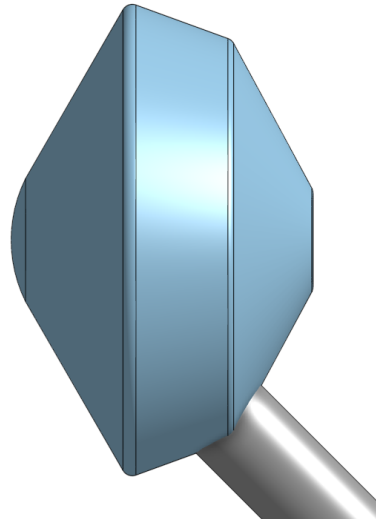


Figure 3.14: 45° Aft-shoulder Sting.

3.6.1 Design 1 - Axial Sting Placement

Due to the very specific nature of this project, the design aspect could be deemed as minimal; however, this is due to the targeted literature review and precise outcomes required for project success. The first design is the current axial sting mounting which is the standard form for stagnation point testing (Figure 3.6). With all engineering design, it is important to assess the current methods, in order to understand whether change will improve the desired outcome.

These sting designs were created in Onshape and altered to different locations around the geometry via assembly mode. This model is used mainly for stagnation points [29], with reference to Figure 3.15, it can be seen that the blue lines depicted as optical fibres have a very tight bend in them. This model could also become problematic due to the near wake of the shoulder and backshell discussed in the literature review. A preliminary screening of this design will take place to understand if this axial sting placement is suitable, before assessing the other designs.

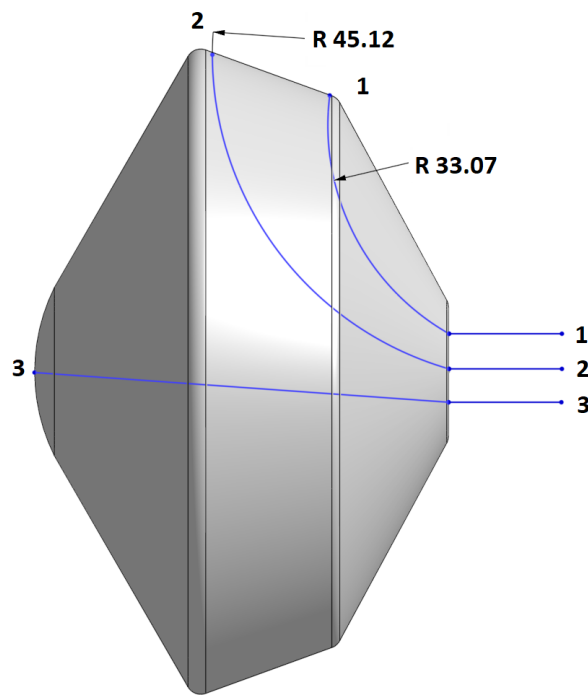


Figure 3.15: Optic fibre bend radius measurements of Axial Sting.

To improve iteration and decision making for the most appropriate sting, a rudimentary bend radius assessment was conducted in Onshape, by placing a dimensioned arc line to measure the bend radius at each testing location. It can be seen that the forebody shoulder recorded 45.12 mm, whereas the aftbody shoulder recorded a bend radius of 33.07 mm. These values far exceed the recommendations established in Table 3.3 of between 53 mm - 106 mm.

3.6.2 Design 2 - Mid-Shoulder Placement

The second design considered involved mounting the sting between the lower forebody and aftbody shoulders. This design was particularly interesting, as it was expected to provide favourable entrance angles to the instrumentation zones (Figure 3.16).

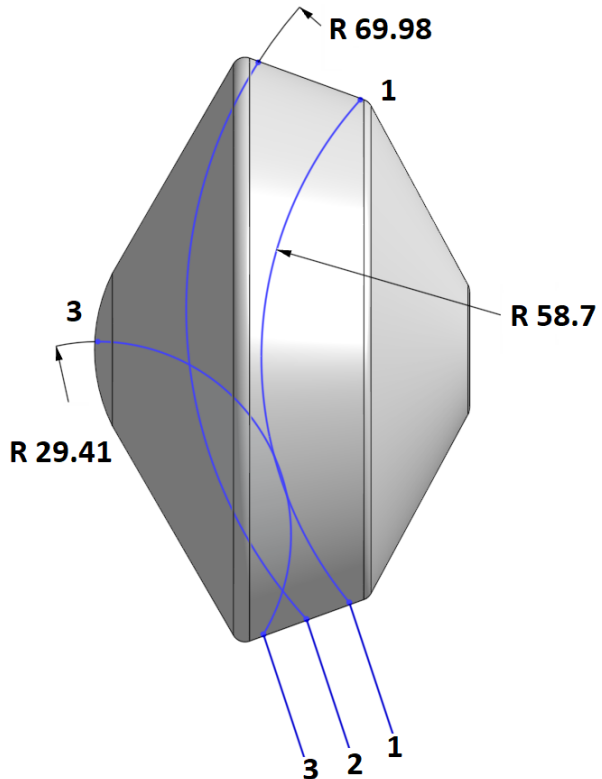


Figure 3.16: Optic fibre bend radius measurements of Mid-shoulder Sting.

Although this method provided an increase in bend radius over the axial sting method, it was determined that it would not be possible to also instrument the stagnation point, with a bend radius of 29.4 mm. The thought was investigated to not require optic fibre measurements at the stagnation point and omit this fibre. However, throughout consultation with the internal stakeholders, it was advised to continue to measure the stagnation regions. The stagnation point would be used as a control point to verify that the initial flow measurements are expected, and to compare with the current through-model radiation testing at UQ [29].

Further issues were noted with the mid-shoulder model due to the surface area of fixation of the model to the sting. Figure 3.5 indicates the mid shoulder area at a 90 mm scale, is only 18.5 mm. This distance was deemed too small to physically mount all surface interactions, and the sting interface and could lead to failure points from the 1 MPa - 3 MPa post-shock pressure on the model.

3.6.3 Design 3 - Backshell Sting Placement

The third design focused on improving the access to the stagnation point, while also remaining mindful of the wake interactions from the sting. By allowing the sting interface to originate from the backshell, this could be a "best of both worlds" when considering bend radius requirements and minimising post-shock wake flow interactions (Figure 3.17).

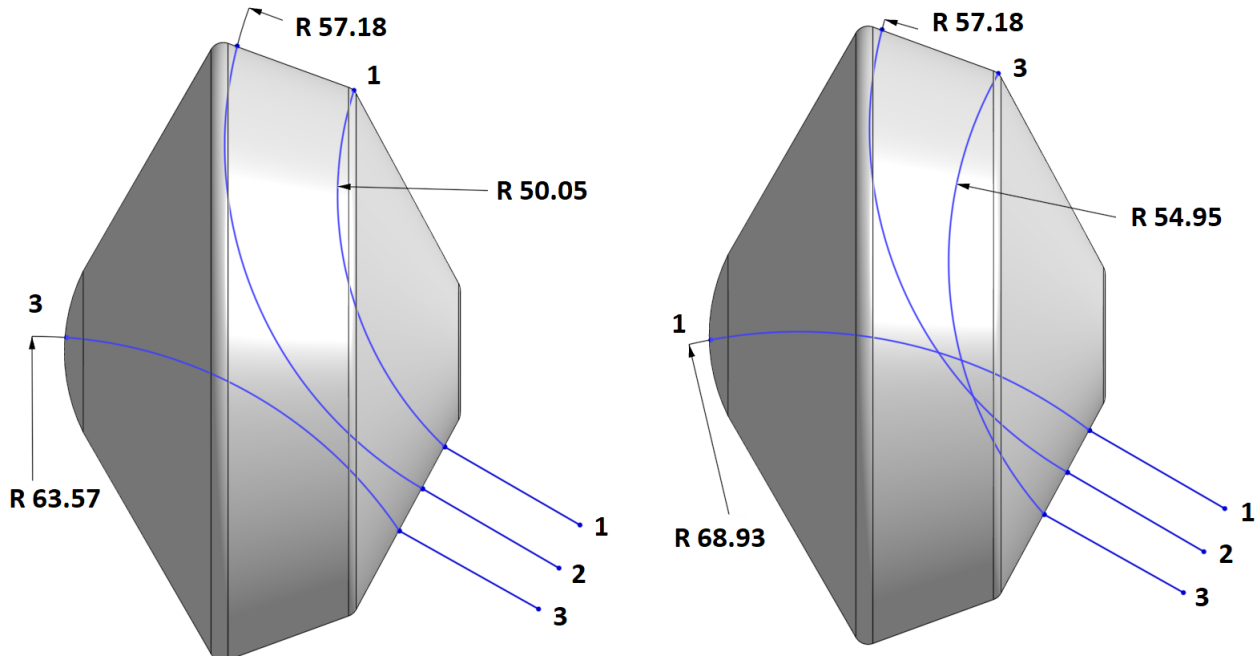


Figure 3.17: Backshell sting interface with two styles of optic fibre wiring.

This model provided promising results with a minimal bend radius value of 50.05 mm (right), further experimentation occurred by changing the orientation of the optic fibres to understand the variety of installation orientations.

The second variant (left) offered an increase of four centimeters to both the stagnation point and aftbody shoulder. It was made evident, that not only the sting interface angle needs to be explored, but also the orientation in which the optic fibres are also installed in the 3D model.

This design is plausible, however, it may not be the most optimal design. This can be due to the bend radius of the fibre towards the aft shoulder (3). With respect to Table 3.3 the maximum short-term bend radius is noted as 53 mm, whereas this position measured 54.95 mm. Therefore, it remains suitable to propose a fourth design which encompasses the learning from the previous methods.

3.6.4 Design 4 - Aft-Shoulder Sting Placement

The final sting interface design, involves the lessons learnt from previous iterations. Throughout the literature, most scale model designs are not representative of the entire vehicle, however, only focus on similar geometry to the locations of interest [5, 29]

Mounting the sting on the bottom aft-shoulder would require a capsule design change, however, this shouldn't impact the oncoming flow inside the tunnel, as the change is in the non-instrumented wake.

The first variation (left) offered the same benefits of the mid-shoulder case, with improved access to the forebody and aft-shoulder locations, with increased bend radius to the stagnation point (Figure 3.18).

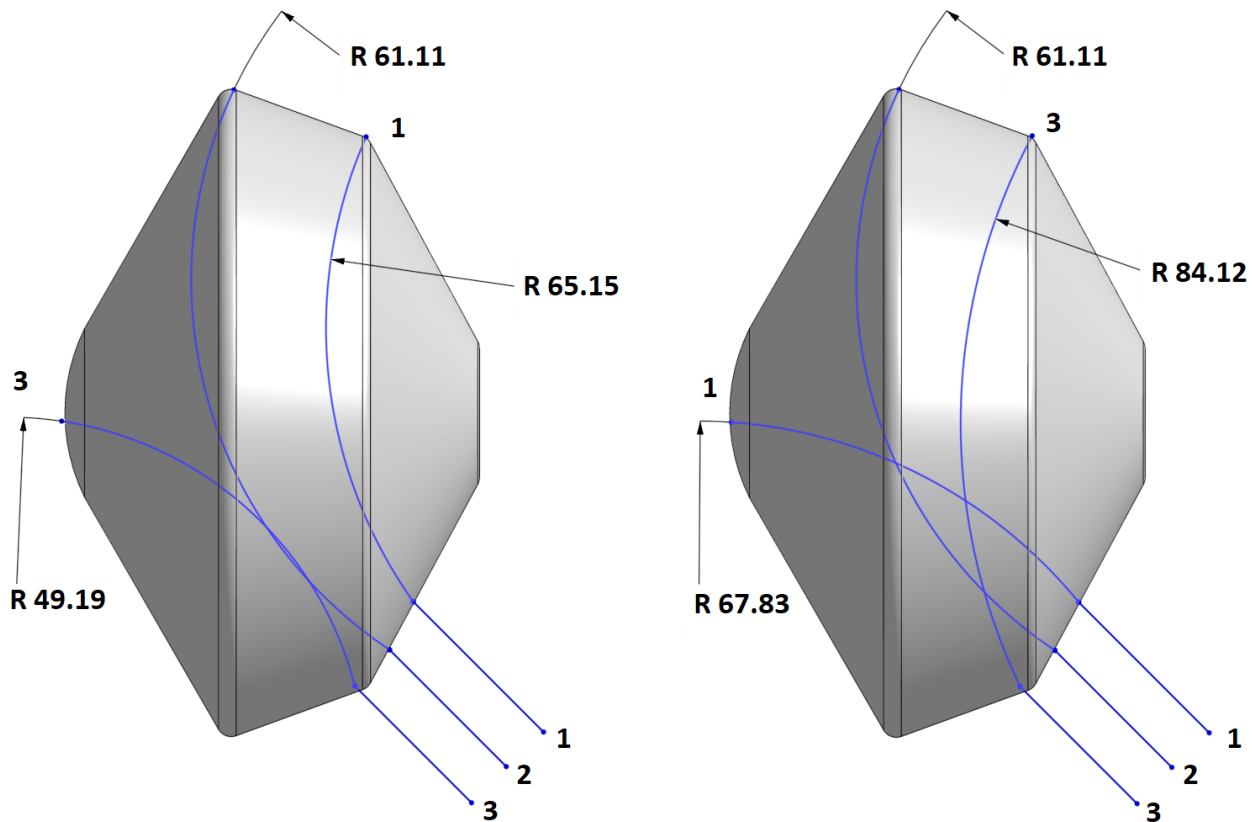


Figure 3.18: Aft-shoulder sting interface with two optic fibre wiring orientations.

The stagnation point does not meet the 53 mm minimum bend radius, so a final variant was examined (right). For this fibre orientation, it was concluded that it was possible to satisfy the requirements of the current $600 \mu\text{m}$ bend radius of over 53 mm short term. Although with a minimum measurement of 61.11 mm to the forebody location, this would be closer to a straight line in practice.

This design and orientation provides the widest range of possible success to instrument all locations of interest, although it requires changes to the geometry of the aftbody.

From removing parts of the bottom aft-shoulder, this design could have easier access for the technicians to install the optic fibres and can open up further testing locations on the backshell itself as described by Dr. Brandis in personal communication.

These designs will be summarised in the following decision matrix to implement further analysis for the design to test and optimise.

3.7 Decision Matrix of Preferred Sting Design

A decision matrix was employed to determine a score for the most appropriate designs, other than just consulting the bend radii requirements. Table 3.4 displays the six possible variations of sting angle interface and the estimation of wake flow interactions. The wake flow value was determined out of 100, with the highest score estimated as the least effect on the near-wake flow interaction of the instrumented zones.

A scoring system was developed summing the minimum and maximum measured bend radii from Figures 3.15 - 3.18, with the addition of a wake flow score. The formula for such is displayed as Equation 3.1.

$$\text{Score} = (\text{Min Bend Radius} + \text{Max Bend Radius} + \text{Minimal Wake Flow Interaction}) \quad (3.1)$$

Table 3.4: Summation of Scores across Sting Designs.

Stings (mm)	Min Bend Radius	Max Bend Radius	Wake Flow	Score	Rank
Axial (Standard)	33.07	45.12	10	88	6
Mid-shoulder	29.41	70	90	184	3
Backshell V1	50.05	63.57	60	173	5
Backshell Cross	54.95	68.93	60	183	4
Aft-shoulder V1	49.19	65.15	80	194	2
Aft-shoulder Cross	61.11	84.12	80	<u>225</u>	1

From consultation of this decision matrix, it is evident that a modification of the aft-shoulder sting will be the best scenario for CN shoulder instrumentation. It is also noted that due to this being a 3D model, the physical installation of optic fibres will be different to this rudimentary assessment.

It is also discovered, that the scaled capsule will be adapted in order to create a suitable mounting surface area for the preferred design. As with the Backshell and Mid-shoulder designs, this was using the available surface area of the model. Since these designs scored poorly due to their tight physical limitations, it appears more suitable to modify the section of the capsule that is not instrumented, in order to improve access to the instrumented side.

In case of any errors with implementation, a smaller diameter optic fibre can be purchased with bend radii of 23 mm - 46 mm, however, with the same wavelength range as the current model, the centre already has the larger fibres Table 3.5.

Table 3.5: 200 μm Optical Fibre Characteristics.

Parameter	Minimum	Maximum
Wavelength Range (nm)	250	1200
Core Diameter (μm)	200	320
Maximum Attenuation (dB/km)	10	8
Numerical Aperture	0.22	0.24
Bend Radius	Short Term	Long Term
Maximum Bend Radius (mm)	23	46

3.8 Chapter Summary

The most important aspect of this chapter was to firstly obtain the dimensions of the Genesis capsule and recreate this accurately at 1.52 m, then to inspect the up-scaling to 4.5 m for Dragonfly. These methods were successful using the Onshape program, which lead to the down scaling to a version suitable for X2.

A review of the current through-model optic fibre experimentation at UQ was required to further constrict the design choices which are most likely to be implemented moving forward [29]. After consultation with the stakeholders and current hypersonic experimenters at UQ, the sting should enable the optic fibres the suitable bending radius but also not impede the near-wake flow of the model. A 90 mm scaled model was also 3D printed to improve the viability and understanding of the physical optic fibre installation process. This lead to the four major sting designs and various orientations of optic fibre installations to optimise the optic fibre requirements.

With the aid of a decision matrix to collate the minimum and maximum bend radius values of each design, an estimation of wake flow interaction was formed to reach a final score. The highest scoring designs both implemented the Aft-shoulder design modification, which will be further investigated.

Chapter 4

Analytical and Simulation Results

"This section is begging for a table."

— Dr. C. James, UQ, 2023 [9].

4.1 Chapter Introduction

This chapter represents the initial analytical, numerical, and simulation results of the proposed design. It is important with experimental design and computer code-based systems to determine analytical estimates of expected results, rather than relying on simulations alone. As without an apparent validation comparison, it remains difficult to trust the values and outputs of engineering simulations. These results will also be compared to published chemistry and flow conditions of previous Titan and Dragonfly research, to further improve the validity of results. The chapter will conclude with the findings from the wide array of testing and recommendations for optimisation and scale model manufacture in the next chapter.

4.2 Determining Boundary Conditions for Simulations

The goal of this project is to better understand the ground testing scale requirements for radiative heat transfer through Titan entry, the region of initial conditions that are important to obtain accurately. The initial conditions for both analytical and computer simulations will be derived from the parameters associated with those expected on Titan, at maximal heating upon atmospheric entry. However, these values have been collated and interpolated between numerous published resources from reduced detail, due to the secrecy related to the project.

Initially, the Dragonfly entry milestones have been noted in Figure 4.1, released from NASA presentations. The points of interest are labelled as entry interface, peak heating and peak deceleration. The altitudes (h), velocity (v), heat flux (q), deceleration (g), and time from atmospheric entry (E) are presented under the ballistic entry phase in Figure 4.1.

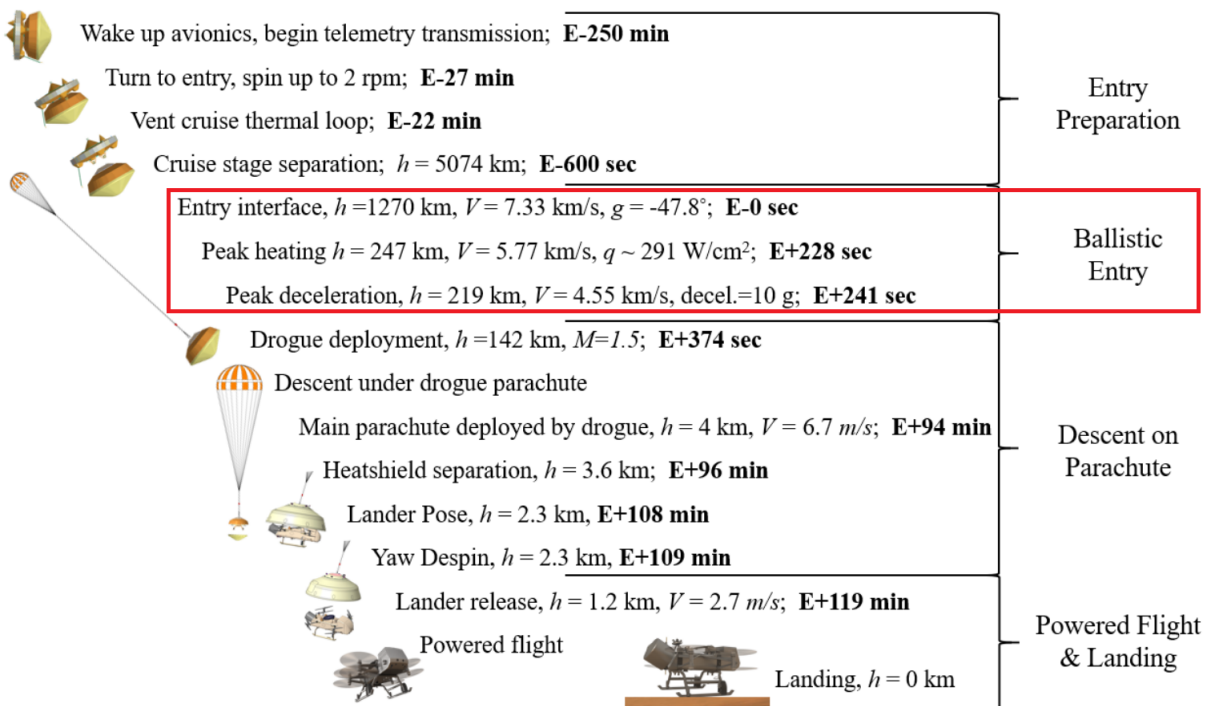


Figure 4.1: Proposed Dragonfly entry milestones in 2023 by NASA Langley [8].

An adapted version of this figure was also discovered in a 2022 NASA presentation, however, these values are similar between comparison (Figure 4.2).

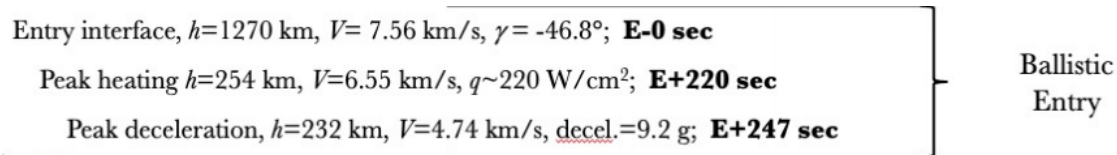


Figure 4.2: Second entry trajectory presentation in 2022 [20].

It is noted that the 2022 released velocities are higher than the more recent 2023 graphic, although resulting in a lower heat flux (q). However, this thesis will use the values from the most recent 2023 graphic (Figure 4.1), until more updated values are published and released, and design towards the highest heat loads.

Table 4.1 displays a summary of the Dragonfly entry parameters which will form the boundary conditions for future analysis.

Table 4.1: Dragonfly Entry and Descent Flight Parameters.

Dragonfly Entry Milestones	Value
Entry interface	1270 km
Entry velocity	7.33 km/s
Peak heating altitude	247 km
Peak heating velocity	5.77 km/s
Max Heat flux	291 W/m ²
Peak deceleration altitude	219 km
Peak deceleration velocity	4.55 km/s
Maximum deceleration	10 g

The main reference material from the literature review was the 2019 study "Features of Afterbody Radiative Heating for Titan Entry" by Johnston, West & Brandis 2019 [7], which provides the most detail towards entry analysis. Although noting this paper was published even earlier than the previous entry figures, a similar trend is evident at peak heating. The time since entry interface at 1270 km, along with the capsule velocity, free-stream density of Titan and expected free-stream atmosphere temperature are noted in Table 4.2.

Table 4.2: Titan Entry Velocity, Density, and Temperature over Time [7].

Time (s)	Velocity (m/s)	Density (kg/m ³)	Temperature (K)
160	7330	4.40E-06	162
180	7290	1.94E-05	162
190	7240	3.89E-05	162
202	7100	8.74E-05	162
211	6890	1.58E-04	162
224	6350	3.56E-04	162
235	5590	6.64E-04	162
241	5070	9.02E-04	162
245	4700	1.09E-03	162
248	4420	1.24E-03	162
254	3850	1.57E-03	162
263	3080	2.12E-03	160
280	1940	3.26E-03	158

It is possible to include the milestones in Table 4.1 to narrow down the peak heating corridor even more with nonlinear interpolation of the values in Table 4.2. The interpolated density at maximum heating, 5770 m/s is 5.87 E-04 kg/m³, while temperature remains at 162 K.

4.2.1 Justification of Boundary Conditions

Since most of Titan's previous ground testing research was conducted on arbitrary conditions and geometries before a dedicated mission was established , it is important to collate an accepted range of initial boundary conditions. Throughout Dragonfly's design timeline the space craft diameter has changed (3.75 m to 4.5 m [7]), a delayed launch window and now to a heavy launch vehicle (Table 2.1).

With reference to the previous Dragonfly entry graphics from 2022 (Figure 4.1) and 2023 (Figure 4.2), and now this detailed trajectory table from 2019, it can be noted the velocity and density values remain consistent and can be used with confidence for the upcoming simulations.

The main query remaining is the entry time windows, which should also be in range over the years of research. In 2022, peak heating was at 220 seconds after atmospheric entry, in 2023 it was noted at 228 seconds, however, the 5.77 km/s peak heating velocity also occurs between 224 s and 235 s in Table 4.2. Therefore, the initial conditions for simulations can be confidently determined, since the determined values remain constant throughout the design lifecycle.

A minor detail included in the study by Johnson et. al (2019) indicates that the maximal CN production, does not necessarily occur at peak heating, as this is a combination of convective and radiative heat flux. Although this study focused on the CN red and CN violet produced between 6.35 km/s and 5.07 km/s, which is still in the range of peak heating at 5.77 km/s noted in the graphics of 2022 and 2023 [7].

It would be very unfortunate for this thesis if there was a wide range of variability in initial conditions, as it's relevance to Dragonfly could come down to an educated guess, as previous research has been. However, in the 2019 to 2023 research window, the entry trajectory, heating and milestones still report to be occurring at similar instances, which improves confidence in initial conditions for simulations in this thesis.

4.3 Analytical Calculations for Dragonfly Entry

Throughout university coursework in Hypersonics and Space Engineering, the author was exposed to the introductory analytical estimations for planetary entry conditions. This section will include the analytical approximations of Dragonfly entry conditions, to be compared with the published values from NASA. It was discovered that the analytical solutions are limited, which will be investigated further within hypersonic numerical simulations later in this chapter.

The following sections will include analytical approximations to hypersonic entry chemistry and thermodynamic conditions behind the shock wave of Dragonfly entry, at the initial conditions expected at peak heating. Since the hypersonic simulations are performed using code, instead of solid models, it is important to follow this procedure in order to understand; how to validate and trust the computer simulations. The final results across a battery of simulations and calculations will be used to inform the engineering mechanical design of the most appropriate scale model inside X2, to replicate the post-shock wave conditions for Dragonfly entry in future work.

In-depth understanding of statistical thermodynamics concepts of outcome probability are required to more accurately model how vibrational, electronic, rotational, and transitional temperature modes interact with atoms and molecules in post-shock chemistry (introduced in section 2.3). This complex quantum assessment arises to improper assumptions in analytical calculations, which can only be used for ‘order of magnitude’ accuracy, before numerical calculations are required.

4.3.1 Analytical Approximation of Initial Atmosphere Conditions

The initial gas conditions need to be determined from the Titan atmosphere composition in order to more accurately estimate the post-shock environment.

The specific gas constant (R) is determined by the Universal Gas constant (8314 J/mol · K) divided by the molecular mass of the gas (displayed in the periodic table). For a mixture of gas, the specific gas constant of that mixture needs to incorporate the percentage of the gases involved. The specific heat and constant pressure (C_p) and specific heat at constant volume (C_v) for the gases and mixture are also displayed in Table 4.3. The ratio of these specific heats is termed as gamma (γ). The subscript mix, refers to the composition mixture.

Table 4.3: Gas Properties for N₂-CH₄ Mixture.

Parameter	Value J/kg-K	Resource
R_{N2}	296.8	8314/28.02 g
R_{CH4}	518.3	8314/16.04 g
$C_{p,N2}$	1039	NASA @ 300 K
$C_{p,CH4}$	2220	NASA @ 300 K
R_{mix}	301.23	$(0.98 \times R_{N2}) + (0.02 \times R_{CH4})$
$C_{p,mix}$	1062.62	$(0.98 \times C_{p,N2}) + (0.02 \times C_{p,CH4})$
γ_{mix}	1.3956	Cp/Cv ratio @ 300 K

The next mathematical procedure using Equations 4.1 - 4.7 will investigate the rudimentary analytical solutions for the peak heating post-shock environment of Dragonfly entry.

Pressure:

$$P_\infty = \rho \cdot R \cdot T \quad (4.1)$$

Enthalpy:

$$h = \frac{v_\infty^2}{2} + C_p \cdot T_\infty \quad (4.2)$$

Speed of Sound:

$$a = \sqrt{\gamma \cdot R \cdot T} \quad (4.3)$$

Mach Number:

$$M = V \cdot a \quad (4.4)$$

Post-shock pressure behind a normal shock wave:

$$P_2 = P_1 \cdot \left(1 + \frac{2\gamma}{\gamma+1} (M_1^2 - 1) \right) \quad (4.5)$$

Post-shock density behind a normal shock wave:

$$\rho_2 = \rho_1 \cdot \left(\frac{(\gamma+1)M_1^2}{2 + (\gamma-1)M_1^2} \right) \quad (4.6)$$

Post-shock Temperature behind a normal shock wave:

$$T_2 = T_1 \cdot \left(1 + \frac{2\gamma}{\gamma+1} (M_1^2 - 1) \right) \cdot \left(\frac{2 + (\gamma-1)M_1^2}{(\gamma+1)M_1^2} \right) \quad (4.7)$$

It is noted that subscript ∞ represents the atmospheric freestream value, pressure P , density is ρ , enthalpy h , sound speed a , Mach number M , and subscript 1 for initial state while subscript 2 for the post-shock state. Further symbols have been explained earlier in this section.

From the previous calculations, the freestream pressure, enthalpy, sound speed, and mach numbers will remain usable as an analytical solution. The analytical results for post-shock conditions at peak heating during Dragonfly entry at 5.77 km/s can be seen in Table 4.4.

The literature review revealed that the analytical estimations for post-shock pressure, density and temperature will not be accurate after accounting for the hypersonic chemical changes. Especially noting a post-shock temperature over 15,000 K would destroy most known substances, however, from every other space mission, this does not occur (Table 4.4).

Table 4.4: Analytical Titan Conditions at 5.77 km/s.

Parameters at Maximum Heat Flux (\dot{q})	Value	Units
Titan Entry Enthalpy	16.82	MJ/kg-K
Titan Local Sound Speed	261.01	m/s
Titan Local Mach Number	22.10	-
Titan Freestream Pressure	28.67	Pa
Titan Freestream Density	5.8761×10^{-4}	kg/m ³
Titan Freestream Temperature	162	K
Pressure Behind Titan Shock	16 320	Pa
Density Behind Titan Shock	3.519×10^{-3}	kg/m ³
Temperature Behind Titan Shock	15 398	K

It was discussed in the literature review that NASA has created a number of computational codes in order to improve the accuracy and speed of the hypersonic environment. Another one of these is the Chemical Equilibrium for Applications code or CEA.

Traditionally, this program is only available via a minimal input on-line interface and used for combustion kinetics. Due to the Memorandum of Understanding signed between UQ and NASA, this CEA code through Linux commands was made available for personalised and in depth post-shock analysis of planetary reentry. The following section will investigate more reliable results expected during Dragonfly entry, the outcome of these results will be used to understand the experimental design required for the X2 hypersonic wind tunnel.

4.4 NASA's Chemical Equilibrium for Applications Code

The post-shock environment of Titan is difficult to predict analytically, therefore more advanced techniques are used to improve the modelling. This subsection introduces NASA's CEA code and it's numerical equilibrium post-shock results, as well as the expected concentrations of atoms and molecules. This code is under strict access control due to the advanced modelling and applications it can be used for, and will not be shared. The initial conditions for analytical results are also used as initial conditions into the CEA program, to compare and further refine the expected results.

Since the purpose of the report is to investigate the radiation effects of CN on the vehicle, it is most important to understand the concentration that is produced in the post-shock environment [7].

4.4.1 Additional Initial Conditions for CEA Calculations

Within the CEA environment, the user has the ability to prepare the available gas model input for the atmosphere being investigated. This file was created by Dr. James after compiling the recent improvements by Dr. Brandis refereed to in the literature review [7, 25]. The input reactants for the freestream state of Titan will be Nitrogen (N_2) and Methane (CH_4), with the possible 33 outcomes from statistical thermodynamics as potential products (Table 4.5).

Table 4.5: Input reactants and output products available from NASA's CEA code.

Reactants	Available Output Products
N_2	$CH_4, CH_3, CH_2, CH, HCN, N_2, C_2, H_2, C_2N_2, CN, NH, HCN, N, C, H, N_2^+, CN^+$
CH_4	$N^+, N^-, C^+, H^+, e^-, C_3, C_4, C_5, CCN, HNC, C_4N_2, CNC, NCN, C_2H, NH^+, C_2H_2$

During the Huygens Titan entry in 2005, trace Argon was recorded and suggested for incorporation into future Titan CEA calculations [3, 24].

4.4.2 Inclusion of Argon in CEA Gas Model

The new gas model that includes argon can be seen in Table 4.6. In the primary referenced 2019 study by Johnston et. al, mentioned to generate the maximal amount of post-shock CN, it was deemed to use the gas model that did not include Argon [7]. Although for studying post-shock CN composition, the non argon model is suggested, although it is still important to understand the potential effects on under or overestimating CN production, temperatures etc. The gas model with Argon is displayed in Table 4.6.

Table 4.6: Reactant Mole Fractions and Products Including Argon.

Reactant	Product
N_2	$CH_4, CH_3, CH_2, CH, HCN, N_2, C_2, H_2, C_2N_2, CN, NH, N, C, H, N_2^+, CN^+, N^+$
CH_4	$N^-, C^+, H^+, e^-, C_3, C_4, C_5, CCN, HNC, C_4N_2, CNC, NCN, C_2H, NH^+, C_2H_2$
Argon	Ar, Ar^+

The first CEA analysis with Nitrogen and Methane at peak heating will be conducted and the post-shock species displayed in order to understand the design requirements.

4.5 CEA Post-shock Equilibrium Conditions N₂ & CH₄

The initial and post-shock conditions with N₂ 98 % & 2% CH₄ by mole fraction, at the expected maximum heating conditions is listed in Table 4.7. It was noted that the CEA gas model would fail to converge if the temperature value was changed from 264 K due to an issue with Carbon species, this will be noted in the recommendations.*

Table 4.7: Post-shock results from N₂ & CH₄ by mole fraction.

Gas Composition	Mole fraction	
Nitrogen (N ₂)	0.98	
Methane (CH ₄)	0.2	
Initial Conditions	Value (Table 4.1)	Units
Density (ρ_1)	5.8761×10^{-4}	kg/m ³
Pressure (p_1)	28	Pa
Temperature (T_1)*	264*	K
Speed of sound (a_1)	332.2	m/s
Velocity (v_1)	5770	m/s
γ_{mix} Cp/Cv	1.3956	-
Enthalpy (h)	16.82	MJ/kg-K
Post-shock Conditions	Value	Units
Density (ρ_2)	4.8552×10^{-3}	kg/m ³
Pressure (p_2)	10 753	Pa
Temperature (T_2)	5716	K
Speed of sound (a_2)	1572.6	m/s
γ_{mix} Cp/Cv	1.1169	-
Enthalpy (h)*	16.47*	MJ/kg-K

*Note: CEA Post-shock Enthalpy is firstly different due to the temperature change between 162 K & 264 K (16.93 MJ/Kg-K), also noting Eq 4.2 that CEA will have a higher Cp value than at 300 K.

4.5.1 CEA Post-shock Species N₂ & CH₄

There are very interesting results between the initial and post-shock conditions displayed in Table 4.7. It was found that over a 10 fold increase in density, 20 fold increase in temperature occurred in the immediate post-shockwave environment. The analysis of these results will be explained all together in the following sections after further simulations are performed.

The CEA post-shock results will be compared from including Argon into the initial mixture. The most appropriate initial conditions and expected post-shock conditions will then be collated and used for Computational Fluid Dynamic (CFD) assessments of the scale models.

The individual concentrations of gas species is presented from the N₂ & CH₄ simulation in Table 4.8. Most interestingly, the concentration of Methane changes from 2% to less than 1 Billionth, in the equilibrium post-shock state at maximal heating. This further verifies the theme in the literature review, that CH₄ dissociation causes vast increases in entry heating [7, 25]. The CN mole fraction was determined as 1.14×10^{-3} from this initial simulation as the same order of magnitude expected by Johnston 2019 and Brandis & Cruden 2017 [7, 25].

Table 4.8: Most notable post-shock species 0.98 N₂ & 0.02 CH₄.

Species	Mole Fraction
CH ₄	$\ll 1 \times 10^{-10}$
N+	1.3664×10^{-5}
e-	1.4290×10^{-4}
C+	1.2176×10^{-4}
CN	1.1443×10^{-3}
C	0.014056
H	0.061285
N	0.34598
N ₂	0.57724

Note: CH₂, CH₃, CH₄, C₂H₂ – acetylene, C₄, C₄N₂ & C₅ were all listed as under 1×10^{-10} mass fraction.

Nitrogen molecule (N₂) mole fraction reduced from 0.98 to 0.577 due to dissociation, while the atomic Nitrogen (N) mole fraction rose from 0 to 0.346. The most common species were presented in this table.

4.5.2 Errors with Analytical Post-shock Equations

It is important to compare the potential errors between the analytical approximations and the CEA model. Table 4.9 represents the multiple of error between the analytical values estimated in Table 4.4 and those revealed from CEA calculations in Table 4.7.

Table 4.9: Factor increase based on analytical and CEA post-shock values.

Parameter	Factor of Change
Enthalpy	2%
Pressure Behind Titan Shock	1.52 x
Density Behind Titan Shock	0.72 x
Temperature Behind Titan Shock	2.69 x

It is noted the vast errors across every parameter, except enthalpy, which will remain the same pre and post-shock due to conservation of momentum, as depicted in Equation 4.2 ($h_1 = h_2$). It is clearly evident that analytical post-shock equations (Equations 4.5 - 4.7) are only suitable for ideal gases without chemistry changes.

4.6 CEA Post-shock Equilibrium Results N₂, CH₄ & Ar

To further understand the required initial conditions for experimentation, the previous simulations will be re-tested by altering the mole fractions of 1.5 % CH₄ & 0.5 % Argon, with unchanged N₂, using the gas model outlined in Table 4.6 with results displayed in Table 4.10.

In order to find initial conditions of the mixture with Argon, a new R value was determined as 299.7 J/kg-K with a Cp of 1077.7 J/kg-K following the same methods outlined in Table 4.3.

With the inclusion of Argon, there were similar post-shock changes seen without Argon. Noting an insignificant increase in density, pressure and temperature as Argon is a heavier species than Methane [7].

Table 4.10: Post-shock results from N₂, 1.5 % CH₄ & 0.5% Ar by mole fraction.

Gas Composition	Mole fraction	
Nitrogen (N ₂)	0.98	
Methane (CH ₄)	0.15	
Argon (Ar)	0.05	
Initial Conditions	Value (Table 4.1)	Units
Density (ρ_1)	3.624×10^{-4}	kg/m ³
Pressure (p_1)	28	Pa
Temperature (T_1)	264	K
Speed of sound (a_1)	329.6	m/s
Velocity (v_1)	5770	m/s
γ_{mix} Cp/Cv	1.3852	-
Enthalpy (h)	16.82	MJ/kg-K
Post-shock Conditions	Value	Units
Density (ρ_2)	5.0468×10^{-3}	kg/m ³
Pressure (p_2)	11 227	Pa
Temperature (T_2)	5822	K
Speed of sound (a_2)	1576.9	m/s
γ_{mix} Cp/Cv	1.1177	-
Enthalpy (h)*	16.49*	MJ/kg-K

*Note: CEA post-shock Enthalpy is firstly different due to the temperature change between 162 K & 264 K (16.93 MJ/Kg-K), also noting Eq 4.2 that CEA will have a higher Cp value than at 300 K.

Minimal changes were observed by the inclusion of trace Argon into the mixture at a large scale, however, the main difference will be the post-shock concentrations of CN, due to the lower initial CH₄. The post-shock species from the inclusion of Argon and change in Methane mole fraction will now be investigated.

4.6.1 CEA Post-shock species N₂, CH₄ & Ar

With the inclusion of Argon, it is expected that a lower amount of CN will be produced, due to the reduction in initial Methane concentration. It is also possible for more molecular Nitrogen to dissociate, due to Argon being a heavier atom than Methane. The molecular weights (g/mol) are provided as revision of the periodic table; Carbon = 12, Hydrogen = 1, CH₄ = 16.04, Argon = 40. The effects of such are displayed in Table 4.11.

Table 4.11: Most abundant Post-shock species including Argon.

Species	Mole Fraction
CH ₄	$\ll 1 \times 10^{-10}$
N+	2.2344×10^{-5}
e-	1.5021×10^{-4}
C+	1.1833×10^{-4}
CN	7.3401×10^{-4}
C	0.014222
Argon	0.03456
H	0.043971
N	0.38065
N ₂	0.52754

Note: CH₂, CH₃, CH₄, C₂H₂ – acetylene, C₄, C₄N₂ & C₅ were all listed as under 1×10^{-10} mass fraction.

A similar trend appeared with post-shock equilibrium Methane concentration below recorded levels, with CN an order of magnitude lower than the previous simulations. The analysis and implications of the post-shock environment with and without Argon will now be summarised, which will provide suitable boundary conditions for the CFD simulations on sting designs.

4.7 Comparison of Post-shock Conditions with Gas Models

Finally after the CEA simulations with and without argon, it is appropriate to summarise these results and determine if the CFD simulations should or should not include Argon, in order to measure the effects of post-shock CN. Comparing the two gas models it *shows negligible difference* on a large scale, however, the change in species is the factor to investigate further.

Table 4.12: Factor increase and percentage difference between initial and post-shock conditions.

Parameter	Increase No Ar	Increase With Ar	% Difference
Density (ρ)	13.69 x	13.92 x	1.68%
Pressure (p)	384.04 x	400.96 x	4.40%
Temperature (T)	21.66 x	22.05 x	1.80%
Speed of sound (a)	4.73 x	4.78 x	1.06%

4.7.1 Comparison of Post-shock Species with Gas Models

After the many stages of analytical and numerical analysis, the final code based results of this chapter are displayed in Table 4.13. It can be confirmed when studying CN production in the immediate post-shock Titan environment, there is a 35% difference between using an atmospheric model with 2% CH₄ over using 1.5% CH₄ & 0.5% Argon by mole fraction.

Table 4.13: Relative mole fraction differences between CH₄ & N₂ and Argon Species.

Species	Difference (%)	Note
N ⁺	-63.52%	Increase with Argon
e ⁻	-5.12%	Increase with Argon
C ⁺	+2.82%	Increase with CH ₄ and N ₂
CN	+35.86%	Increase with CH ₄ and N ₂
C	-1.18%	Increase with Argon
H	+28.25%	Increase with CH ₄ and N ₂
N	-10.02%	Increase with Argon
N ₂	+8.61%	Increase with CH ₄ and N ₂

It is important to integrate the relevant literature to understand the accuracy and verification of these outcomes. In the primary referenced 2019 study by Johnston et. al, the immediate post-shock concentration of CN remains similar [7]. It was noted that their research used slightly increased CH₄ mole fraction at 0.022. Figure 4.3 displays the mass fractions of CN, compared to the distance and time away from the shock wave interface from that report.

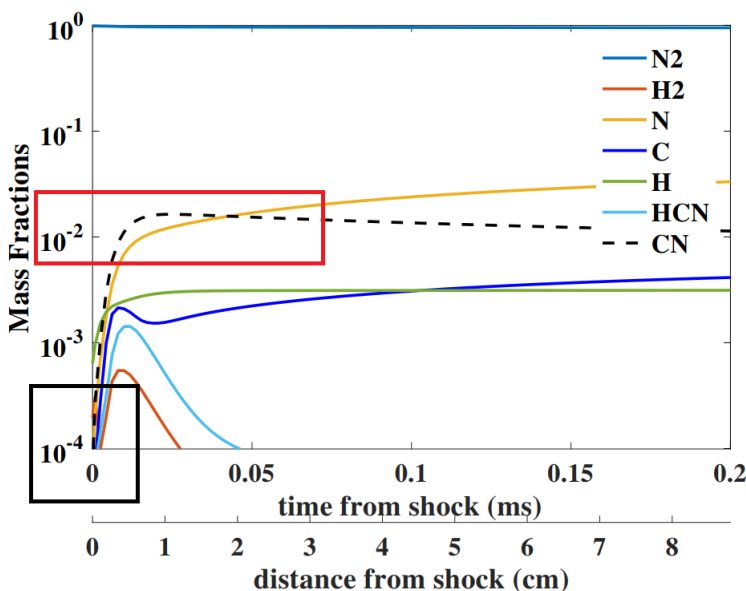


Figure 4.3: CN production with time and distance from shock wave [7].

Since CEA computes the immediate post-shock environment, the findings from the previous section will compare the graph values at the 0 mark on the x axis (black box). The previous non Argon experiment at 0.02 CH₄ at 5.77 km/s calculated mass fractions of 1.4×10^{-3} , whereas Johnston 2019 reported 4.7 km/s and 0.022 CH₄ calculated approximately 1×10^{-3} mass fraction of CN immediate post-shock (Figure 4.3).

It is also noted that the mass fraction of CN increases with distance and time from the shock wave (red box). It was concluded from this research that "The chemical processes along near-shock streamlines are shown to be mostly in equilibrium, with only the dissociation processes remaining in non-equilibrium beyond a short time beyond the shock." [7].

However, the reduction in CN production with the incorporation of Argon directly relates to this article by the authors mentioning "Ar was replaced with additional CH₄ for conservatism". The decision to model Titan entry radiative heating without Argon directly reflects and verifies the claim for this thesis to omit it from future analysis and experiments.

4.8 Summary of Initial Conditions and CEA results

Throughout this Chapter the focus has been an in-depth and multi factorial analysis on the most appropriate initial conditions to use as input into analytical and NASA CEA code, as well as the expected outcomes. Due to the nature of this project and the precise niche of the current mission design, it was very important to conduct a proper analysis of boundary conditions, otherwise all simulations and experiments would be deemed unusable for Dragonfly. Table 4.14 displays the most appropriate initial and expected outcomes for future computational and experimental endeavours.

Table 4.14: Summary of Initial and Post-shock conditions of Titan at Maximum heating.

Initial Conditions	Value	Units	Mole Fractions
Density (ρ_1)	5.8761×10^{-4}	kg/m ³	N ₂ 0.98
Pressure (p_1)	28	Pa	CH ₄ 0.02
Temperature (T_1)*	162*	K	
Velocity (v_1)	5770	m/s	
Enthalpy (h)	16.82	MJ/kg-K	
Post-shock Conditions	Value	Units	Mole Fractions
Density (ρ_2)	4.8552×10^{-3}	kg/m ³	CH ₄ $\ll 1 \times 10^{-10}$
Pressure (p_2)	10 753	Pa	CN 1.1443×10^{-3}
Temperature (T_2)	5716	K	N 0.34598
γ_{mix} Cp/Cv	1.1169	-	N ₂ 0.5772

*Note: The Post-shock CEA values are using a temperature of 264 K in CEA

4.9 Computational Fluid Dynamic Assessment of Designs

The computational analysis will now be displayed for the selected scale models. This first section will first focus on the CFD provided in the literature of the Dragonfly vehicle. It was deemed a more accurate approach to understanding the in-flight case to use images provided by NASA researchers, rather than introducing errors with different codes and skill levels.

4.9.1 Dragonfly Full Scale Simulations

Figure 4.4 was presented by Dr. Michael Wright, the lead EDL engineer for Dragonfly at a design review in 2023 [20]. This image displays the percentage of CN produced in the post-shock environment (left) and also the expected temperature ranges at maximum heating through Dragonfly entry. This figure follows the expected pattern which emerged in Table 4.14 and Figure 4.3 that the concentration of CN increases away from the stagnation point and towards the foreshoulder and aft-shoulder of the vehicle (Figure 4.4).

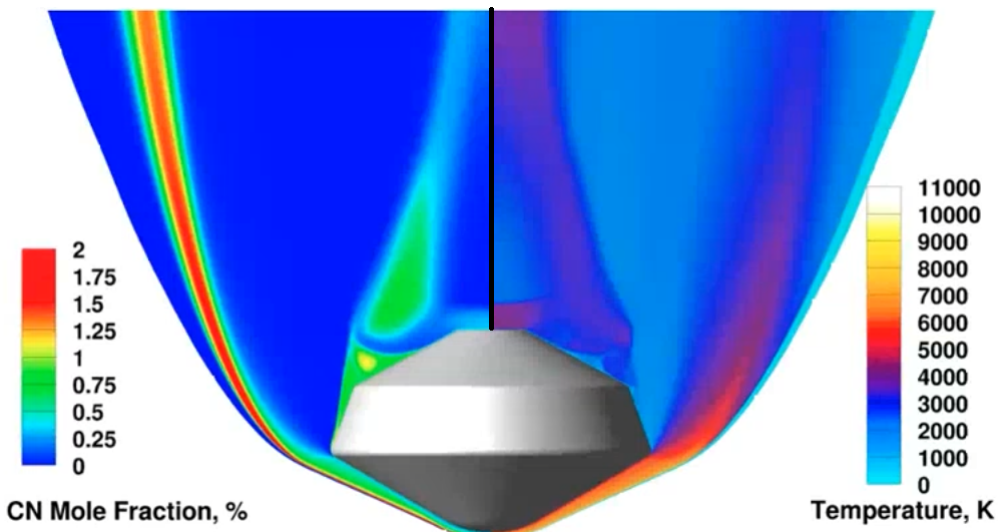


Figure 4.4: NASA Simulations of CN mole fraction and Temperature [20].

This figure also validates the expected post-shock temperatures estimated in the previous CEA analysis of Table 4.14, with temperature in orange ranging from 5000 K - 6000 K (Figure 4.4).

Further expectations of Dragonfly streamline and post-shock parameters have been previously displayed in Figure 2.10, Figure 2.11 & Figure 3.9, which all illustrates a similar trend in the near shoulder environments.

4.10 Ansys Fluent Analysis of Control

Since the streamline analysis of the stings presented in Chapter three will be conducted in Ansys Fluent, it is important to provide a control without sting integration, to ensure the addition of a sting will result in an undisturbed instrumentation zone.

The simulated streamline flow patterns at 90 mm scale can be seen in Figure 4.5 of 98 % N₂ and 2% CH₄ by mole fraction at the initial velocity of 5.77 km/s.

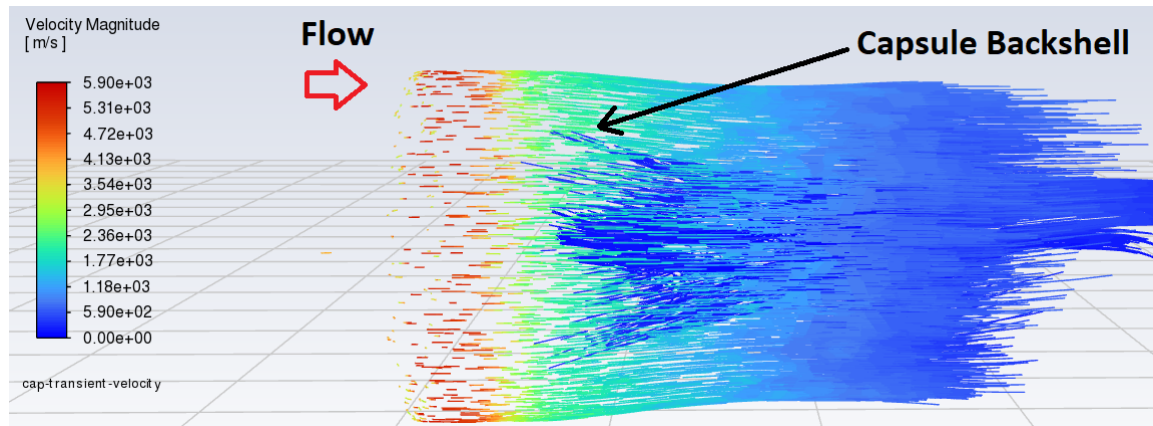


Figure 4.5: 90 mm capsule normal wake streamlines at 5.77 km/s.

This image was created by capturing the initial impulse of flow using individual streamlines of a transient Ansys Fluent simulation. By focusing on the initial impulse this shows the outline of the capsule backshell, as well as the external boundaries of the flow around the capsule shoulders (Figure 4.5).

Figure 4.6 illustrates the same simulation once the flow has developed in the analysis which indicates minimal changes in the boundaries of flow in the near wake regions.

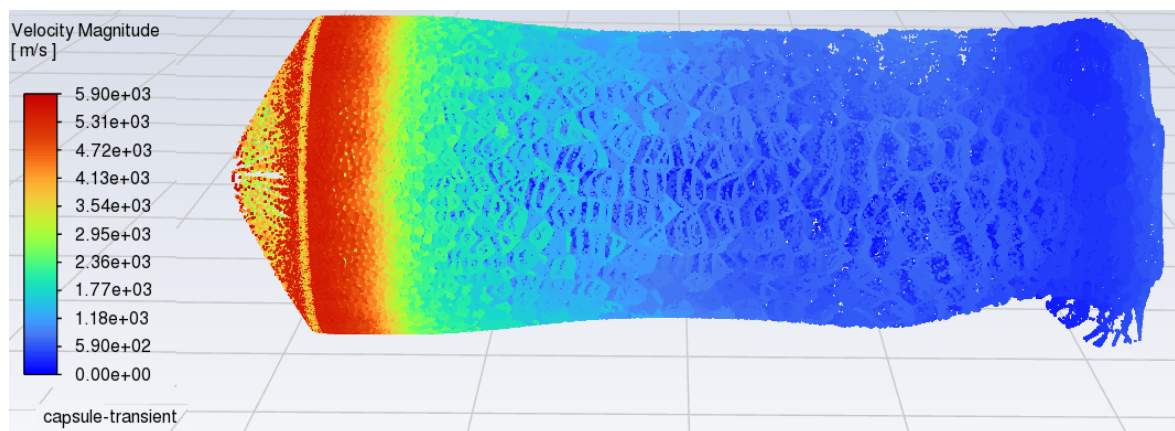


Figure 4.6: 90 mm capsule transient velocity at 5.77 km/s.

The Ansys simulations will not provide the same level of detail as those displayed by NASA, however, this is adequate for investigating the flow field of different stings.

This initial control analysis has demonstrated the expected outcome of an Ansys Fluent streamline simulation, now the preferred aft-shoulder sting will be assessed in order to learn if this design will satisfy the flow field required for experimental analysis.

4.11 Ansys Fluent 90 mm Aft-shoulder Model

The method for these simulations involved creating an enclosure in Ansys Spaceclaim, while calling a boolean function to remove the solid model and label it as a void in Ansys DesignModler. The direction of flow was labelled as the velocity inlet with the pressure outlet at the far wake, while the other four remaining sides of the enclosure were labelled as walls.

The enclosure was designated as fluid, which would create the mid-section representation displayed as the capsule and sting are empty space (Figure 4.7).

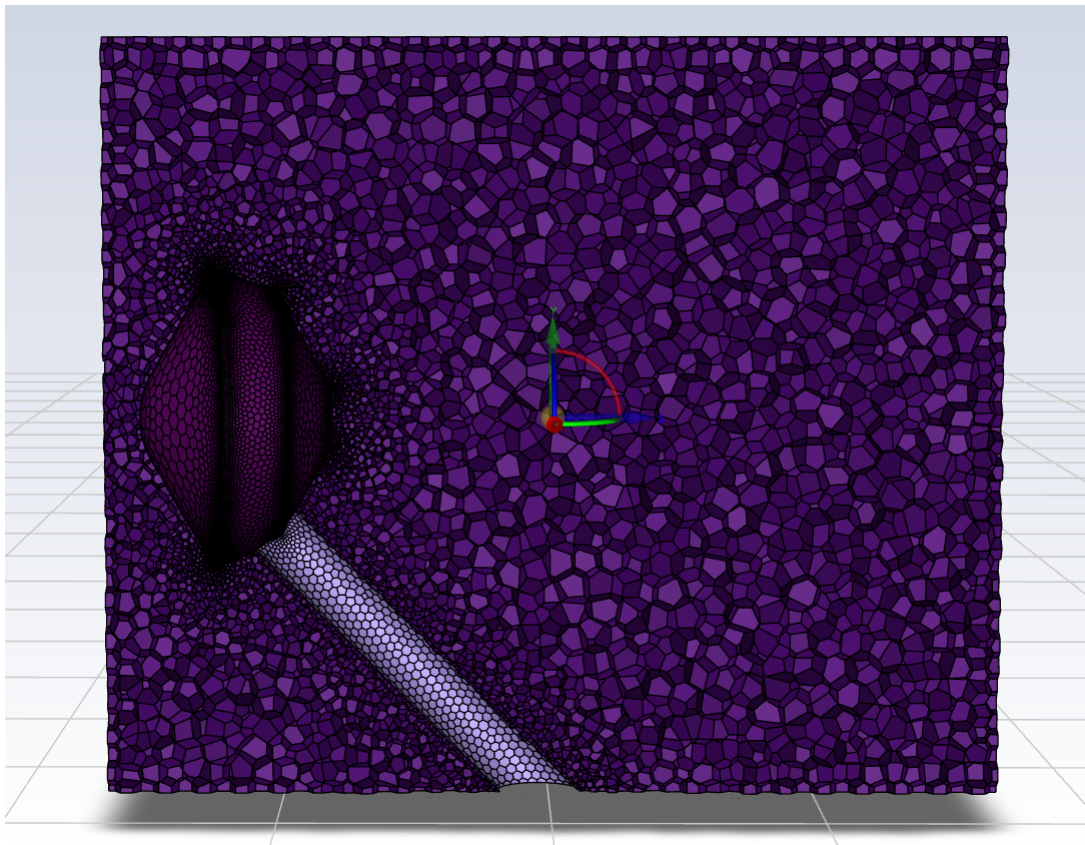


Figure 4.7: Fluid enclosure and volumetric meshing of aft-shoulder simulation.

To improve the reliability of the simulation, a high degree of surface meshing was incorporated on the forebody and aft shoulders to improve the quality of streamline measurements (Figure 4.7).

It was deemed necessary to analyse this sting in both as a steady impulse to see the streamline interaction as soon as the flow impacted the model, as well as the transient nature to visualise the long term flow effects.

The side-by-side comparison of streamline particles impacting the capsule with the aft-shoulder sting are illustrated in Figure 4.8. It is evident that there is *no observable difference* to the top instrumentation zone with the addition of the aft-shoulders sting.

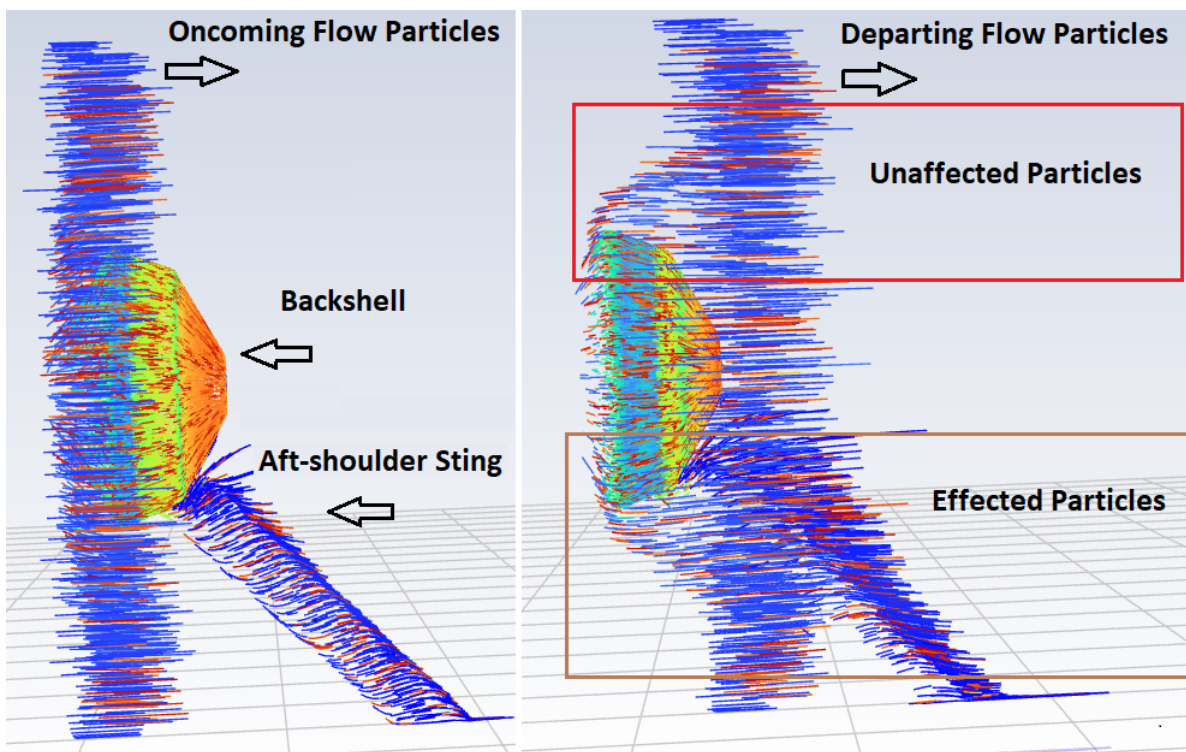


Figure 4.8: Streamline effect from before and after 5.77 km/s impulse with aft-shoulder sting.

The red rectangle labelled as ‘Unaffected Particles’ has the similar flow pattern over the forebody and aft-shoulders as originally shown in Figure 4.5.

Due to the nature of the particles at the sting interface labelled as ‘Effected Particles’ it is possible over a longer time frame that the particles may impact the top instrumentation zone.

A transient analysis was performed again, similar to the control geometry to understand the particle effects after the initial flow impact. Figure 4.9 depicts the transient flow analysis of the diagonally located sting.

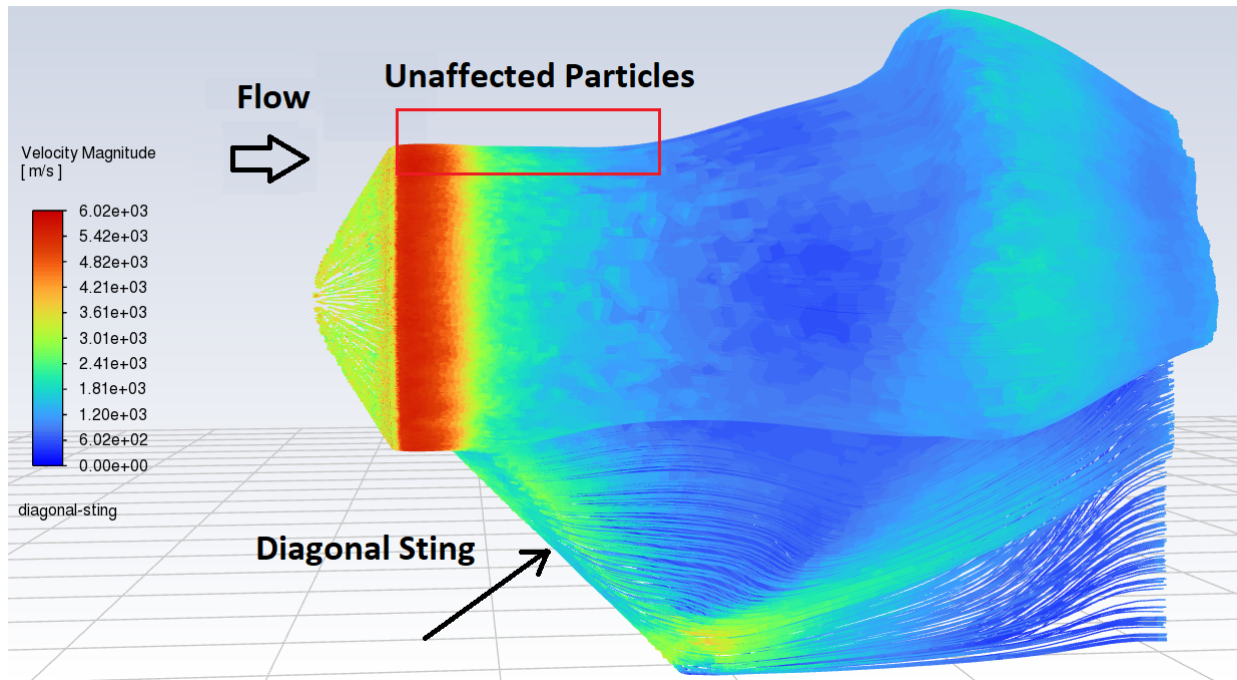


Figure 4.9: Transient analysis of Aft-shoulder sting at 5.77 km/s.

It can be seen that over a longer time frame the top instrumentation zone still displays "Unaffected Particles", which further clarifies the steady impulse assessment. The far wake flow of this simulation shows large disturbances, however, that is most likely to have occurred from a small enclosure of the simulation. Larger enclosures with longer wake zones were attempted, although the computing power and licences of Ansys student prohibited the volumetric meshing requirements.

It was deemed as unimportant to measure further down the wake region, as the volumetric meshing would decrease away from the capsule surfaces, which was the purpose of the analysis.

After satisfying both the bend radius requirements and unaffected streamline characteristics, the aft-shoulder sting can be confidently used for hypersonic experimentation.

To ensure the material selection of the capsule will survive the experimental testing, a Finite Element Analysis (FEA) of the capsule geometry was performed in Ansys Static Structural.

4.12 Ansys Static Structural Assessment of 90 mm Model

To demonstrate more mechanical engineering aspects for this report, an FEA impact assessment was conducted to understand any deformation inside X2. Although the previous CFD models were a solid capsule, this would not be suitable to test structural deformation, as the final product would be considerably hollow to allow for optic fibre integration. The shell feature was utilised in Onshape, to remove most of the capsule material and leave a 5 mm surface thickness.

The surface meshing from this impact assessment is displayed in Figure 4.10.

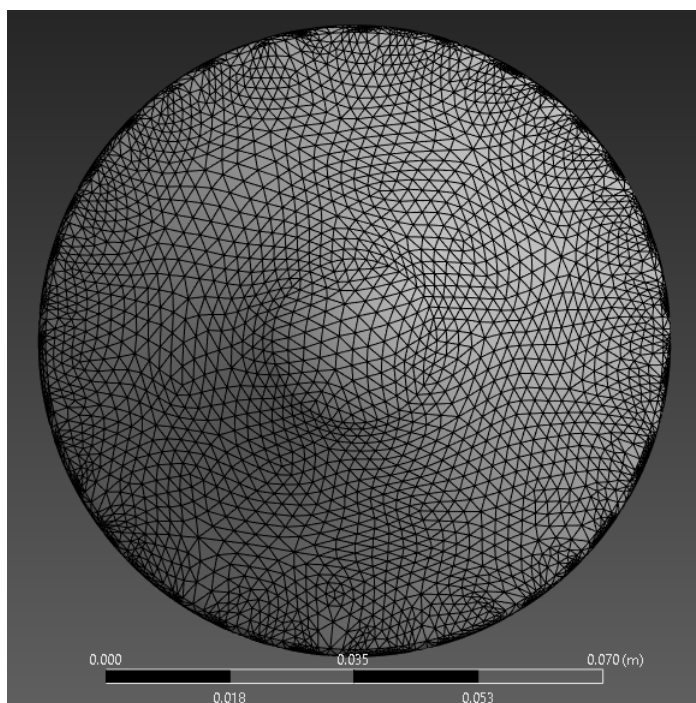


Figure 4.10: Forebody Meshing at 90 mm diamter with 5 mm shell model.

The pressure on the scale model was estimated as 3 MPa via using the Modified-Newtonian Approximation and estimated as 20x the expected pitot pressure. With reference to the hypersonic experiments at UQ in Chapter two & three, the forebody will be made of stainless steel.

A point load of 3 MPa was used to replicate the impact of flow, with estimated deformation of 4.9e-5 m, which is 0.049 mm. This minimal deformation provides reassurance that the model will survive the impact, as the model will be used multiple times throughout a PhD campaign.

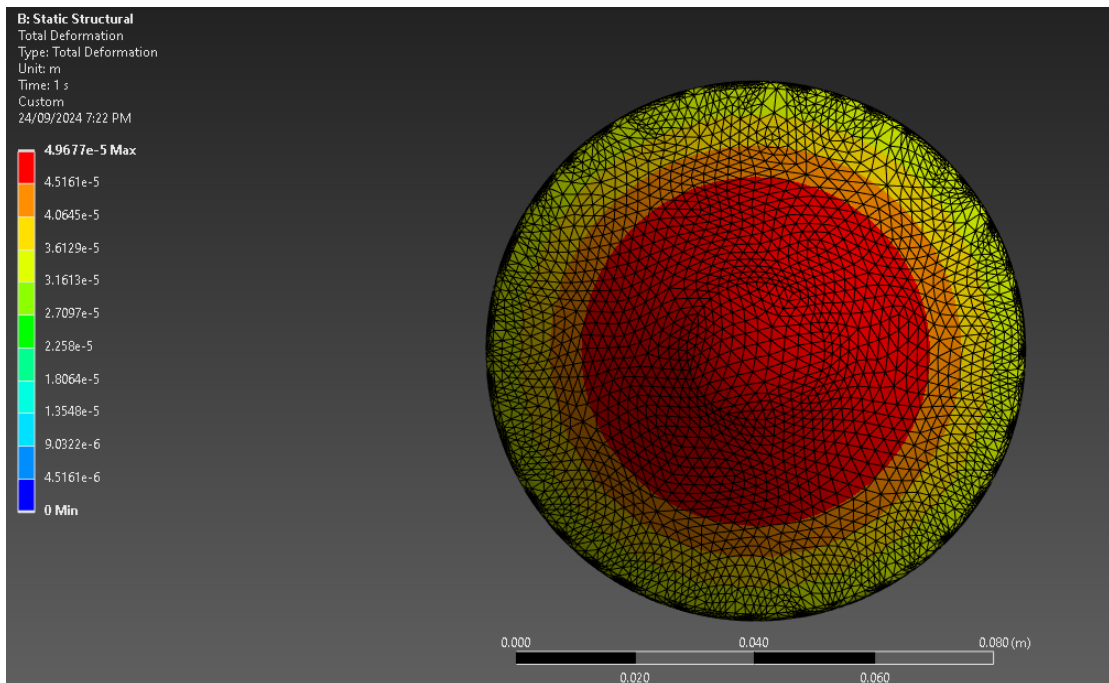


Figure 4.11: Forebody Deformation at 90 mm diameter with 5 mm shell model.

During X2 experimentation, the rupture of the two thin steel diaphragms will most likely impact the scale model at speeds close to 5 km/s. The minimal deformation recorded from this analysis, gives a factor of safety towards debris strikes from testing.

4.13 Chapter Summary

Chapter four detailed many initial boundary conditions required to understand the hypersonic flight environment of Titan entry. The entry trajectory information was analysed from a number of released publications and presentations over a five year period, to confirm the initial conditions should remain unchanged before launch.

The analytical and numerical results were established and compared with the differences noted between them. Furthermore, the CEA gas models were compared with and without the inclusion of trace Argon, which was very important to understand the CN concentration for further investigations.

Solid model simulations were also integrated for the scale model and compared to with the aft-shoulder sting. These results verified that the aft-shoulder sting should remain free from streamline interference to the instrumentation zones. Finally, a FEA analysis was conducted of the expected impact of the hypersonic test conditions, which demonstrated the minimal effect in deformation. The analysis phase of the initial design lifecycle has concluded, the next chapter will focus on design changes from these results.

Chapter 5

Optimised Design & Experimental Scaling

"I have not failed. I've just found 10,000 ways that won't work."

— Thomas A. Edison

5.1 Chapter Introduction

This Chapter represents the incorporation from the lessons learned in the previous design process after inclusion of the results from initial findings.

The preliminary findings indicated that the capsule itself needs to be modified to account for the most effective sting design. The CAD modifications required to include the aft-shoulder sting will be investigated, while an ANSYS re-simulation of this improved design will be used to validate the streamline suitability for experimental testing in X2.

After the final design concept has been computationally validated, another investigation will determine the chemical accuracy of the scaled model. It was noted in the literature review, that the post-shock atmospheric chemistry does not linearly scale with geometry. NASA's CEA program will be used to further understand if a 90 mm model will produce the similar CN concentrations immediately post-shock, even though this size will be suitable for the optic fibre instrumentation.

5.2 Optimised Design

The optimised design from the findings of Chapter four is displayed in Figure 5.1, this model remained at 90 mm diameter to ensure the optic fibres will access the testing locations. The three notable changes occurred at the bottom mid-shoulder, aft-shoulder and a segment of the backshell in the shadow region of flow (Figure 5.1).

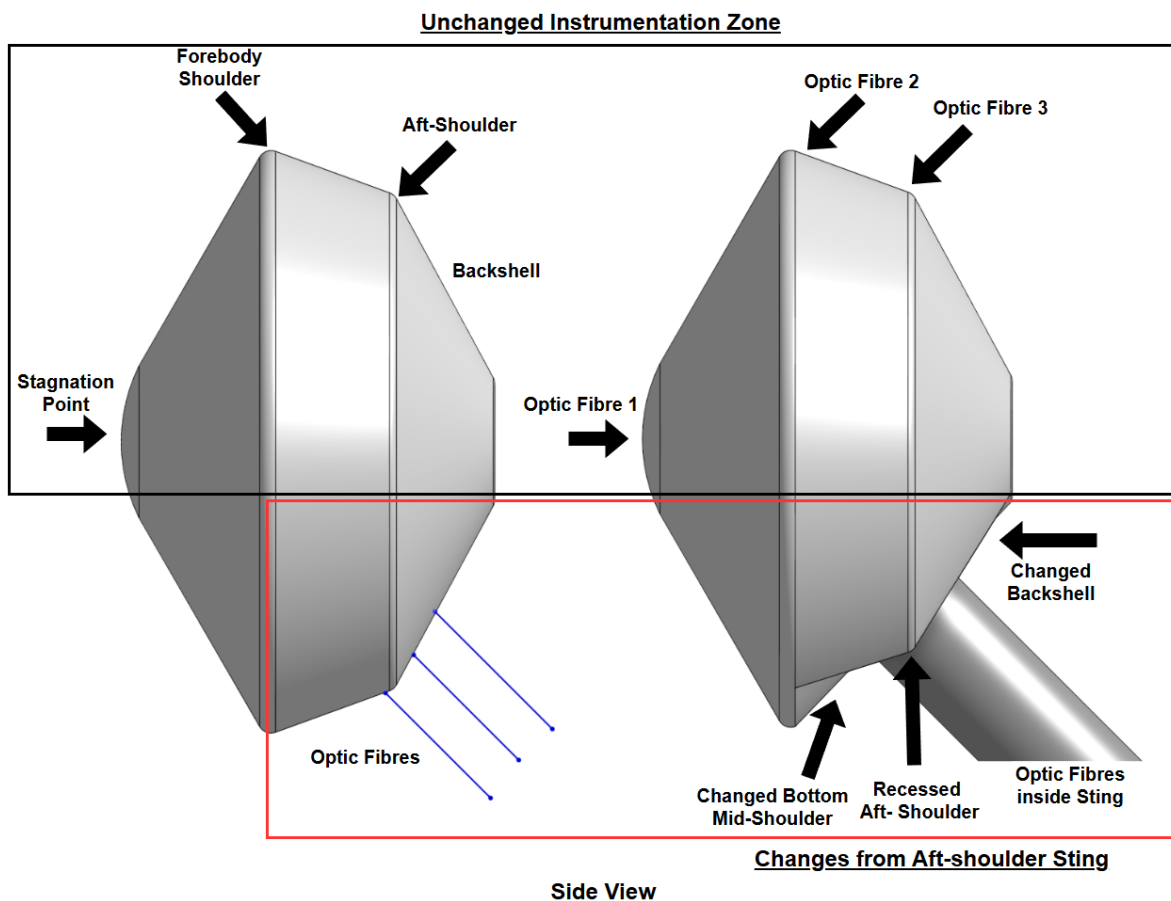


Figure 5.1: Comparison of initial aft-shoulder design and optimised design.

The optic fibres interface at the same 45° angle on the bottom aft-shoulder. Since the profile to the instrumentation zone is the same, the bend radius measurements will also be identical as those displayed in the decision matrix (Table 3.4). The changes were possible by reducing the polar coordinates of the 3D revolved surfaces to leave a 30° recessed section. This will be used to form a flat interface for the sting shown in Figure 5.2.

A focused view of the changes to the bottom/back sections of the optimised design are shown in Figure 5.2.

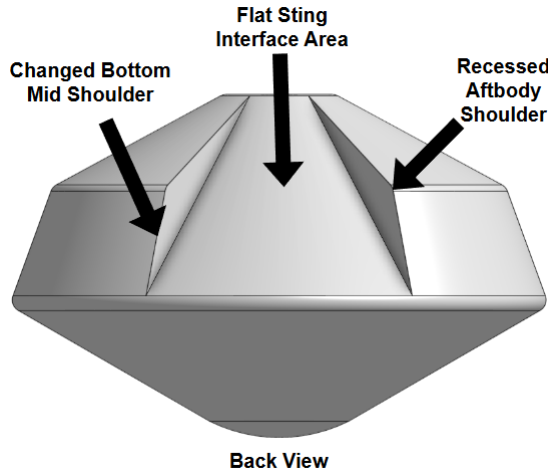


Figure 5.2: Variation of model geometry to house sting.

5.3 Ansys Fluent Methodology of Optimised Design

The same pre-processing procedure outlined in Chapter four was followed for re-assessment. A fluid enclosure was created in Spaceclaim, while the capsule and sting were subtracted; in order to create an empty void in the fluid domain.

The volumetric meshing density was also increased by 30% compared to those completed in Chapter four to improve resolution of CFD, with an increased height of the fluid domain, consisting of 627,359 nodes, 757,603 faces & 112,225 cells.

The initial conditions outlined in Table 5.1 remain unchanged from Chapter four. Ansys Fluent has access to the "Gokcen" 21 species Titan reaction scheme, however, the post-shock mole fraction values are not usable, hence the requirement of NASA's CEA for accurate post-shock chemistry.

Table 5.1: Initial Conditions for Optimised Design Simulations in Ansys Fluent.

Parameter	Initial Condition
Nitrogen Mole Fraction	0.98
Methane Mole Fraction	0.02
Velocity	5.77 km/s
Gauge Pressure	28 Pa
Temperature	162 K
Gas Model	Titan 21 species Gokcen

5.4 Results from Optimised Design Analysis

The simulation style that showed the clearest streamline interaction was under the pathlines graphic section, as a single pulse flow. The initial and intermediate results of the single pulse is displayed in Figure 5.3, in the same manor as in Chapter 4.5.

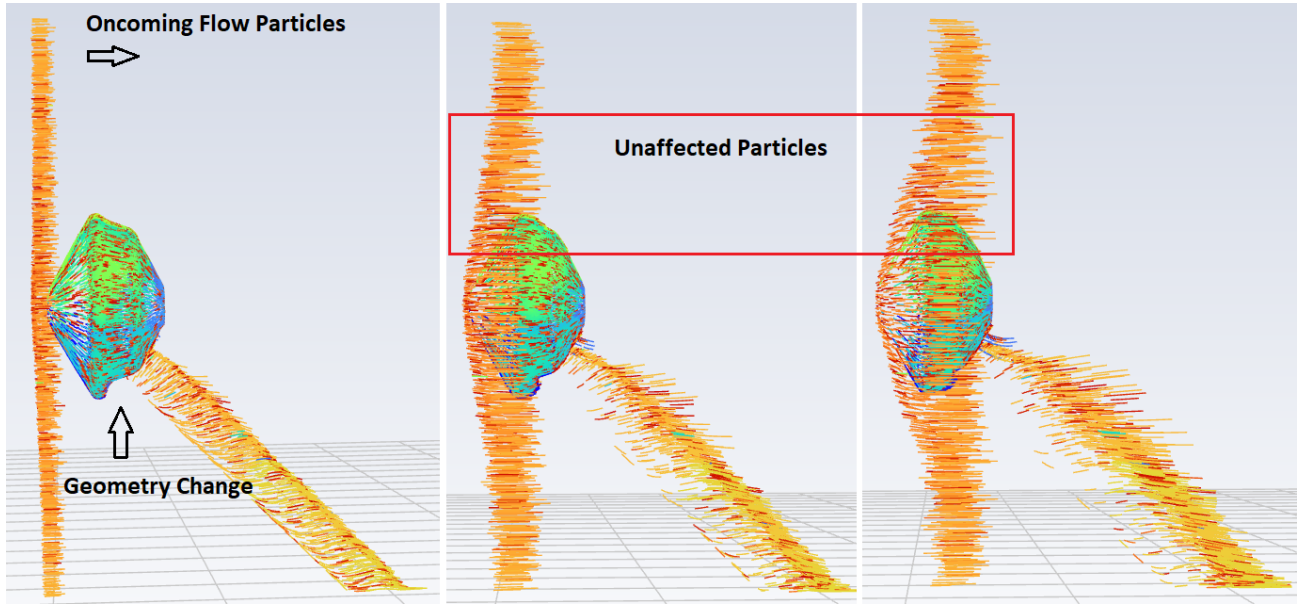


Figure 5.3: Ansys Fluent CFD Results for Optimised Design.

This simulation illustrates similar unaffected areas inside the top instrumentation area, as compared with the original NASA CFD shown in Figure 2.10, Figure 2.11, Figure 3.9, and especially in Section 4.9.1 from full scale Dragonfly simulations presented by Wright 2023 (Figure 4.4) [20].

The streamline results from the optimised model is the required evidence for this project to move to the next phase. It has been determined that the minor geometry change required to incorporate a diagonally mounted, aft-shoulder sting *does not influence the instrumentation zone* for the optical fibre installation locations. The post-shock chemical mole fractions were unable to be calculated in Ansys.

5.5 Comparison of Results with Literature

Further evidence for the Titan atmosphere interactions was found when analysing flight stability assessments of Dragonfly entry. A major design concern remains while investigating the orientation of the capsule during the two hour EDL phase.

Since the ending of the Cassini mission orbiting Titan's host planet Saturn, there is no close orbiting satellite for Dragonfly to communicate with throughout Dragonfly's descent. Therefore, Dragonfly needs to maintain a stable orientation so the high gain antenna in the backshell can communicate with Earth [10, 36].

Figure 5.4 illustrates a comprehensive CFD analysis of Dragonfly entry through Titan's atmosphere. The relevant optical fibre instrumentation zones and proposed sting zone was incorporated into the image, to further visualise the goal of this project. These zones are also outlined in Figure 5.1.

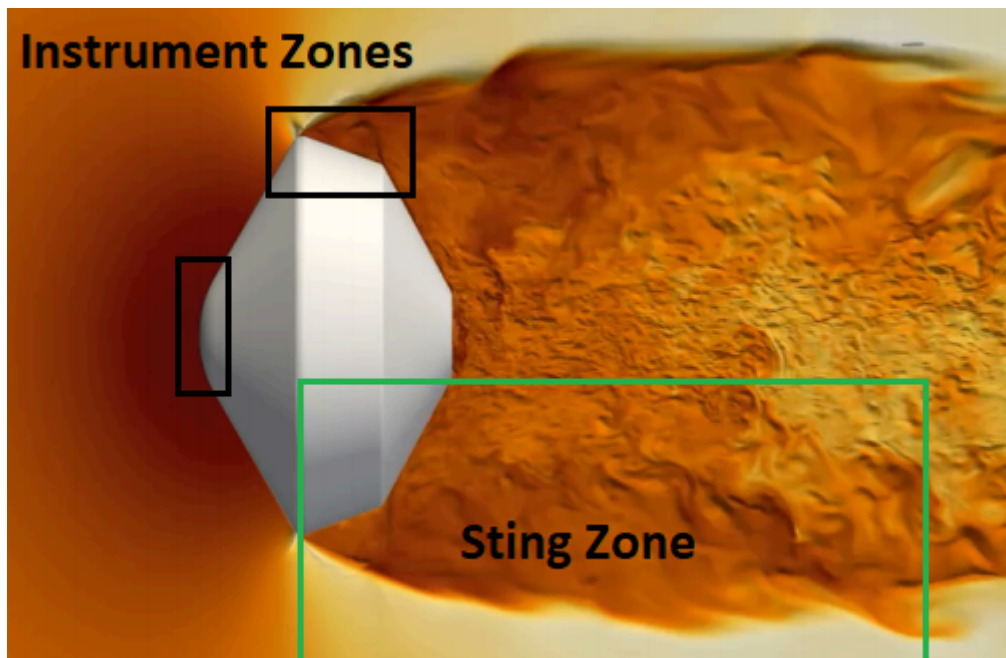


Figure 5.4: CFD Results from Dragonfly Stability Presentation [36].

The testing locations requested by Dr. Brandis can also be visualised in Figure 5.5, while showing a radiative and convective heat flux over the top section of Dragonfly at full scale. Since the capsule is axis-symmetric, as per the CFD from the tested stings, it is suitable to observe one section and infer that across the geometry [37].

Most notably, this study was conducted by American University staff, examining the entry trajectory and parameters outlined from the principle reference for this thesis [7]. It is interesting that these paper published in January 2024, references the values from the outdated Dragonfly diameter (Figure 5.5). The aim of this University research was to identify the effects of self-absorption of the post-shock chemistry expected upon Dragonfly entry, which it would be suitable to use a previous diameter value.

The radiative heat flux can be seen as orders of magnitude higher than the convective heat flux, which validates the earlier claims throughout the literature review. Most notably, on the top left corner (green box) of this graph, the distance resembles that of the previous 3.75 m diameter Dragonfly [37].

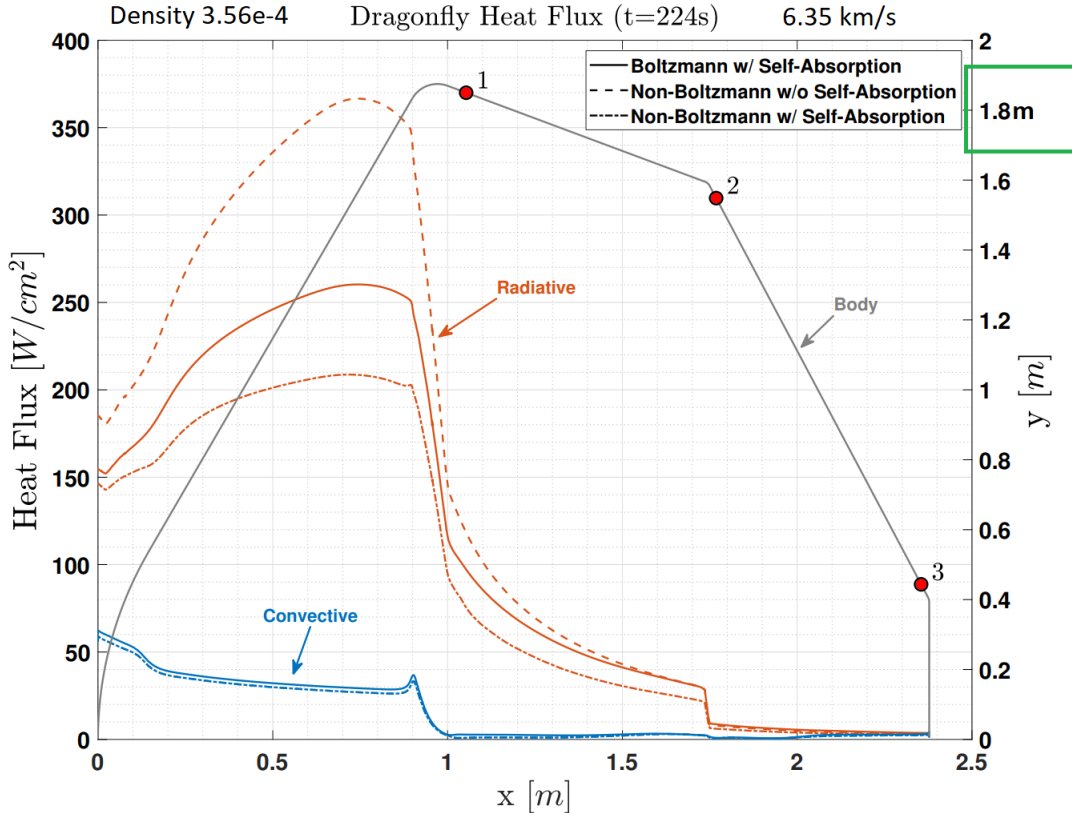


Figure 5.5: Radiative & Convective Heat flux for 3.75 m diameter Dragonfly [36].

It can be seen the density and velocity associated with this graph is from an earlier timestamp at 224 seconds, whereas peak heating has been refined to the 230 second mark after entry interface (Table 2.3).

It is clearly evident that Universities require the current and publicly available entry trajectory, convective and radiative heat flux values from the most current design, to remain relevant and to aid understanding the Titan environment.

With reference to studies being published in 2024 which are based off out-dated 2019 designs and entry values, further highlights the need for Universities to interact directly with NASA, to offer more meaningful and relevant research along the project lifecycle.

Finally, this geometry profile is suitable for scaled Dragonfly entry testing inside X2 at UQ. Although the model itself will need to be further designed to house the optic fibres and

improve the ease of manufacturing before experimentation can occur. The reason that a final design was not developed in detail was due to the remaining analysis that needs to occur, to further understand the non-equilibrium post-shock environment expected.

Scaling can be usually accurately completed at a low scaling factor (5-10) and without proper alterations made this can become unsuitable for analysis of non-equilibrium flows [13]. With reference to [29], the current through-model spectroscopy analysis at UQ is based off the 40 cm diameter Hayabusa asteroid re-entry capsule. Although the model size being instrumented is of 80 mm diameter, which is a scaling factor of only 1:5. Whereas this thesis is examining a capsule from 4.5 m to 90 mm, which is a 1:50 scale.

5.5.1 Design Feedback from Industry Advisors

The goal of this thesis was to understand if a scaled Dragonfly capsule could be used inside the X2 hypersonic wind tunnel. These findings were presented to the industry supervisors at UQ and NASA, in order to understand the next steps required to begin experimentation.

The Industry advisors mentioned that the design should take into account the optic fibre mounting sections. As when designing a two or three part model, the measurement sites are on the shoulders or would-be joints. A two-piece model could be used to ensure that the stagnation point, fore-shoulder and aft-shoulder locations are on the same piece (Figure 5.6).

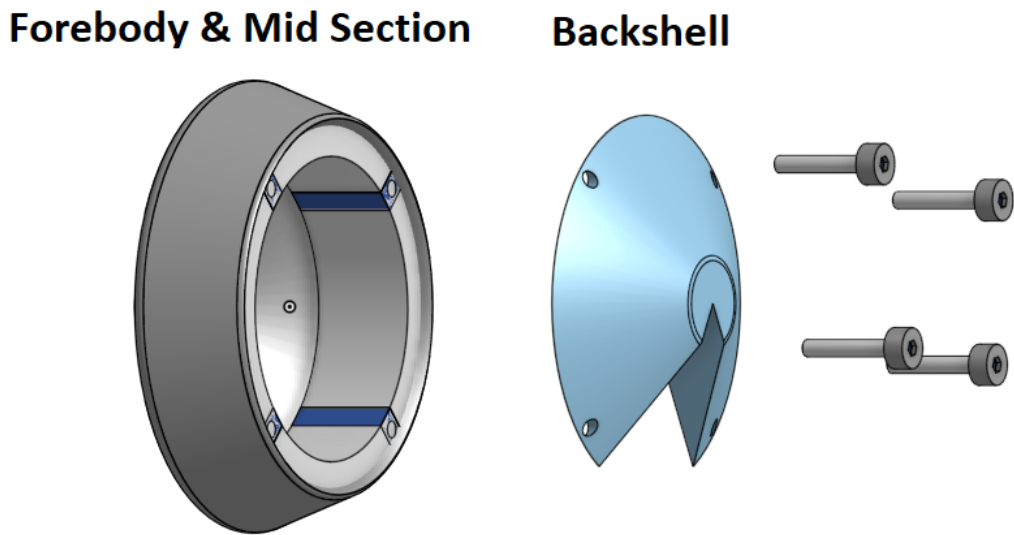


Figure 5.6: Variation of model geometry to house sting.

Another option could be to include a three-piece model, which would then allow the expected damaged forebody to be replaced with a new machined section.

The manufacturability of the final model will be investigated, after the appropriate chemical scaling simulations are completed from the recommendations listed in the concluding chapter.

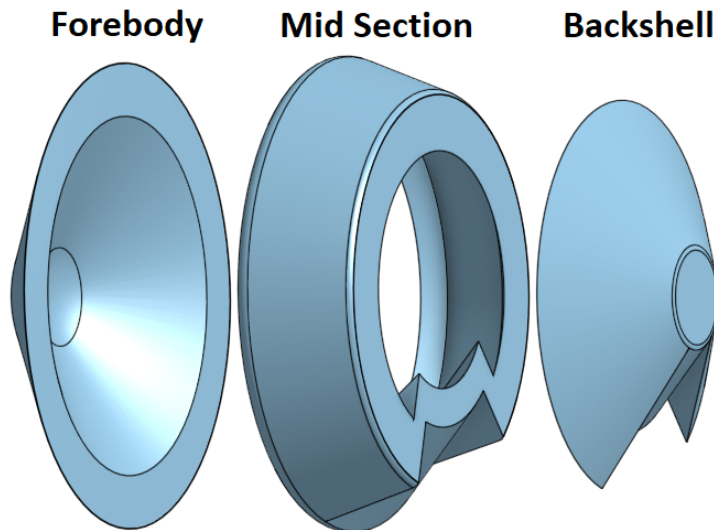


Figure 5.7: Variation of model geometry to house sting.

Therefore, it is recommended to further analyse the scaling requirements needed to replicate the CN concentrations as they are vastly increased from the stagnation point towards the fore and aft shoulders [7]. Further comments of chemical scaling and experimental testing will be mentioned in the future recommendations in Chapter 6.

5.6 Scaling for Hypersonic Wind Tunnel Testing

As mentioned throughout this report, additional work needs to be conducted to better understand the chemical reactions with scaling the Dragonfly geometry down from 4.5 m diameter. With experimental design, it is important to understand what phenomena is trying to be replicated and measured. This thesis is aimed at understanding the feasibility of through-model CN radiation experimentation for Dragonfly entry at an approximate 1:50 scale. Therefore, further advice is required from the Industry Advisors to prioritise the specific post-shock parameters to replicate, in order to create comparable CN radiative effects over the scaled model.

The chemical reactions of atmospheric particles occurs by statistical thermodynamics, with the outcome of atomic and molecular collisions resulting from probability. Therefore, it is increasingly difficult to replicate the same probability when ground testing. The scaling of in-flight and ground testing post-shock conditions will be briefly summarised.

5.6.1 Analytical Binary Scaling Approximations

Binary scaling can be used to replicate the post-shock environment at scale, however, this does not guarantee the concentration of atoms and molecules will also be replicated accurately. Anderson 2006 comments that "Binary scaling is used for primarily dissociating flows when non-equilibrium effects become important" [13]. The equations for binary scaling between the flight case and laboratory model is shown in Equations 5.1 - 5.3.

$$\rho_{X2} = \frac{\rho_\infty \cdot D_{\text{flight}}}{D_{X2}} \quad (5.1)$$

$$T_{X2} = \frac{h_0}{\frac{M_{X2}^2 \cdot \gamma \cdot R}{2} + C_p} \quad (5.2)$$

$$V_{X2} = M_{X2} \cdot \sqrt{\gamma \cdot R \cdot T_{X2}} \quad (5.3)$$

The subscript "flight", refers to the full scale Dragonfly diameter of 4.5 m, while the subscript X2 refers to the values required in the wind tunnel. The symbols for density, temperature, mach number, enthalpy, specific gas constant, gamma, specific heat at constant pressure and subscript infinity for freestream values are unchanged. The apparent conditions required inside X2 to replicate peak heating of Dragonfly entry are outlined in Table 5.2.

Table 5.2: X2 Freestream Conditions at 5770 m/s (Max heating).

Initial Condition	Value	Units
Titan Density _∞	5.8761×10^{-4}	kg/m ³
Titan Pressure _∞	28.67	Pa
Titan Temperature _∞	162	K
Titan Enthalpy ₁₌₂	16.82	MJ/Kg-K
X2 90 mm Scaled	Value	Units
X2 Density _∞	2.938×10^{-2}	kg/m ³
X2 Temperature _∞	761.3	K
X2 Pressure _∞	6737.6	Pa
X2 Velocity _∞	5658.05	m/s
CEA Post-shock	Value	Units
CEA Density ₂	4.855×10^{-4}	kg/m ³
CEA Pressure ₂	10 753	Pa
CEA Temperature ₂	5716	K

It can be seen that a 50 fold increase in density should be used in order to replicate a 50 fold decrease in vehicle diameter. This is the principle relationship as to why binary scaling is used for ground testing the flight environment.

It has been confirmed by the Industry Advisors that these conditions can be replicated inside the X2 wind tunnel. However, this does not mean that the same concentrations of CN will occur behind the shock wave and over the scaled geometry.

5.6.2 CEA CN Results from Density Scaling

The final aspect of this thesis is to evaluate the CN concentration at equilibrium post-shock when the density is scaled to the same factor of the scale model using CEA. As the statistical thermodynamic principles from the probability of collisions needs to be suitably scaled, therefore as demonstrated by binary scaling the density of the gas is the driving factor.

The CEA results from the post-shock environment with a 50 fold increase in density are displayed in Table 5.3.

Table 5.3: CEA Results from 1:50 density scaling at 5770 m/s (Max heating).

CEA Initial	Value	Units
50x Density _∞	2.938×10^{-2}	kg/m ³
Pressure _∞	2322	Pa
Temperature _∞	264	K
Velocity _∞	5770	m/s
Mach Number	22.25	-
CEA Post-shock	Value	Units
CEA Density ₂	3.416×10^{-1}	kg/m ³
CEA Pressure ₂	896 350	Pa
CEA Temperature ₂	7022	K
Enthalpy ₂₌₁	16.43	MJ/kg-K
γ	1.146	-
Sound Speed	1733	m/s

*Note: The post-shock values and CN concentration could be different from initial 162 K & 264 K.

The post-shock values after CEA analysis from a 50 fold increase in initial density create an 11.63x increase in post-shock density, 386x increase in pressure, 26.6x increase in temperature. These values are similar increases to those experienced in the original non-Argon simulation displayed in Table 4.12.

Noting the post-shock species listed in Table 5.4, indicate a wide variety of difference between simulations at the flight and scaled densities. The main findings from the scaled case is there was a 3 fold increase in CN production immediately post-shock, which can be attributed to the increased temperature of 7022 K (Table 5.4).

Table 5.4: Most notable post-shock species at 1:50 scaled density.

Parameter	Flight Case	1:50 Scale Model Case	Difference
Freestream Density _∞	$5.8761 \times 10^{-4} \text{ kg/m}^3$	$2.938 \times 10^{-2} \text{ kg/m}^3$	50 x
CEA Density ₂	$4.855 \times 10^{-4} \text{ kg/m}^3$	$3.416 \times 10^{-1} \text{ kg/m}^3$	704 x
CEA Temperature ₂	5716 K	7022 K	1.23 x
Species	Flight Mole Fraction	1:50 Scale Mole Fraction	Difference
CH ₄	$\ll 1 \times 10^{-10}$	$\ll 1 \times 10^{-10}$	-
N+	1.3664×10^{-5}	3.7103×10^{-3}	271 x
e-	1.4290×10^{-4}	1.8042×10^{-3}	12.6 x
C+	1.2176×10^{-4}	1.2449×10^{-3}	10.2 x
CN	1.1443×10^{-3}	3.4302×10^{-3}	3 x
C	0.014056	0.01250	0.9 x
H	0.061285	0.06389	1.04 x
N	0.34598	0.27259	0.8 x
N ₂	0.57724	0.64709	1.12 x

Note: CH₂, CH₃, CH₄, C₂H₂ – acetylene, C₄, C₄N₂ & C₅ were all listed as under 1×10^{-10} mass fraction.

Interestingly, there was a 271x increase in ionised N⁺, a 10x increase in ionised C⁺, which can be seen in the decrease in atomic Nitrogen and Carbon. Although there was an increase in the initial Nitrogen molecule count, which needs to be investigated further.

It can be seen that using the analytical Binary scaling of density for the model size, does not recreate the same chemical phenomena required. This reiterates the fact that additional computational models needs to be created in order to replicate the immediate post-shock CN concentration and also determine the post-shock CN concentrations over the shoulders before conclusive experimentation can start.

Although the primary objective has been determined that a 90 mm model can be designed for X2 for radiative through-model investigation of Dragonfly. Further analysis is required to accurately replicate the post-shock flight environment on Titan.

5.7 Chapter Summary

Chapter five presented an optimised capsule and sting design, informed from the CFD analysis performed in Chapter four. The Ansys Fluent meshing methodology and initial conditions for re-assessment was outlined, while noting the programs limitations towards post-shock chemistry.

The streamline results were displayed over three time steps of the hypersonic flow interaction expected in X2. This analysis provided the desired outcome that a minor change to the bottom aft-shoulder segment of the capsule, will not impede the hypersonic flow of the instrumentation zone at the top shoulders of the model.

The Ansys Fluent final assessment was compared to very high resolution CFD performed by NASA, with emphasis on the similar near-wake interactions at the instrumentation zones.

The primary discoveries and their importance to the future work regarding experimental Dragonfly entry testing will be summarised in the final concluding chapter.

Chapter 6

Conclusion

"If you can't explain it simply, you don't understand it well enough."

6.1 Chapter Introduction

— Albert Einstein

This chapter will include a summary of the thesis with a mention of the recommendations to take this project from Undergraduate to Higher Degree by Research level.

The aim of this thesis was to; perform an engineering feasibility study for a scale model of the Dragonfly entry capsule, suitable for through-model radiation experiments in the X2 facility at UQ. This aim was achieved which lead to a brief introduction into the hypersonic chemistry to be replicated in X2.

6.1.1 Literature

The overarching theme of the reviewed literature was towards the unknown radiative heating from CN molecules over the forebody and aftbody shoulders of the entry vehicle. The variability between vehicle diameters and launch windows was examined with conclusions that over the last five year period, the Titan entry trajectory remained the same. Temperature models of atoms and molecules was introduced to aid with understanding of the vast thermal engineering challenges which Dragonfly will encounter.

Previous Titan entry experiments were also compared between UQ, NASA and Oxford University displaying that the UQ radiance results need to be updated. The current CFD predictions of Dragonfly were also examined, showing that radiative heating can form up to 90% of shoulder heating. Finally, the experimental apparatus for through-model optic fibre stagnation point testing was illustrated to explain the direction of the project.

6.1.2 Methodology & Initial Analysis

It was recommended in the literature and by the Industry Advisors to replicate the Genesis capsule directly from published articles and scale this up to 4.5 m. This process was completed in OnShape then scaled down to 80 mm, 90 mm & 100 mm to verify if the optic fibre bend radius requirements would be feasible inside X2. A 90 mm Dragonfly prototype vehicle was 3D printed to compare the current 600 μm optic fibre bend radius.

An axial still along with three off centre sting interface variations were created with their respective optic fibre bend radius dimensions examined. The likelihood of near wake flow interference over the top shoulders was also a major design consideration. It was determined that a variation of a bottom mounted aft-shoulder sting would meet both the wake flow and optic fibre requirements.

The analytical and CEA post-shock results were compared at Dragonfly peak heating of Titan gas models with inclusion or exclusion of Argon. The CN volume was 35% higher immediately post-shock when 2% Methane was used instead of 1.5% CH₄ & 0.5% Argon by mole fraction. These post-shock values were compared to the currently literature, to validate the assumptions determined to arrive at suitable initial conditions for further analysis.

Ansys Fluent was used to determine the streamline effects of a control case then if the aft-shoulder sting would be suitable for development. The streamline analysis indicated that a bottom aft-mounted shoulder sting would not impede the flow of the instrumentation zones.

6.1.3 Optimisation & Experimental Design

Due to the requirement of the aft-shoulder sting, the scale capsule was modified to improve the interface angle and optic fibre accessibility. These alterations involved removing sections of the backshell, aftbody shoulder and mid-shoulder. Ansys Fluent was utilised again to validate that these minor changes in the shadow region would not impede the instrumentation zones.

6.2 Implications to the Scientific Community

A multitude of research papers were referenced the change in heat flux and CN concentration across the Dragonfly aeroshell with note to other wake flow CFD provided by NASA. These high detail CFD images aided in validation that the streamline results from Ansys would be representative of the flight environment on Titan.

Two further model designs were shown and an entry level study of CN concentrations at scale was performed. These initial results indicate that the flight environment and CN concentrations could be replicated in X2 at UQ.

The goal of this project is to investigate the process of experimentation at the shoulder and backshell of a scaled Dragonfly capsule. Therefore, as it is known that CN concentration increases away from the immediate shock wave environment, further computationally expensive simulations should be conducted, before scale model manufacture and X2 experimentation occurs.

6.3 Future Experimental Recommendations

There is years of research left to be conducted after the findings of this feasibility study. Firstly, the next computational analysis required is to determine the CN concentrations across the forebody, shoulders and backshell. This will be performed using the "Eilmer 5" software at UQ at full size and at 90 mm.

The CN concentrations will also be examined across a variety of initial conditions to understand it's radiative effects further.

For the experiments themselves another UQ created program is required to understand the fill pressures required inside X2. Dr. C James has developed a python wind tunnel simulation code (PITOT3), which can be used in conjunction with the NASA CEA program, to determine the ground testing experimental requirements. Since this thesis has investigated the in-flight conditions of Dragonfly at peak heating, the next phase is to determine the required fill pressures for each section of X2 to replicate them over the scaled model.

6.4 Chapter Conclusion

This thesis was successfully able to design a scaled geometry profile of NASA Dragonfly suitable for through-model radiation measurements in X2. These findings will be shared with the Industry Advisors and the recommendations will be implemented towards hypersonic experimentation of Dragonfly radiative heating.

References

- [1] Aaron Brandis DS, Allen G, Stern E, Wright M, Mahzari M, Johnston C, et al.: Aerothermodynamics for Dragonfly's Titan Entry Presented by Aaron Brandis.
- [2] Lab JHUAP.: Dragonfly. [Accessed 06-04-2024]. <https://dragonfly.jhuapl.edu/index.php>.
- [3] Baillion M.: Aerothermodynamic Requirements and Design of the Huygens Probe.
- [4] Desai PN, Lyons DT. Entry, Descent, and Landing Operations Analysis for the Genesis Entry Capsule. *Journal of Spacecraft and Rockets*. 2008 Jan;45(1):27–32.
- [5] James CM, Ravichandran R, Smith DR, Cullen TG, Morgan RG. Scaled apollo capsule heat flux measurements in the X3 expansion tube. vol. 1 PartF. American Institute of Aeronautics and Astronautics Inc, AIAA; 2020. .
- [6] James CM. Radiation from Simulated Atmospheric Entry into the Gas Giants [PhD thesis]. The University of Queensland. School of Mechanical and Mining Engineering; 2018. A thesis submitted for the degree of Doctor of Philosophy at The University of Queensland in 2018.
- [7] Johnston CO, West TK, Brandis AM. Features of Afterbody Radiative Heating for Titan Entry. In: AIAA Aviation 2019 Forum; 2019. .
- [8] Winski RG, Pensado AR. Dragonfly Entry and Descent Flight Mechanics Modeling and Analysis. In: AIAA SCITECH 2023 Forum; 2023. .
- [9] Brown D, Webster G, Chicoine RA, Rickman J, Barnstorff K.: Mars Science Laboratory Landing Media Contacts Science Payload Investigations Alpha Particle X-ray Spectrometer: Chemistry and Camera: Engineering Investigation MSL Entry, Descent and Landing Instrument Suite.
- [10] McQuaide ME, Ellison DH, Englander JA, Jesick MC, Ozimek MT, Roth DC. Dragonfly Phase B Mission Design. In: AAS/AIAA Astrodynamics Specialist Conference. AAS-170. Big Sky, MT; 2023. .
- [11] NASA Science.: NASA's Dragonfly to Proceed with Final Mission Design Work. Available from: <https://science.nasa.gov/missions/dragonfly/nasas-dragonfly-to-proceed-with-final-mission-design-work/>.

- [12] Mcquaide M, Ellison D.: Dragonfly Phase B Mission Design. Available from: <https://www.researchgate.net/publication/373256268>.
- [13] Anderson DJ. Hypersonic and High-Temperature Gas Dynamics. Reston, VA: American Institute of Aeronautics and Astronautics; 2006.
- [14] Miller RA, Tang CY, Santos JAB, White TR, Cruden BA. Aftbody Heat Flux Measurements During Mars 2020 Entry. *Journal of Spacecraft and Rockets*. 2023;p. 1–14. <https://doi.org/10.2514/1.a35783>.
- [15] Potter DF. Modelling of Radiating Shock Layers for Atmospheric Entry at Earth and Mars [PhD thesis]. The University of Queensland. School of Mechanical and Mining Engineering; 2011.
- [16] Vargas J, Lopez B, Silva MLD. Heavy Particle Impact Vibrational Excitation and Dissociation Processes in CO₂. *Journal of Physical Chemistry A*. 2021;125:493–512. <https://doi.org/10.1021/acs.jpca.0c05677>.
- [17] Fortescue P, Swinerd G, Stark J. Spacecraft Systems Engineering. John Wiley & Sons; 2011.
- [18] Martin MS, Mendeck GF, Brugarolas PB, Singh G, Serricchio F, Lee SW, et al. In-flight experience of the Mars Science Laboratory Guidance, Navigation, and Control system for Entry, Descent, and Landing. *CEAS Space Journal*. 2015 May;7(2):119–142.
- [19] Brandis AM, Johnston CO. Characterization of Stagnation-Point Heat Flux for Earth Entry. In: 45th AIAA Plasmadynamics and Lasers Conference; 2014. .
- [20] Wright MJ, Edquist KT.: Dragonfly Entry and Descent Overview. [cited 2024 Oct 18]. Available from: <https://nescacademy.nasa.gov/video/1ce99ca8fd314a3a8a335a27b8e7071b1d>. Available from: <https://ntrs.nasa.gov/citations/20220008862>.
- [21] Lorenz RD. Dragonfly: Entry and Descent on Titan Year after the Huygens Probe. In: AIAA SCITECH 2023 Forum. Laurel, MD 20723, USA: Johns Hopkins Applied Physics Laboratory; 2023. .
- [22] Brandis A. Experimental Study and Modelling of Non-equilibrium Radiation During Titan and Martian Entry [PhD thesis]. The University of Queensland. School of Mechanical Engineering; 2009.
- [23] Brandis A, Stern E, Santos J, Hwang H, Gulhan A, Karlgaard C, et al.: Dragonfly Entry Aerosciences Measurements (DrEAM) Suite Science Objectives. [cited 2024 Oct 18]. Available from: <https://ntrs.nasa.gov/citations/20230012150>. Available from: <https://ntrs.nasa.gov/citations/20230012150>.
- [24] Brandis AM, Cruden BA. Titan Atmospheric Entry Radiative Heating. In: AIAA Aviation 2017. Denver, CO, United States: American Institute of Aeronautics and Astronautics; 2017. ARC-E-DAA-TN42338, cited 2024 Oct 19, Ames Research Center. Available from: <https://ntrs.nasa.gov/citations/20170010202>.

- [25] Brandis AM, Morgan RG, McIntyre TJ, Jacobs PA. Nonequilibrium Radiation Intensity Measurements in Simulated Titan Atmospheres. *Journal of Thermophysics and Heat Transfer*. 2010 Mar 29;24(2):291–300. <https://doi.org/10.2514/1.45002>.
- [26] Sopek T, Glenn A, Clarke J, Mare Ld, Collen P, McGilvray M. Radiative Heat Transfer Measurements of Titan Atmospheric Entry in a Shock Tube. *Journal of Thermophysics and Heat Transfer*. 2024 Jun 25;p. 1–23.
- [27] Tibère-Inglesse AC, Johnston CO, Brandis AM, Cruden BA. Dragonfly backshell radiation measurements in the EAST facility. *American Institute of Aeronautics and Astronautics (AIAA)*; 2023. .
- [28] Tibère-Inglesse A, Bensassi K, Brandis AM, Cruden BA. Shock tube radiation measurement in expanding air flows. *American Institute of Aeronautics and Astronautics Inc, AIAA*; 2022. .
- [29] Subra H, Allison R, Lock S, Liu Y, Uren M, Hawken R, et al. Through-Model Fibre Optic Emission Spectroscopy for Studying Planetary Entry Radiative Heat Flux. In: 10th ESA Radiation of High Temperature Gases Workshop. Brisbane, QLD, Australia: Centre for Hypersonics, The School of Mechanical and Mining Engineering, The University of Queensland; 2024. .
- [30] Gollan RJ.: The Computational Modelling of High-Temperature Gas Effects with Application to Hypersonic Flows.
- [31] Brandis AM, White TR, Saunders DA, Hill JP, Johnston CO. Simulation of the Schiaparelli Entry and Comparison to Aerosciences Flight Data. *Journal of Spacecraft and Rockets*. 2022;59:166–177. <https://doi.org/10.2514/1.A35049>.
- [32] Cruden BA, Brandis AM, White TR, Mahzari M, Bose D. Radiative heating during mars science laboratory entry: Simulation, ground test, and flight. vol. 30. American Institute of Aeronautics and Astronautics Inc.; 2016. p. 642–650.
- [33] Eichmann TN, Potter D, McIntyre TJ, Brandis A, Mallon M, Morgan RG, et al. Radiation measurements in a simulated non-terrestrial atmosphere. In: 16th Australasian Fluid Mechanics Conference; 2007. p. 2–7.
- [34] Jo SM, Rostkowski P, Doostan A, Kim JG, Panesi M. Influence of Non-Boltzmann Radiation around Titan Atmospheric Entry Vehicles. In: AIAA SCITECH 2023 Forum. National Harbor, Maryland, USA: AIAA; 2023. .
- [35] Allison R. Through-Model Fibre Optic Emission Spectroscopy in the X2 Expansion Tube. [Undergraduate thesis]. The University of Queensland. School of Mechanical and Mining Engineering; 2023.
- [36] Stern E, Kazemba C, Mckown Q, Owens B. Dragonfly: A Case Study in Dynamic Stability Characterization. In: International Planetary Probe Workshop 2023; 2023. [cited 2024 Oct 23]. Available from: https://ntrs.nasa.gov/api/citations/20230012570/downloads/ippw_dragonfly_dynamics.pdf.

- [37] Thomas CE, Knutson A, Candler GV, Jo SM, Panesi M. Characterizing the Effects of Radiation During Dragonfly's Titan Entry Using a Coupled Simulation Approach. 2024 Jan 4;<https://doi.org/10.2514/6.2024-0450>.
- [38] Wei H, Morgan RG, McIntyre TJ, Brandis AM, Johnston CO.: Experimental and Numerical Investigation of Air Radiation in Superorbital Expanding Flow.
- [39] Tibère-Inglesse AC, McGuire SD, Mariotto P, Laux CO. Experimental study of recombining nitrogen plasmas: II. Electronic population distributions and nonequilibrium radiation of atoms. *Plasma Sources Science and Technology*. 2021;30. <https://doi.org/10.1088/1361-6595/ac2221>.
- [40] Tibère-Inglesse AC, McGuire SD, Mariotto P, Laux CO. Experimental study of recombining nitrogen plasmas: I. Vibronic population distributions and nonequilibrium molecular radiation. *Plasma Sources Science and Technology*. 2019;28. <https://doi.org/10.1088/1361-6595/ab2cc4>.
- [41] Nelson HF, Park C, Whiting EE. Titan atmospheric composition by hypervelocity shock-layer analysis. *Journal of Thermophysics and Heat Transfer*. 1991;5:157–165. <https://doi.org/10.2514/3.243>.
- [42] Wright MJ, Bose D, Olejniczak J. Impact of flowfield-radiation coupling on aeroheating for Titan aerocapture. *Journal of Thermophysics and Heat Transfer*. 2005;19:17–27. <https://doi.org/10.2514/1.10304>.
- [43] Walpot LM, Caillault L, Molina RC, Laux CO, Blanquaert T. Convective and radiative heat flux prediction of Huygens entry on Titan. *Journal of Thermophysics and Heat Transfer*. 2006;20:663–671. <https://doi.org/10.2514/1.20901>.
- [44] Porat H.: Measurement of Radiative Heat Transfer in Simulated Titan and Mars Atmospheres in Expansion Tubes.
- [45] Gu S, Morgan RG, McIntyre TJ, Brandis AM. An Experimental Study of CO₂ Thermochemical Nonequilibrium. *AIAA Journal*. 2022;60:1283–1292. <https://doi.org/10.2514/1.J061037>.
- [46] Hk SGSGE, Hao J, Wen CY. State-Specific Study of Air in the Expansion Tunnel Nozzle and Test Section. *AIAA Journal*. 2022;60:4024–4038. <https://doi.org/10.2514/1.J061479>.

Appendix

```
1      '''Johnson and Brandis Dragonfly Proposed Entry Trajectory into Titan
2          '',
3          '''Johnston CO, West TK, Brandis AM. Features of Afterbody Radiative
4              Heating for
5              Titan Entry. In: AIAA Aviation 2019 Forum; 2019. .'''
6
7      import numpy as np
8      from scipy.interpolate import CubicSpline
9
10     CpN2_300 = 1039 # J/kg -K
11     CpCH4_300 = 2220 # J/kg -K
12     Cp_mix = (0.98 * 1039) + (0.02 * 2220)
13     print(f'Cp mixture is {Cp_mix} J/kg -K') #
14
15     '''Find R for N2 98% and CH4 2%'''
16     ''' Methane % at 247 km?'''
17     gamma = 1.396 # previous tests
18     R_N2 = 296.8 # J/kg -K
19     R_CH4 = 518.3 # J/kg -K
20     R_Argon = 208.13 # J/kg -K
21     Rmix = (0.98 * R_N2) + (0.02 * R_CH4)
22
23     gamma_Argon = 1.67
24     Cp_argon = 523 # J/kg -K
25
26     print(f'R mixture is {Rmix}')
27     MX2 = 10
28
29     gamma_Argon = 1.67
30     Cp_argon = 523 # J/kg -K
31     Titan_interface = 1270 # km
```

```
32 Ve = 7330 # m/s
33 q_y_max = 247 # km
34 v_y_max = 5770 # m/s
35 q_max = 291 #W/cm^2
36
37 y_g_max = 219 # km
38 v_g_max = 4550 # m/s
39
40 yo = 40000 #40 km Scale height
41
42 Dflight = 4.5 #m
43 Rnose = 1.309 #m
44 D_X2 = 0.09 #m 90 mm
45 mass = 2255 # kg entry mass pre ablation
46
47 Area_Dfly = (np.pi * Dflight ** 2) / 4
48
49 def pressure(rho, Rmix, T):
50     pressure = rho * Rmix * T
51     return pressure
52
53 def enthalpy(v_inf, Cp_mix, T_inf):
54     enthalpy = (v_inf**2 / 2) + (Cp_mix * T_inf)
55     return enthalpy
56
57 rho_flight = 0.00058761
58
59 def rho_lab(density, D_flight, D_x2):
60     rho_x2 = (density * D_flight) / D_x2
61     return rho_x2
62
63 # Mach 10 nozzle in X2
64 def T_X2(ho, MX2, gamma, Rmix, Cp_mix):
65     T_X2 = (ho / ((MX2**2 * gamma * Rmix / 2) + Cp_mix))
66     return T_X2
67
68 def V_X2(MX2, gamma, Rmix, T_X2):
69     V_X2 = MX2 * np.sqrt(gamma * Rmix * T_X2)
70     return V_X2
71
72 def sound_speed(gamma, R, Temperature):
73     return np.sqrt(gamma * R * Temperature)
74
75 def Mach(velocity, sound_speed):
```

```

76     return velocity / sound_speed
77
78 def normal_shock_relations(M1, gamma):
79     """Calculate downstream Mach number M2 in a normal shock."""
80     M2 = np.sqrt((1 + 0.5 * (gamma - 1) * M1**2) / (gamma * M1**2 -
81                 0.5 * (gamma - 1)))
82     return M2
83
84 def shock_P2_P1(M1, gamma):
85     """Calculate the pressure ratio across the shock (p2/p1)."""
86     pressure_ratio = 1 + 2*gamma/(gamma + 1) * (M1**2 - 1)
87     return pressure_ratio
88
89 def shock_density_ratio(M1, gamma):
90     """Calculate the density ratio across the shock (2 / 1)."""
91     density_ratio = ((gamma + 1) * M1**2) / (2 + (gamma - 1) * M1**2
92         )
93     return density_ratio
94
95 def T2_T1_ratio(M1, gamma):
96     """Calculate the temperature ratio across the shock (T2/T1).
97         """
98     left = 1 + ((2 * gamma) / (gamma + 1)) * (M1**2 - 1)
99     right = ((2 + (gamma - 1) * M1**2) / ((gamma + 1) * M1**2 ))
100    T2_T1 = left * right
101    return T2_T1
102
103    ''' Dictionary of Table Values of Entry Trajectory'''
104 entry_dict = {
105     "time": [160, 180, 190, 202, 211, 224, 235, 241, 245, 248, 254,
106             263, 280],           # List of time values
107     "velocity": [7330, 7290, 7240, 7100, 6890, 6350, 5590, 5070,
108                 4700, 4420, 3850, 3080, 1940],      # List of velocity values
109     "density": [4.4e-6, 1.94e-5, 3.98e-5, 8.74e-5, 1.58e-4, 3.56e-4,
110                 6.64e-4, 9.02e-4, 1.09e-3, 1.24e-3, 1.57e-3, 2.12e-3, 3.26e-3
111                 ],        # List of density values
112     "temperature": [162, 162, 162, 162, 162, 162, 162, 162, 162,
113                     162, 160, 158]   # List of temperature values
114 }
115
116    # New dictionary to store interpolated values
117 interpolated_dict = {
118     "time": [],
119     "velocity": [],
120

```

```
112     "density": [] ,
113     "temperature": []
114 }
115
116 # Define the new range of time for interpolation (you can adjust this
117 # as needed)
117 time_interp = np.linspace(min(entry_dict["time"]), max(entry_dict["time"]),
118                           num=100) # 50 points between the min and max time
119
120 # Perform cubic spline interpolation for each variable
121 cs_velocity = CubicSpline(entry_dict["time"], entry_dict["velocity"])
122 cs_density = CubicSpline(entry_dict["time"], entry_dict["density"])
123 cs_temperature = CubicSpline(entry_dict["time"], entry_dict["temperature"])
124
125 # Interpolate the values at the new time points
126 velocity_interp = cs_velocity(time_interp)
127 density_interp = cs_density(time_interp)
128 temperature_interp = cs_temperature(time_interp)
129
130 # Store the interpolated values in the new dictionary
131 interpolated_dict["time"] = time_interp
132 interpolated_dict["velocity"] = velocity_interp
133 interpolated_dict["density"] = density_interp
134 interpolated_dict["temperature"] = temperature_interp
135
136 for i in range(len(interpolated_dict["time"])):
137     time = interpolated_dict["time"][i]
138     velocity = interpolated_dict["velocity"][i]
139     density = interpolated_dict["density"][i]
140     temperature = interpolated_dict["temperature"][i]
141
142     print(f"When Titan velocity is {velocity:.0f} m/s, Titan
143           Freestream Density is {density:.8f} kg/m^3.")
144     titan_freestream_P = pressure(density, Rmix, temperature)
145     print(f"When Titan velocity is {velocity:.0f} m/s, Titan
146           Freestream Pressure is {titan_freestream_P:.2f} Pa.")
147     enthalpy_titan = enthalpy(velocity, Cp_mix, temperature)
148     print(f"When Titan velocity is {velocity:.0f} m/s, Titan Entry
149           Enthalpy is {enthalpy_titan/1e6:.2f} MJ/Kg-K.")
150     rho_X2 = rho_lab(density, Dflight, D_X2)
151     print(f"When Titan velocity is {velocity:.0f} m/s, X2 Freestream
152           density is {rho_X2:.8f} kg/m^3.")
153     Temp_X2 = T_X2(enthalpy_titan, MX2, gamma, Rmix, Cp_mix )
```

```

149     print(f"When Titan velocity is {velocity:.0f} m/s, X2 Freestream
150         Temperature is {Temp_X2:.2f} K.")
151 Velocity_X2 = V_X2(MX2, gamma, Rmix, Temp_X2)
152     print(f"When Titan velocity is {velocity:.0f} m/s, X2 Freestream
153         Velocity is {Velocity_X2:.2f} m/s.")
154 Pressure_X2 = pressure(rho_X2, Rmix, Temp_X2)
155     print(f"When Titan velocity is {velocity:.0f} m/s, X2 Freestream
156         Pressure is {Pressure_X2:.2f} Pa.")
157     print()
158 Titan_soundspeed = sound_speed(gamma, Rmix, temperature)
159     print(f"When Titan velocity is {velocity:.0f} m/s, Titan local
160         sound speed is {Titan_soundspeed:.2f} m/s.")
161 Titan_Mach = Mach(velocity, Titan_soundspeed)
162     print(f"When Titan velocity is {velocity:.0f} m/s, Titan local
163         Mach number is {Titan_Mach:.2f}.")
164
165 Mach_behind = normal_shock_relations(Titan_Mach, gamma)
166     print(f"When Titan velocity is {velocity:.0f} m/s, Mach number
167         behind Titan bow shock is {Mach_behind:.2f}.")
168
169 Pressure_PostDfly_shock = shock_P2_P1(Titan_Mach, gamma)
170     print(f"When Titan velocity is {velocity:.0f} m/s, Pressure
171         behind Titan bow shock is {(Pressure_PostDfly_shock *
172             titan_freestream_P)/1000:.2f}.kPa ")
173
174 Density_PostDfly_shock = shock_density_ratio(Titan_Mach, gamma)
175     print(f"When Titan velocity is {velocity:.0f} m/s, Density behind
176         Titan bow shock is {(Density_PostDfly_shock * density):.6f}.
177             kg/m^3 ")
178
179 Temperature_PostDfly_shock = T2_T1_ratio(Titan_Mach, gamma)
180     print(f"When Titan velocity is {velocity:.0f} m/s, Temperature
181         behind Titan bow shock is {(Temperature_PostDfly_shock *
182             temperature):.2f} K.")

183     print('---' * 20)

184     ''' Ballistic Equations '''
185
186 def y_f_max(yo, Cd, rho, Area, mass, flight_angle):
187     ymax_decel = yo * np.log((Cd * rho * Area * yo) / (mass * np.sin(
188         np.radians(flight_angle))))
189     return ymax_decel

```

```
180 alt_gmax = y_f_max(yo, 0.7, 5.3, Area_Dfly, mass, 90.0)
181
182 print(f" Altitude of g Max for Titan entry is {alt_gmax:.2f} m")
183
184 titan_surface_dens = 5.3 # 219 km gmax
185
186 V_gmax = 7.5 * (np.e **-0.5)
187 print(f"velocity at g max is {V_gmax:.2f} m/s, 4.55 km/s expected")
188
189 def enthalpy(v_inf, Cp_mix, T_inf):
190     enthalpy = (v_inf**2 / 2) + (Cp_mix * T_inf)
191     return enthalpy
192
193 enthalpy_analytical = enthalpy(5770, 1060.62, 162)
194 print(f"enthalpy analytical 162 {enthalpy_analytical:.4f} J/kg-K")
195 enthalpy_264 = enthalpy(5770, 1060.62, 264)
196 print(f"enthalpy analytical 264 {enthalpy_264:.4f} J/kg-K")
197
198 print(f'R mixture is {Rmix}')
199 print(f'Cp mixture is {Cp_mix} J/kg-K')
200
201 Cp_with_argon = (0.98 * 1039) + (0.015 * 2220) + (0.05 * Cp_argon)
202 print(f'Cp with argon is {Cp_with_argon:.4f} J/kg-K')
203
204 Rmix_with_argon = (0.98 * R_N2) + (0.015 * R_CH4) + (0.005 * R_Argon)
205 print(f'Rmix argon is {Rmix_with_argon} # J/kg-K')
206
207 def equation_Cv(Cp, R):
208     Cv = Cp - R
209     return Cv
210
211 Cv_mix = equation_Cv(Cp_mix, Rmix)
212 print(f'Cv mixture is {Cv_mix:.4f} J/kg-K')
213
214 Cv_with_argon = equation_Cv(Cp_with_argon, Rmix_with_argon)
215 print(f'Cv argon is {Cv_with_argon:.4f} J/kg-K')
216
217
218 def equation_gamma(Cp, Cv):
219     gamma = Cp/Cv
220     return gamma
221
222 gamma_mix = equation_gamma(Cp_mix, Cv_mix)
223 print(f'gamma mix is {gamma_mix:.4f}')
```

```
224  
225 gamma_argon = equation_gamma(Cp_with_argon, Cv_with_argon)  
226 print(f'gamma argon is {gamma_argon:.4f}')  
227  
228 enthalpy_argon = enthalpy(5770, Cp_with_argon, 162)  
229 print(f'Enthalpy with argon is {enthalpy_argon:.4f} J/kg-K')
```

Listing 6.1: Dragonfly Entry Trajectory Code